SIMPLE MODELS OF COMPLEX SYSTEMS

BY JOHN BARTON

A dissertation submitted to the

Graduate School—New Brunswick

Rutgers, The State University of New Jersey

in partial fulfillment of the requirements

for the degree of

Doctor of Philosophy

Graduate Program in Physics and Astronomy

Written under the direction of

Professor Joel L. Lebowitz

and approved by

_____

_____

_____

_____

_____

New Brunswick, New Jersey

October, 2012

ABSTRACT OF THE DISSERTATION

Simple models of complex systems

by John Barton

Dissertation Director: Professor Joel L. Lebowitz

When the complete description of a complex system of interest is out of reach, simple models which are more amenable to theoretical approach can give a qualitative understanding. In addition, the techniques and ideas developed in investigating simple model systems form a foundation for research on complex phenomena. In this thesis, composed of two parts, we study some representative models from statistical mechanics. In the first part we explore the ABC model, which describes three species of particles with asymmetric interactions. In the second part we consider the inverse Ising problem, using experimental data to infer an effective Ising model.

Acknowledgements

I have had a great time working and learning as a graduate student at Rutgers, and I owe a great deal of thanks to all of those who have helped me along the way.

First, I would like to thank my advisor, Joel Lebowitz, who has been a wonderful mentor throughout my time as a student. I am grateful also for the guidance of Gene Speer, who has been very much like a second advisor to me. Through discussions and by example Joel Lebowitz and Gene Speer have shown me what it is to be a scientist, and so much more. Without their help, this work would not have been possible.

I would also like to thank my collaborators in research Simona Cocco, Rémi Monasson, and Eduardo Sontag, from whom I have learned much and am still learning. My thanks to the many scholars with whom I have enjoyed interesting discussions, and in particular to Thierry Bodineau, Pablo Hurtado, and Tobias Kuna.

Finally, I am grateful for the support and companionship of many friends and family over my years here at Rutgers. In particular I would like to thank my wife Chioun for constant encouragement.

Dedication

To my parents, who have supported every step of the journey.

Table of Contents

List of Tables

List of Figures

Chapter 1

Introduction

Broadly speaking, the goal of statistical mechanics is to derive the macroscopic properties of a system given the microscopic rules governing its evolution. This goal has been largely accomplished in equilibrium statistical mechanics, where rules for constructing appropriate statistical ensembles provide a means of computing, formally if not practically, the macroscopic properties of a system in equilibrium. However, little is known in general about the statistics of systems out of equilibrium.

Simplified model systems whose macroscopic behavior can be determined explicitly from microscopic laws are thus of great interest. The techniques and intuition developed in studying such models can then be applied to help understand more complex systems, both in and out of equilibrium. Simple phenomenological models may also be helpful in qualitatively understanding the macroscopic collective behavior of complex systems which are difficult to approach directly.

An example is the asymmetric simple exclusion process (ASEP) [20] (see also related reviews [10, 21]), a prototypical model exhibiting a nonequilibrium steady state and one closely related to the ABC model presented in this thesis. The ASEP consists of particles and holes (empty sites) on a one-dimensional lattice. Particles hop to the left

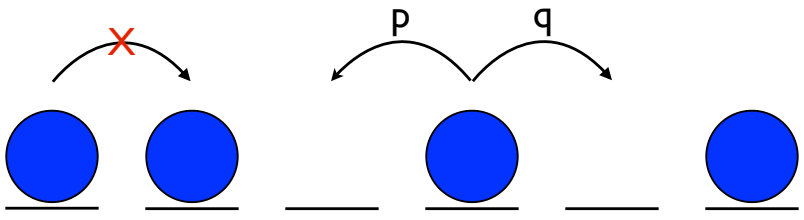

Figure 1.1: A section of a one-dimensional lattice for the ASEP, illustrating nearest neighbor hopping dynamics.

and right with stochastic rates p and q, respectively, subject to hard core exlusion (see Fig. 1.1). Work on the ASEP and closely related models has spanned several decades, and a rigorous description of its macroscopic properties has required the development of novel analytical techniques [2, 22, 23]. The ASEP has also been used as a model for such diverse subjects as traffic flow [53] and the motion of molecular motors in cells [34], as well as in the study of biopolymers [41].

In this thesis we summarize investigations and applications of several statistical mechanical models. The first two Chapters deal with the properties of the ABC model, a dynamical model of three particle species on a one-dimensional lattice which perform nearest neighbor exchanges with spatially asymmetric exchange rates. As the dynamics of the standard ABC model only consists of particle exchanges, the number of particles of each species is conserved. If the boundary conditions of the lattice are taken to be closed, or if the boundary conditions are periodic but the number of particles of each species is equal, then the stationary measure is an equilibrium Gibbs measure with a long-range Hamiltonian, despite the strictly local dynamics. However, the ABC model displays novel behavior not found in standard equilibrium systems with short range interactions. These include a finite temperature phase transition in one dimension leading to phase separation, with particles of the same type gathered together in large domains.

The first Chapter details collaborative work with Joel Lebowitz and Eugene Speer, where we consider a grand canonical version of the ABC model [7]. Background and results for the canonical ABC model are also discussed in Section 2.2. We add chemical potentials to the standard ABC model Hamiltonian and allow the number of particles of each species to fluctuate. In this case we find that, as for the canonical ensemble, the grand canonical ensemble is the stationary measure satisfying detailed balance for a natural dynamics. We obtain the full phase diagram of the model, finding a phase transition when the chemical potentials are all equal at a temperature different from that of the canonical model, thus demonstrating inequivalence of ensembles.

In the second Chapter, based on collaborative work with Eugene Speer and Joel Lebowitz, we consider a generalized version of the canonical ABC model with external

fields applied to the particles [7]. With this modification the interactions need not be invariant under cyclic permutation of the particle species as in the standard ABC model. Here we made heavy use of conserved quantities to probe the analytical structure of this generalized model when direct solution of the nonlinear Euler-Lagrange equations for the particle densities proved difficult. Our main result, which we are able to prove rigorously in special cases but conjecture to hold in general, is the description of the phase plane including a second order phase transition for certain values of the average particle densities and external fields, analogous to that of the standard ABC model. We have also found connections between our model and certain unresolved questions about the generalized Lotka-Volterra family of ODEs, which includes the well-known Lotka-Volterra predator-prey equations.

The final Chapter outlines work in progress on the inverse Ising problem, undertaken jointly with Remi Monasson, Simona Cocco, Joel Lebowitz, and Eugene Speer [6]. In contrast with the "forward" Ising problem, the description of the collective behavior of some Ising spins based upon their interactions, the inverse Ising problem involves using a set of observables – in this case the single-spin magnetizations and pairwise correlations – to infer the interaction structure. The inverse Ising problem thus belongs to the general category of inverse problems, whose goal is to use measurements of a system to infer the parameters which characterize its behavior [63].

Inverse problems in general present some mathematical difficulties which are not present in the corresponding forward problem. Often the inverse problem is ill-posed, that is, a solution may not exist, or solutions may not be unique or stable under small changes in the observed data. A problem whose solution changes greatly in response to small perturbations in the data is also referred to as ill-conditioned.

In recent years effective Ising models have proved useful for describing several biological phenomena of interest, including the activity of networks of neurons [15, 24, 56, 59] and elements of protein structure and protein-protein interactions [60, 67]. These effective Ising models must be inferred from data, bringing into focus the need for efficient solutions of the inverse Ising problem. Standard methods of solution such as Boltzmann learning, which involves iterative Monte Carlo simulations followed by small updates

to the interaction parameters [1], or perturbative expansions [51, 54, 58] can be slow, or suffer from limited ranges of applicability.

In Chapter 4, we describe an efficient method of solution of the inverse Ising problem, originally developed by Cocco and Monasson [16, 17], referred to as the Selective Cluster Expansion (SCE) algorithm. Here we describe joint efforts to improve the algorithm, and demonstrate its viability by analyzing real data from multielectrode recordings of networks of neurons.

Chapter 2

The grand canonical ABC model

2.1 Introduction

In this chapter we study the phase diagram of the three species ABC model on an interval as a function of the chemical potentials and the temperature. The system is defined microscopically on a lattice of N sites in which each site is occupied by either an A, a B, or a C particle. The energy is of mean field type, with an interaction which has cyclic symmetry in the particle types but is reflection asymmetric:

$$E_N(\underline{\zeta}) = \frac{1}{N} \sum_{i=1}^{N-1} \sum_{j=i+1}^{N} [\eta_C(i)\eta_B(j) + \eta_A(i)\eta_C(j) + \eta_B(i)\eta_A(j)]. \tag{2.1}$$

Here the configuration $\underline{\zeta}$ of the model is an N-tuple $(\zeta_1, \ldots, \zeta_N)$, with $\zeta_i = A$, B, or C, and $\eta_\alpha(i)$, $\alpha = A, B, C$, is a random variable which specifies whether a particle of species α is present at site i: $\eta_\alpha(i) = 1$ if $\zeta_i = \alpha$ and $\eta_\alpha(i) = 0$ otherwise, so that always $\sum_\alpha \eta_i(\alpha) = 1$.

We remark that we may also regard the model as a reflection asymmetric mean field three state Potts model. The asymmetry of the interaction gives this model system very different behavior from that of the usual symmetric mean field model [61]. Similar but short-range (in fact, nearest neighbor) reflection asymmetric interactions occur in chiral clock models [3, 29, 46]; see Remark 2.5.1 below. A simple comparison of reflection symmetric and asymmetric nearest neighbor interactions in one dimension is given in Appendix A.2.

The equilibrium probability of a configuration $\underline{\zeta}$ is given by the grand canonical Gibbs measure

$$\mu_{\beta,\lambda}(\underline{\zeta}) = \Xi^{-1} \exp[-\beta E_N(\underline{\zeta}) + \sum_\alpha \lambda_\alpha N_\alpha(\underline{\zeta})], \tag{2.2}$$

where β is the inverse temperature, λ_A, λ_B, and λ_C are β times the chemical potentials, $N_\alpha = \sum_{i=1}^{N} \eta_\alpha(i)$ with $\sum_\alpha N_\alpha = N$, and Ξ is the usual grand canonical partition function. We prove here that in the scaling limit ($N \to \infty$, $i/N \to x \in [0,1]$) the equilibrium density profiles $\rho(x)$ are unique and spatially nonuniform when the λ_α's are not all the same. When $\lambda_A = \lambda_B = \lambda_C$ the densities are spatially uniform above a critical temperature $\hat{T}_c = \hat{\beta}_c^{-1}$, with $\hat{\beta}_c = 2\pi/\sqrt{3}$; below $\hat{T}_c$ the profiles have a natural extension to periodic functions with a period three times the length of the system.

One may compare the behavior described above with that of the same system in the canonical ensemble, in which the N_α are taken as fixed. The results are quite different, that is, we have inequivalence of ensembles (see [13, 43] for recent reviews). We give in Section 2 a brief history of the ABC model with fixed particle number and a summary of results for that system. In Section 3 we describe a stochastic evolution satisfying detailed balance with respect to the measures $\mu_{\beta,\lambda}(\underline{\zeta})$, and in Section 4 we establish the phase diagram. Section 5 gives a discussion of some related models and problems.

A different generalization of the ABC model to a system with fluctuating particle numbers is discussed in [39, 40]. In that model vacancies are permitted and it is the total number of particles which fluctuates, while the differences $N_\alpha - N_\gamma$ are conserved. The model is formulated on a ring and is initially specified by dynamical rates, but it is observed that in the case when all the N_α are equal, the case considered in detail, it may be equivalently described by a grand canonical equilibrium model on the ring or on the interval. A striking feature is the existence of a first-order phase transition, at low temperatures, from a low-density to high-density state.

2.2 The ABC model in the canonical ensemble

The ABC model was introduced by Evans et al. [33] (see also [5, 9, 11, 14, 26, 32] and [37, 38] for a related model) as a one dimensional system consisting of three species of particles, labeled A, B, C, on a ring containing N lattice sites; we will typically let $\alpha = A$, B, or C denote a particle type, and make the convention that $\alpha + 1$, $\alpha + 2$, ... denote the particle types which are successors to α in the cyclic order ABC. The

system evolves by nearest neighbor exchanges with asymmetric rates: if sites i and $i+1$ are occupied by particles of different types α and γ, respectively, then the exchange $\alpha\,\gamma \to \gamma\,\alpha$ occurs at rate $q < 1$ if $\gamma = \alpha + 1$ and at rate 1 if $\gamma = \alpha - 1$. That is,

$$AB \underset{1}{\overset{q}{\rightleftharpoons}} BA,$$
$$BC \underset{1}{\overset{q}{\rightleftharpoons}} CB,$$
$$CA \underset{1}{\overset{q}{\rightleftharpoons}} AC.$$

The total numbers N_α of particles of each species are conserved and satisfy $\sum_\alpha N_\alpha = N$. In the limit $N \to \infty$ with $N_\alpha/N \to r_\alpha$, where $r_\alpha > 0$ for all α, the system segregates into pure A, B, and C regions, with rotationally invariant distribution of the phase boundaries.

We remark that for a general choice of the N_α the steady state of the ABC model on the ring is nonequilibrium. In order for detailed balance to hold, the forward and reverse transition rates along a closed loop in the configuration space must be equal. The rate for a given particle, say an A, to make one loop around the ring and return to its starting point is q^{N_B} when traveling to the right, and q^{N_C} in the reverse direction. Hence the detailed balance condition is violated if the number of particles of each species is not equal.

In the weakly asymmetric version of the system introduced by Clincy et al. [14], in which $q = e^{-\beta/N}$, the stationary state for the equal density case $N_A = N_B = N_C$ is a Gibbs measure of the form $\exp\{-\beta E_N\}$, so that the parameter $\beta = T^{-1}$ plays the role of an inverse temperature. The energy E_N is given by (2.1), and the condition $N_A = N_B = N_C$ ensures that this is translation invariant, despite the appearance of a preferred starting site for the summations.

Ayyer et. al. [5] studied the weakly asymmetric system on an interval, that is, again on a one-dimensional lattice of N sites but now with zero flux boundary conditions, so that a particle at site $i = 1$ (respectively $i = N$) can only jump to the right (respectively left). For this system the steady state is *always* Gibbsian, given by $\exp\{-\beta E_N\}$ with E_N as in (2.1), whatever the values of N_A, N_B, and N_C. When $N_A = N_B = N_C$ the steady state of the system thus agrees with that on the ring, so that the invariance

under rotations on the ring then implies a rather surprising "rotation" invariance of the Gibbs state on the interval. We describe the results of [5] in some detail, since the work of the current chapter depends heavily on them.

To identify typical coarse-grained density profiles at large N, [5] considers the scaling limit

$$N \to \infty, \qquad i/N \to x, \quad x \in [0,1]. \tag{2.3}$$

For this limit there exists a Helmholtz free energy functional $\beta^{-1}\mathcal{F}(\{n\})$ of the density profile $n(x) = (n_A(x), n_B(x), n_C(x))$. $\mathcal{F}$ is the difference of contributions from the energy and entropy:

$$\mathcal{F}(\{n\}) = \beta\mathcal{E}(\{n\}) - \mathcal{S}(\{n\}), \tag{2.4}$$

where $\mathcal{E}(\{n\})$ and $\mathcal{S}(\{n\})$ are the limiting values of the energy and entropy per site:

$$\mathcal{E}(\{n\}) = \int_0^1 dx \int_x^1 dz \sum_\alpha n_\alpha(x) n_{\alpha+2}(z), \tag{2.5}$$

$$\mathcal{S}(\{n\}) = -\int_0^1 dx \sum_\alpha n_\alpha(x) \ln n_\alpha(x). \tag{2.6}$$

We will write $\mathcal{F} = \mathcal{F}^{(\beta)}$ when we need to indicate explicitly the β dependence. Only the canonical ensemble was considered in [5], so that for some fixed positive mean densities r_A, r_B, r_C satisfying $r_A + r_B + r_C = 1$ the profiles $n(x)$ in (2.4)–(2.6) satisfy the conditions

$$0 \le n_\alpha(x) \le 1, \quad \sum_\alpha n_\alpha(x) = 1, \quad \text{and} \quad \int_0^1 n_\alpha(x)dx = r_\alpha. \tag{2.7}$$

The typical profiles in the scaling limit are those which minimize $\mathcal{F}$; it was shown in [5] that such minimizers always exist and satisfy the ELE derived from $\mathcal{F}$. To obtain the ELE one defines

$$\begin{aligned} \mathcal{F}_\alpha(x) &= \frac{\delta\mathcal{F}}{\delta n_\alpha(x)} \\ &= \log n_\alpha(x) + \beta \int_0^x [n_{\alpha+1}(z) - n_{\alpha+2}(z)]\, dz + 1 + \beta r_{\alpha+2} \end{aligned} \tag{2.8}$$

to be the variational derivative taken as if the profiles $n_A(x)$, $n_B(x)$, and $n_C(x)$ were independent; the constraints (2.7) then imply that at a stationary point of $\mathcal{F}$ both

$\mathcal{F}_A - \mathcal{F}_C$ and $\mathcal{F}_B - \mathcal{F}_C$ are constant. After simple manipulations (see also Section 2.4 below) this yields the ELE satisfied by the typical profiles $\rho(x)$:

$$\frac{d\rho_\alpha}{dx} = \beta\rho_\alpha(\rho_{\alpha-1} - \rho_{\alpha+1}), \qquad \alpha = A, B, C. \tag{2.9}$$

These are to be solved subject to (2.7) (written in terms of ρ rather than n).

It follows from (2.9) that all relevant solutions satisfy

$$\prod_\alpha \rho_\alpha(x) = K \tag{2.10}$$

for some constant K with $0 < K \leq 1/27$. This may be seen directly, for example, by computing

$$\frac{d}{dx}\sum_\alpha \log \rho_\alpha = 0. \tag{2.11}$$

Now employing (2.7) and (2.10), we have that

$$(\rho_A - \rho_C)^2 = (\rho_A + \rho_C)^2 - 4\rho_A\rho_B \tag{2.12}$$

$$= (1 - \rho_B)^2 - 4K/\rho_B. \tag{2.13}$$

This expression leads to a differential equation for $\rho_B(x)$ (and, with similar manipulations, for the other particle densities as well) which is independent of the other density profiles. For $K = 1/27$ the solutions are constant, with value $1/3$; for $K < 1/27$ they have the form

$$\rho_\alpha(x) = y_K(2\beta(x - 1/2) + t_\alpha), \qquad 0 \leq x \leq 1, \tag{2.14}$$

with $y_K(t)$ a solution, periodic with period τ_K, of the equation

$$\frac{1}{2}y'^2 + \frac{1}{2}Ky - \frac{1}{8}y^2(1 - y)^2 = 0; \tag{2.15}$$

here $t = 2\beta x + \text{constant}$. y_K is uniquely specified by requiring that it take on its minimum value at the points $t = n\tau_K$, $n \in \mathbb{Z}$. The phase shifts t_α in (2.14) satisfy

$$t_A = t_B + \tau_K/3 \qquad \text{and} \qquad t_C = t_B - \tau_K/3. \tag{2.16}$$

Remark 2.2.1. Equation (2.15) describes a particle of unit mass and zero energy oscillating in a potential $U_K(y) = Ky/2 - y^2(1 - y)^2/8$. The constant solution $y = 1/3$

appears for $K = 1/27$. For $K < 1/27$, $y_K(t)$ is an even function which is strictly increasing on the interval $[0, \tau_K/2]$; it was shown in [5] that τ_K is a strictly decreasing function of K. Because the potential is quartic in y the solution is an elliptic function. Further properties of the function y_K are summarized in Proposition A.1.1 of Appendix A.1.

Equation (2.14) indicates that nonconstant solutions of the ELE are obtained by viewing $y_K(t)$, and its translates by one-third and two-thirds of a period, in some "window" of length 2β. If one is given β and $r = (r_A, r_B, r_C)$ then one must determine K and one of the phase shifts, say t_B, so that

$$r_\alpha = \frac{1}{2\beta} \int_{-\beta}^{\beta} y_K(t + t_\alpha)\, dt, \qquad \alpha = A, B, C. \tag{2.17}$$

The solutions which minimize $\mathcal{F}$ were completely determined in [5]. In stating the result, we use the following terminology: a solution is *of type n* if $(n-1)\tau_K < 2\beta \leq n\tau_K$, that is, if the window contains more than $n-1$ and at most n periods of the function y_K.

Theorem 2.2.2. *Suppose that r_A, r_B, and r_C are strictly positive. Then:*

(a) If $r_A = r_B = r_C = 1/3$ then for the equations (2.9) *with* (2.7) *there exist (i) the constant solution, (ii) for $\beta > n\beta_c = 2\pi n\sqrt{3}$, $n = 1, 2, \ldots$, a family of solutions, of period $\tau_K = 2\beta/n$ and hence of type n, differing by translation, and (iii) no other solutions. The minimizers of the free energy are, for $\beta \leq \beta_c$, the (unique) constant solution and, for $\beta > \beta_c$, any type 1 solution.*

(b) For values of r other than $(1/3, 1/3, 1/3)$ there exists for all β a unique type 1 solution of these equations which is a minimizer of the free energy.

(c) At zero temperature ($\beta \to \infty$) the system segregates into either three or four blocks, each containing particles of only one type.

2.3 Dynamics of the grand canonical ABC model

We now turn to consideration of the ABC model on the interval when the number of particles can fluctuate; we will abbreviate this as the GCABC model. In Section 1 the corresponding grand canonical measure $\mu_{\beta,\lambda}$ (see (2.2)) was presented in the equilibrium

setting as a Gibbs measure obtained from the energy function (2.1) and chemical potentials $\beta^{-1}\lambda_\alpha$. Just as for the canonical Gibbs measure, however, one may alternatively view this as the stationary measure for some dynamics; we describe two possibilities here.

In the first dynamics we consider there are particle exchanges between adjacent sites, with the same rates as for the canonical dynamics. To allow the number of particles to fluctuate, however, we introduce two new possible transitions. First, if the particle at site $i = 1$ is of type α then with a rate equal to $Ce^{-\lambda_\alpha}$ the entire configuration is translated by one site to the left, the particle at site $i = 1$ disappears, and a particle of species $\alpha + 1$ is created at site $i = N$. Second, with a rate equal to $Ce^{-\lambda_{\alpha+1}}$ the reverse transition occurs. Here C is a constant which we shall in the future take equal to 1. This dynamics satisfies the detailed balance condition with respect to the Gibbs measure (2.2): if a transition $\underline{\zeta} \to \underline{\zeta}'$ arises from an exchange of particles the argument is as for the canonical model [5], while if it comes from a transition of the new type, say in the "forward" direction as described above, then $E_N(\underline{\zeta}) = E_N(\underline{\zeta}')$ but N_α decreases by 1 and $N_{\alpha+1}$ increases by 1, and the detailed balance condition $e^{-\lambda_\alpha}\nu_\beta(\underline{\zeta}) = e^{-\lambda_{\alpha+1}}\nu_\beta(\underline{\zeta}')$ follows.

Remark 2.3.1. One may also obtain this dynamics by considering a ring of N sites, with each site occupied by an A, B, or C particle and with a marker located on one of the bonds between adjacent sites. Adjacent particles exchange across any unmarked bond with the usual ABC rates, while the marker may move one bond to its left or right, and in doing so it changes the species of the particle it passes: with $\nsim$ and — denoting a marked and unmarked bond, respectively, the transition $\nsim\ \alpha\ — \ \to\ — \ (\alpha+1)\ \nsim$ occurs with a rate equal to $e^{-\lambda_\alpha}$ and the reverse transition with a rate equal to $e^{-\lambda_{\alpha+1}}$. If one then obtains a configuration on the interval from a ring configuration by letting the marked bond identify the boundaries of the interval—effectively by cutting the ring at the marked bond—one sees easily that the inherited dynamics on the interval is precisely the dynamics discussed above. A slight variation of this idea was mentioned in [5].

We define the second dynamics only for the case in which all the λ_α are equal. We obtain it by first defining a dynamics for the *constrained ring:* a ring of $3N$ sites populated by A, B, and C particles but with a restriction to configurations $(\xi_i)_{i=1}^{3N}$ which satisfy

$$\xi_{i+N} = \xi_i + 1 \tag{2.18}$$

(addition on the site index is modulo $3N$); that is, if an A particle is on site i then there must be a B particle at site $i+N$ and a C particle at site $i+2N$, etc. The dynamics for the constrained ring is given by a modification of the usual rules of the canonical ABC model on a ring: exchanges occur simultaneously across three equally spaced, unmarked bonds in the usual ABC manner, with rate 1 for the favored exchanges and rate $q = e^{-\beta/N}$ for the unfavored ones.

We consider now any fixed block of N consecutive sites on the constrained ring and ask for the induced dynamics on configurations in this block. Two types of transitions occur: nearest-neighbor exchanges at standard ABC rates for a system of size N and inverse temperature β (i.e., rates 1 and $q = e^{-\beta/N}$) and a transition corresponding to an exchange on the constrained ring across the boundaries of the block. To understand the latter, suppose the configuration within the block has the form $(\alpha+2)\,\underline{\zeta}\,(\alpha+1)$, with $\underline{\zeta}$ any configuration on $N-2$ sites; then (2.18) implies that the particles immediately to the left and right of the block are of type α, and a transition from $(\alpha+2)\,\underline{\zeta}\,(\alpha+1)$ to $\alpha\,\underline{\zeta}\,\alpha$ occurs at rate 1. The reverse transition occurs at rate q, and no such transition occurs when the block configuration is $(\alpha+2)\,\underline{\zeta}\,\alpha$. Then using $\lambda_A = \lambda_B = \lambda_C$ one checks, just as for the dynamics considered above, that if one identifies the block with an interval of N sites then this dynamics satisfies the detailed balance condition with respect to the grand canonical Gibbs measure (2.2).

On the constrained ring there are equal numbers of A, B, and C particles, from (2.18), so that the energy E_{3N} (that is, the energy given by (2.1) with N replaced by $3N$ throughout), and thus the restriction of the Gibbs measure $Z^{-1}\exp\{-\beta E_{3N}\}$ to particle configurations satisfying (2.18), is well defined and independent of the starting point of the summations [33]. Moreover, this is the invariant measure for the constrained ring dynamics defined above, as one again checks by verifying detailed balance. With

the discussion above this shows that the restriction of $Z^{-1}\exp\{-\beta E_{3N}\}$ to the block of N sites is the Gibbs measure (2.2). One may also verify this from the fact that if $\underline{\xi}$ is a constrained ring configuration and $\underline{\zeta}$ the portion of that configuration within the block then

$$E_{3N}(\underline{\xi}) = E_N(\underline{\zeta}) + N/3. \tag{2.19}$$

Thus we can study the GCABC with $\lambda_A = \lambda_B = \lambda_C$ by studying directly the constrained ring.

2.3.1 The scaling limit for the constrained ring

To identify typical coarse-grained density profiles at large N on the constrained ring we consider the scaling limit (2.3) with N replaced by $3N$ ($N \to \infty$ with $i/3N \to x \in [0,1]$) and find the appropriate free energy functional. The scaling limit of the energy per site is still given by (2.5), but because the full microscopic configuration under the constraint (2.18) is determined by the configuration of the first N sites the entropy per unit site is only 1/3 of (2.6). This leads to a free energy functional

$$\beta\mathcal{E}(\{n\}) - \frac{1}{3}\mathcal{S}(\{n\}) = \frac{1}{3}\mathcal{F}^{(3\beta)}(\{n\}). \tag{2.20}$$

Here $\mathcal{E}(\{n\})$ and $\mathcal{S}(\{n\})$ are as in (2.5) and (2.6) and n is a constrained density profile, that is, one which satisfies the continuum equivalent of (2.18):

$$n_\alpha(x) = n_{\alpha+1}(x + 1/3), \tag{2.21}$$

where the addition $x + 1/3$ is taken modulo 1. $\mathcal{F}^{(3\beta)}$ is the free energy functional at temperature 3β of the (unconstrained) canonical system on an interval, as defined in (2.6); equivalently, because there are equal numbers of particles of each species, this is the free energy functional on a ring [5].

Typical (coarse-grained) profiles at inverse temperature β on the constrained ring, for large N, correspond then to continuum density profiles $\rho(x)$ which satisfy the constraint (2.21) and minimize the free energy over all such constrained profiles. It follows from (2.14) and (2.16), however, that the typical profiles (minimizers) for the canonical free energy, which are a priori unconstrained, do in fact satisfy (2.21). Thus by

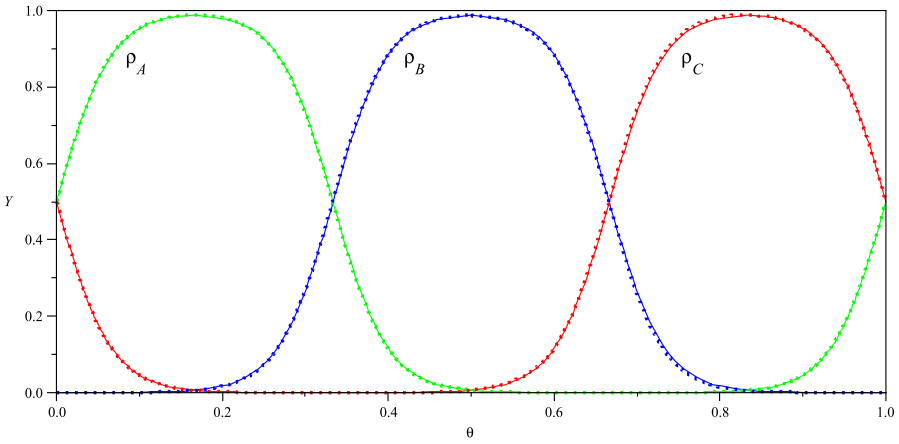

Figure 2.1: Typical profiles in a large system. The dotted curves are time-averaged occupation numbers in a constrained ring of size $N = 1800$ at inverse temperature $\beta = 10.152$. The solid curves are the corresponding elliptic functions obtained from the exact solution of [5] at temperature $\beta = 30.456$.

(2.20) the typical profiles for the constrained ring are the same as the typical profiles of an unconstrained system on the ring at inverse temperature 3β. This is illustrated in Figure 2.1, where we plot time-averaged profiles from Monte-Carlo simulations of the constrained ring at $\beta = 10.152$ and the exact solution [5] for the unconstrained ring at $\beta = 30.456$, showing close agreement. (We can use time averaging rather than spatial coarse graining for this comparison because the time scale for the profile to drift around the ring is much larger than the simulation time scale.)

It follows from this discussion that when the chemical potentials are equal the critical temperature $\hat{\beta}_c$ for the grand canonical ensemble on an interval, which is represented by the part of the constrained ring between two markers, is $\hat{\beta}_c = \beta_c/3$. Typical configurations are constant if $\beta < \hat{\beta}_c$ and for $\beta > \hat{\beta}_c$ are a portion of the typical profile for the canonical system at inverse temperature 3β; the latter is periodic and in the GCABC system we see a randomly-selected one-third of a period (for example, at $\beta = 10.152$, one third of the profile shown in Figure 2.1), rescaled to length one. These properties are confirmed in Section 2.4 by direct analysis of the grand canonical system in the scaling limit.

2.4 The phase diagram of the GCABC model

In this section we discuss the GCABC model directly in the scaling limit (2.3). From (2.2) we see that the new free energy functional $\hat{\mathcal{F}}(\{n\})\,\big(=\hat{\mathcal{F}}_{\beta,\lambda}(\{n\})\big)$, which is the negative of the pressure multiplied by β, is obtained by adding chemical potential terms to the free energy functional of the canonical model:

$$\hat{\mathcal{F}}(\{n\}) = \mathcal{F}(\{n\}) - \sum_\alpha \lambda_\alpha \int_0^1 dx\, n_\alpha(x), \tag{2.22}$$

with $\mathcal{F}$ given by (2.4). The profiles now are constrained only by

$$0 \le n_\alpha(x) \le 1 \quad \text{and} \quad \sum_\alpha n_\alpha(x) = 1. \tag{2.23}$$

We will always normalize the chemical potentials so that $\sum_\alpha \lambda_\alpha = 0$. This choice is arbitrary, since adding the same constant to each λ_α just shifts the free energy by a constant; our choice is convenient in most cases, although with this normalization we cannot conveniently consider the limit in which just one of the λ_α becomes infinite.

Just as for the canonical model [5] it can be shown on general grounds that for every β, λ the free energy functional has at least one minimizing profile $\rho(x)$ which belongs to the interior of the constraint region, i.e., satisfies $0 < \rho_\alpha(x) < 1$ for all α, x (and of course $\sum_\alpha \rho_\alpha(x) = 1$ for all x). From this it follows that $\rho(x)$ will satisfy

$$\frac{\delta}{\delta\rho_A(x)}\left[\hat{\mathcal{F}}(\{\rho\})\Big|_{\rho_C=1-\rho_A-\rho_B}\right] = (\mathcal{F}_A(x) - \lambda_A) - (\mathcal{F}_C(x) - \lambda_C) = 0, \tag{2.24}$$

$$\frac{\delta}{\delta\rho_B(x)}\left[\hat{\mathcal{F}}(\{\rho\})\Big|_{\rho_C=1-\rho_A-\rho_B}\right] = (\mathcal{F}_B(x) - \lambda_B) - (\mathcal{F}_C(x) - \lambda_C) = 0, \tag{2.25}$$

with $\mathcal{F}_\alpha(x)$ as in (2.8), so that $\mathcal{F}_\alpha(x) - \lambda_\alpha$ is independent of α. But one finds from (2.8) that $\sum_\alpha \rho_\alpha \partial\mathcal{F}_\alpha(x)/\partial x = 0$, so that

$$\mathcal{F}_\alpha(x) - \lambda_\alpha = C \tag{2.26}$$

for some C independent of x and α. Differentiating (2.26) leads again to (2.9):

$$\frac{d\rho_\alpha}{dx} = \beta\rho_\alpha(\rho_{\alpha-1} - \rho_{\alpha+1}), \qquad \alpha = A, B, C. \tag{2.27}$$

Moreover, (2.26) implies that $\mathcal{F}_\alpha(0) - \lambda_\alpha = \mathcal{F}_{\alpha+1}(1) - \lambda_{\alpha+1}$, which with (2.8) yields the boundary condition

$$\rho_\alpha(0)e^{-\lambda_\alpha} = \rho_{\alpha+1}(1)e^{-\lambda_{\alpha+1}}, \qquad \alpha = A, B, C. \tag{2.28}$$

Note that (2.28) is consistent with the (first) dynamics described in Section 2.3.

Equations (2.27) and (2.28) may be taken as the ELE of the model (it is easy to verify that these imply (2.26)). Solutions of (2.27) are, by the analysis of [5], of the form (2.14), with phase shifts satisfying (2.16). It remains only to consider the effect of the boundary condition (2.28).

Let us begin by considering the case $\lambda_A = \lambda_B = \lambda_C$, in which (2.28) becomes $\rho_\alpha(0) = \rho_{\alpha+1}(1)$. Certainly the constant profile with $\rho_\alpha(x) = 1/3$ for all α, x satisfies this condition and hence is a solution for all β. From (2.16) we see that a nonconstant solution (2.14) will satisfy this condition if and only if

$$y_K(t_\alpha - \beta) = y_K(t_\alpha + \beta - \tau_K/3), \qquad \alpha = A, B, C. \tag{2.29}$$

The properties of y_K mentioned in Remark 2.2.1 imply that (2.29) can hold if and only if $(t_\alpha - \beta) \pm (t_\alpha + \beta - \tau_K/3)$ is an integer multiple of τ_K. The choice of the positive sign here leads to no solutions consistent with (2.16); the negative sign gives $2\beta = (3n-2)\tau_K/3$ for $n = 1, 2, 3, \ldots$. Since the minimal period of solutions of (2.9) is $2\beta_c = 4\pi\sqrt{3}$, a nonconstant solution of (2.9) and (2.28) can exist only if $\beta > \beta_c/3$; thus as in Section 2.3 we find that $\hat{\beta}_c = \beta_c/3$ is the critical inverse temperature for the GCABC model. There is no constraint on the t_α other than (2.16), so that there is a one-parameter family of solutions differing by translation.

Following the usage of [5] it is natural to refer to the solutions just discussed for which $2\beta = (3n-2)\tau_K/3$ as being of *type* n. We will, again as in [5], extend this classification to the case of general λ: a solution (2.14) of (2.27) and (2.28) will be said to be *of type* 1 if $2\beta \le \tau_K/3$ and *of type* n, $n = 2, 3, \ldots$, if $(3n-5)\tau_K/3 < 2\beta \le (3n-2)\tau_K/3$. With this terminology we can state our main result.

Theorem 2.4.1. *(a) If $\lambda_A = \lambda_B = \lambda_C$ then for the equations* (2.27) *and* (2.28) *there exist (i) the constant solution, (ii) for $\beta > (n-2/3)\beta_c = 2\pi(n-2/3)\sqrt{3}$, $n = 1, 2, 3, \ldots$, a family of solutions of type n, differing by translation, and (iii) no other solutions. The minimizers of the free energy functional $\hat{\mathcal{F}}$ are, for $\beta \le \beta_c/3$, the (unique) constant solution and, for $\beta > \beta_c$, any type 1 solution.*

(b) If not all λ_α are equal then there exists for all β a unique minimizer of the free energy

functional $\hat{\mathcal{F}}$; moreover, this minimizer is a type 1 solution of (2.27) *and* (2.28).

We give the proof of part (a) of this theorem here; the more technical proof of (b) is presented in Appendix A.1.

Proof of Theorem 2.4.1(a): The discussion at the beginning of this section establishes the first statement of the theorem; it remains to show that the type 1 solution, when it exists, minimizes the free energy. We do so by reducing this problem to the corresponding one for the canonical ensemble; the argument is similar to the consideration of the constrained ring system in Section 2.3. For any profile $n(x) = (n_A(x), n_B(x), n_C(x))$ (where it is understood that $0 \le n_\alpha(x) \le 1$ and $\sum_\alpha n_\alpha(x) = 1$) define the *tripled* profile $\Theta(\{n\})$ by

$$(\Theta(\{n\}))_\alpha(x) = \begin{cases} n_\alpha(3x), & \text{if } 0 \le x < 1/3, \\ n_{\alpha-1}(3x-1), & \text{if } 1/3 \le x < 2/3, \\ n_{\alpha-2}(3x-2), & \text{if } 2/3 \le x < 1. \end{cases} \tag{2.30}$$

The profiles which have the form $\Theta(\{n\})$ for some n are precisely those satisfying (2.21); in particular, each $\Theta(\{n\})$ gives equal mean densities to the three species.

Now a simple computation shows that for any profile $\{n_\alpha(x)\}$,

$$\mathcal{F}^{(\beta)}(\{n\}) = \mathcal{F}^{(3\beta)}(\{\Theta(\{n\})\}) - \beta/3. \tag{2.31}$$

(Note that this free energy differs by an overall factor, plus an additive constant, from that of (2.20); the difference arises because here we started from the energy and entropy per site on the interval of size N, and in (2.20) from the energy and entropy per site on the ring of size $3N$.) Thus the problem of finding the minimizer(s) of $\hat{\mathcal{F}}^{(\beta,0)}(\{n\}) = \mathcal{F}^{(\beta)}(\{n\})$ over all profiles n is equivalent to finding the minimizer(s) of $\mathcal{F}^{(3\beta)}(\{n\})$ over all profiles satisfying (2.21). On the other hand, the minimizers of $\mathcal{F}^{(3\beta)}$ over all equal-density profiles are given in Theorem 2.2.2(a): the constant solution if $3\beta \le \beta_c$ and the solution of (minimal) period 6β if $3\beta > \beta_c$ (this is the type 1 solution for the canonical model). Because these are either constant or periodic, they satisfy (2.21) and hence are also the minimizers over all such profiles. But these minimizers are precisely the images under Θ of the profiles identified as minimizers in Theorem 2.4.1(a). □

Remark 2.4.2. In the argument above the essential role of the tripling map Θ is to convert the problem of minimizing $\hat{\mathcal{F}}$ with respect to arbitrary variations in the profiles to the previously solved problem of minimizing under variations which preserve the condition $\int_0^1 dx\, n_\alpha(x) = 1/3$. Other conclusions may be obtained similarly; we mention briefly two examples.

(a) It was shown in [5] that, for $\beta < (2/3\sqrt{3})\beta_c$ and any $r = (r_A, r_B, r_C)$, $\mathcal{F}(\{n\})$ is convex as a functional of profiles satisfying (2.7). Via Θ this implies that $\hat{\mathcal{F}}(\{n\})$ is, for $\beta < (2/3\sqrt{3})\hat{\beta}_c$, convex as a function of profiles satisfying (2.23).

(b) The two point correlation functions on the interval are related to those on the constrained ring by

$$\langle n(x)n(y)\rangle_{\text{interval}} = \langle n(x/3)n(y/3)\rangle_{\text{ring}}. \tag{2.32}$$

The latter (denoted below simply as $\langle\cdot\rangle$) may be computed in the high temperature phase by a calculation parallel to that of [11]. On the constrained ring a perturbation $n_\alpha(x) = 1/3 + a_\alpha \cos(2\pi m x) + b_\alpha \sin(2\pi m x)$ of the constant solution satisfies (2.21) and $\sum_\alpha n_\alpha(x) = 1$ if and only if $m = 3k + j$ for $j = 1$ or 2, and

$$a_{\alpha+1} = -\frac{1}{2}a_\alpha + (-1)^j \frac{\sqrt{3}}{2} b_\alpha, \qquad b_{\alpha+1} = -\frac{1}{2}b_\alpha - (-1)^j \frac{\sqrt{3}}{2} a_\alpha. \tag{2.33}$$

One may thus treat a_A and b_A as the independent parameters. The probability of the profile $\{n_\alpha(x)\}$ is $\exp\{-3N\mathcal{F}^{(3\beta)}(\{n\})\}$, and to quadratic order in the perturbation,

$$\mathcal{F}^{(3\beta)}(\{n\}) \simeq \text{constant} + \frac{9}{8\pi m}\left[2\pi m + (-1)^j\sqrt{3}\beta\right]\left(a_A^2 + b_A^2\right). \tag{2.34}$$

Thus

$$\langle a_A^2\rangle = \langle b_A^2\rangle = \frac{4\pi m}{27N(2\pi m + (-1)^j\sqrt{3}\beta)}, \qquad \langle a_A b_A\rangle = 0. \tag{2.35}$$

Summing over all the fluctuations, i.e., over m, we obtain

$$\langle n_\alpha(x)n_\alpha(y)\rangle_c \;=\; \frac{4\pi}{27N}\sum_{k=0}^{\infty}\sum_{j=1}^{2}\frac{m\cos[2\pi m(x-y)]}{2\pi m + (-1)^j\sqrt{3}\beta}\Bigg|_{m=3k+j}. \tag{2.36}$$

All connected two-point functions $\langle n_\alpha(x)n_\gamma(y)\rangle_c$ may be obtained on the constrained ring from (2.36) via (2.21), and then on the interval using (2.32). Note that (2.36) diverges as $\beta \nearrow \hat{\beta}_c$.

2.4.1 The canonical free energy $F(r)$

The free energy in the canonical model, for mean densities r_A, r_B, r_C satisfying $r_A + r_B + r_C = 1$, is given by

$$F(r) = F(r_A, r_B, r_C) = \min_{\{n(x)\}} \mathcal{F}(\{n(x)\}), \tag{2.37}$$

with the minimum taken over all profiles $n(x)$ satisfying the constraints (2.7). The grand canonical free energy may then be computed in two ways:

$$\hat{F}(\lambda) = \inf_{\{n(x)\}} \hat{\mathcal{F}}(\{n\}) \tag{2.38}$$

$$= \inf_{\sum_\alpha r_\alpha = 1 r_\alpha \geq 0} \left\{ F(r) - \sum_\alpha \lambda_\alpha r_\alpha \right\}, \tag{2.39}$$

where the infimum in (2.38) is over all profiles. We can obtain information on the structure of $F(r)$ from the above results for the minimization problem (2.38), together with the trivial remarks that a unique minimum for (2.38) implies a unique minimum for (2.39) and that such a unique minimum implies that the surface $y = F(r)$ lies above the plane $y = \hat{F}(\lambda) + \sum_\alpha \lambda_\alpha r_\alpha$ and touches it at a single point.

In particular, the fact that when $\beta \leq \hat{\beta}_c$ there is for all λ a unique minimizer for (2.38) implies that for such β the function $F(r)$ is convex. When $\beta > \hat{\beta}_c$ the minimizer for (2.38) is unique except in the case $\lambda_A = \lambda_B = \lambda_C = 0$, when the plane mentioned above is horizontal. In that case the minimum occurs at points lying above a certain simple closed curve $\Gamma\,(= \Gamma_\beta)$ in the plane $\sum_\alpha r_\alpha = 1$, with the point $r_A = r_B = r_C = 1/3$ in its interior; sample curves are shown in Figure 2.2. Γ may be parametrized as $r^*(t)$, $0 \leq t \leq \tau_K$, where K is the parameter in the type 1 solution of Theorem 2.4.1(a) and

$$r^*_\alpha(t) = \frac{3}{\tau_K} \int_{-\tau_K/6}^{\tau_K/6} y_K(s + t_\alpha + t)\, ds. \tag{2.40}$$

(The fact that this curve is simple follows, for example, from Proposition A.1.1(d).) The three-fold symmetry then implies that the surface $y = F(r)$ has a "tricorn" shape.

In particular, the dependence of the mean densities on the chemical potentials is given by

$$r_\alpha(\lambda) = \frac{\partial}{\partial \lambda_\alpha} \hat{F}(\lambda). \tag{2.41}$$

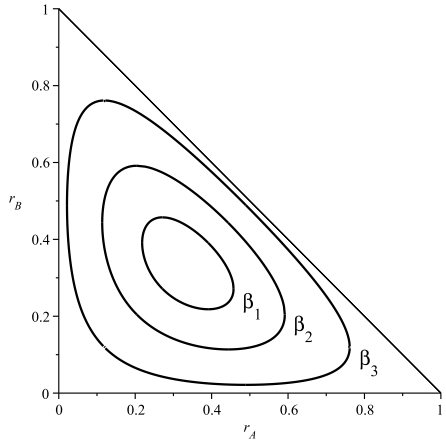

Figure 2.2: Curves Γ_β in the r_A-r_B plane along which $F(r)$ achieves its minimum value, for $\beta_1 = 3.75$, $\beta_2 = 4.25$, and $\beta_3 = 6.05$ ($\hat{\beta}_c = 2\pi/\sqrt{3} \simeq 3.63$).

Remark 2.4.3. It follows from (2.39) that the dependence of the mean densities on the chemical potentials is given by

$$r_\alpha(\lambda) = \frac{\partial}{\partial \lambda_\alpha} \hat{F}(\lambda). \tag{2.42}$$

The minimizing profile for a particular value of λ will be the canonical profile at the value of r determined by (2.42). As discussed in [5] this will be a fraction of a full period of some non-constant period solution of the ELE; see Figure 2.1 above and Figure 4 of [5].

2.5 Concluding remarks

It is natural to compare the phase diagram obtained here for the one dimensional reflection asymmetric ABC model with that of the corresponding symmetric model, that is, the mean field three state Potts model (see [61],[42]). We will define the latter by replacing the sum over $j > i$ in (2.1) by a sum over all $j \neq i$ and dividing by 2; this yields

$$E_N^*(\underline{\zeta}) = \frac{1}{2N}[N_A N_C + N_C N_B + N_B N_A] = \frac{1}{4N}[N^2 - (N_A^2 + N_B^2 + N_C^2)]. \tag{2.43}$$

The energy (2.43) is related to that of the standard mean field Potts model [42] by a choice of energy scale and a shift of the ground state energy. It is, as is usual for mean

field models, independent of dimension and geometry. There is thus no spatial structure in the system and the canonical measure just gives equal weights to all configurations.

The canonical free energy functional with prescribed values of $r_\alpha = \int_0^1 n_\alpha(x)\,dx$ is

$$\mathcal{F}^*(\{n\}) = \frac{\beta}{2}[r_A r_C + r_B r_A + r_C r_B] - \mathcal{S}(\{n\}), \tag{2.44}$$

with $\mathcal{S}(\{n\})$ still given by (2.6). For all β the minimizers of $\mathcal{F}^*$ are the constant density profiles $\rho_\alpha(x) = r_\alpha$, and there are no phase transitions of any kind in the canonical system. The corresponding minimum value

$$F^*(r) = \frac{\beta}{2}\sum_\alpha r_\alpha r_{\alpha+2} - \sum_\alpha r_\alpha \log r_\alpha = \frac{\beta}{4}\sum_\alpha r_\alpha^2 + \frac{\beta}{4} - \sum_\alpha r_\alpha \log r_\alpha \tag{2.45}$$

of $\mathcal{F}^*(\{n\})$ is in fact just the value of $\mathcal{F}(\{n\})$ evaluated at these constant profiles (this follows from our choice of the factor $1/2$ in (2.43)), and hence is an upper bound for the free energy $F(r)$ of (2.37).

The situation is quite different for the grand canonical ensemble. Here the analogue of (2.38) is

$$\hat{F}^*(\lambda) = \inf_r \Big\{ F^*(r) - \sum_\alpha \lambda_\alpha r_\alpha \Big\} \tag{2.46}$$

The analysis of $F^*(\lambda)$ leads to a phase diagram completely different from that of the reflection asymmetric grand canonical model considered in Sections 3 and 4 above [61]. In particular, (2.46) exhibits a first order phase transition for $\lambda_A = \lambda_B = \lambda_C$ at $\beta_c^* = 8\log 2$. For $\beta < \beta_c^*$ the minimizer is $r_A = r_B = r_C = 1/3$; for $\beta > \beta_c^*$ there are three minimizers, each rich in one of the three species, and at $\beta = \beta_c^*$ all four of these states are minimizers.

2.5.1 Higher dimensions

As was already noted and is well known, the standard mean field models with symmetric interactions do not depend on the dimension or topology of the spatial structure of the system considered. This is clearly not the case for models with reflection asymmetric interactions, such as the one-dimensional ABC model considered here. We comment now on various possible generalizations of such reflection asymmetric mean field models to higher dimensions. A generalization of the ABC model from the ring to to the torus

in two or more dimensions was considered in [31]; in that case the ABC dynamics were generalized to higher dimensions but the resulting model is not an equilibrium system, in contrast to the models considered below.

We take for simplicity the dimension to be two and the lattice to be an $N \times N$ square in $\mathbb{Z}^2$. Let us consider first a situation in which the mean field interactions are symmetric in the vertical direction but of the form (2.1) in the horizontal direction. This yields an energy of the form

$$\tilde{E}(\underline{\zeta}) = \frac{1}{N^2} \sum_{k,l}^{N} \sum_{i=1}^{N-1} \sum_{j=i+1}^{N} \sum_{\alpha} \eta_\alpha(i,k)\eta_{\alpha+2}(j,l) \tag{2.47}$$

$$= \sum_{i=1}^{N-1} \sum_{j=i+1}^{N} \sum_{\alpha} \tilde{\eta}_\alpha(i)\tilde{\eta}_{\alpha+2}(j), \tag{2.48}$$

where

$$\tilde{\eta}_\alpha(i) = \frac{1}{N} \sum_{k=1}^{N} \eta_\alpha(i,k). \tag{2.49}$$

The energy functional $\tilde{\mathcal{E}}$ obtained from (2.48) in the scaling limit is identical to that given in (2.5) with $n_\alpha(x)$ replaced by $\tilde{n}_\alpha(x) = \int_0^1 n(x,y)\,dy$. The entropy term (compare (2.6)),

$$-\tilde{\mathcal{S}} = \sum_{\alpha} \int_0^1 \int_0^1 n_\alpha(x,y) \log n_\alpha(x,y)\,dx\,dy, \tag{2.50}$$

is clearly minimized, subject to a specified $\{\tilde{n}_\alpha(x)\}$, by setting $n_\alpha(x,y) = \tilde{n}_\alpha(x)$, and so density profiles which minimize $\beta\tilde{\mathcal{E}} - \tilde{\mathcal{S}}$ depend only on x and are the same as for the one dimensional case, both for the canonical and grand canonical ensembles.

Remark 2.5.1. The two-dimensional chiral clock model [3, 29, 46] also contains interactions—in that case, nearest-neighbor ones—which are reflection symmetric in the vertical direction but not in the horizontal one. When the parameter Δ (in the notation of [46]) has value $1/2$ the energy, up to an additive constant and a rescaling, is

$$\sum_{i=1}^{N-1} \sum_{k=1}^{N} \sum_{\alpha} \eta_\alpha(i,k)\eta_{\alpha+2}(i+1,k) - \sum_{i=1}^{N} \sum_{k=1}^{N-1} \sum_{\alpha} \eta_\alpha(i,k)\eta_\alpha(i,k+1), \tag{2.51}$$

so that the interactions in the horizontal direction have a form reminiscent of (2.1).

A second possibility is to take the reflection asymmetry to be the same in the x and

y directions. In this case (2.1) takes the form

$$E_{N^2}(\underline{\zeta}) = \frac{1}{N^2} \sum_{\alpha} \sum_{i,k=1}^{N-1} \sum_{j=i+1 l=k+1}^{N} \eta_{\alpha}(i,k)\eta_{\alpha+2}(j,l). \tag{2.52}$$

The analysis of this model seems considerably more complicated and we will attempt no discussion here.

Chapter 3

A generalized ABC model

3.1 Introduction

The standard ABC model on an interval was considered in [5], and reviewed briefly in Chapter 2. It is an equilibrium system on a $1D$ lattice of N sites with closed boundary conditions. Each site is occupied by one of three types of particles, denoted by A, B, and C, which interact via a cyclic mean field type pair potential which is however not spatially reflection symmetric. In this chapter we generalize this model by introducing an additional interaction in which each of the particle types moves in a separate background potential that depends linearly on position, breaking the cyclic symmetry in the standard ABC model. The equilibrium state of the standard ABC model may also be obtained as the steady state for certain nearest neighbor exchange dynamics [5, 32, 33], and the generalized model considered here may be obtained by a modification of the exchange rates; see Appendix B.1 for details.

To define the model we introduce the occupation variables $\eta_\alpha(i)$, with $\eta_\alpha(i) = 1$ (0) if site i is (is not) occupied by a particle of type α. As each site is occupied by exactly one particle,

$$\sum_\alpha \eta_\alpha(i) = 1. \tag{3.1}$$

The energy of a configuration $\underline{\eta}$ is defined to be

$$E(\underline{\eta}) = \frac{1}{N} \sum_\alpha \sum_{i=1}^N \left(\sum_{j=1}^N \Theta(j-i) \eta_\alpha(i) \eta_{\alpha+2}(j) + i\, \xi_\alpha\, \eta_\alpha(i) \right), \tag{3.2}$$

Here $\alpha+1$ corresponds to the species following α in the ABC cyclic order, $\Theta(j-i) = 1$ (0) for $j > i$ ($j \leq i$), and the ξ_α may be thought of as constant background electric fields, with ξ_α acting on particles of type α. We will consider the model in the canonical

ensemble, with specified particle numbers of each type

$$\sum_{i=1}^{N} \eta_\alpha(i) = N_\alpha, \qquad \sum_\alpha N_\alpha = N. \tag{3.3}$$

The canonical Gibbs measure for this system is then given by

$$\mu_\beta(\underline{\eta}; N_\alpha) = \frac{1}{Z} e^{-\beta E(\underline{\eta})}, \tag{3.4}$$

with Z the usual canonical partition function. We will assume $N_\alpha > 0$ for all α throughout; if one of the particle species is absent, the model simply reduces to the weakly asymmetric simple exclusion process (WASEP) [10, 52].

Note that if one adds the same constant to each of the ξ_α then the energy (3.2) is only changed by an overall constant. We may therefore set $\sum_\alpha \xi_\alpha = 0$, without loss of generality. We will refer to the case where $\xi_A = \xi_B = \xi_C = 0$ as the "standard" ABC model. This is the model considered in [5].

The energy (3.2) may also be written in a different form, in which the contribution of the external fields is expressed through a modified mean field interaction. Using (3.1) and (3.3) we have

$$\begin{aligned} \sum_{i=1}^{N} i\, \eta_\alpha(i) = -\sum_{i=1}^{N}\sum_{j=1}^{N} \Theta(j-i)\eta_\alpha(i)\left(\eta_{\alpha+1}(j) + \eta_{\alpha+2}(j)\right) \\ + N_\alpha\left(N - \frac{N_\alpha}{2} + \frac{1}{2}\right). \end{aligned} \tag{3.5}$$

Substituting (3.5) in (3.2) and rearranging sums, we obtain

$$\begin{aligned} E(\underline{\eta}) = \frac{1}{N}\sum_\alpha \Bigg(\sum_{i=1}^{N}\sum_{j=1}^{N} \Theta(j-i)\, 3\, v_{\alpha+1}\, \eta_\alpha(i)\, \eta_{\alpha+2}(j) \\ + \xi_\alpha \frac{N_\alpha}{2}\left(N + N_{\alpha+2} - N_{\alpha+1} + 1\right) \Bigg), \end{aligned} \tag{3.6}$$

where the v_α are given by

$$v_\alpha = \frac{1}{3}\Big(1 + \xi_{\alpha+1} - \xi_{\alpha+2}\Big), \tag{3.7}$$

so that

$$\sum_\alpha v_\alpha = 1. \tag{3.8}$$

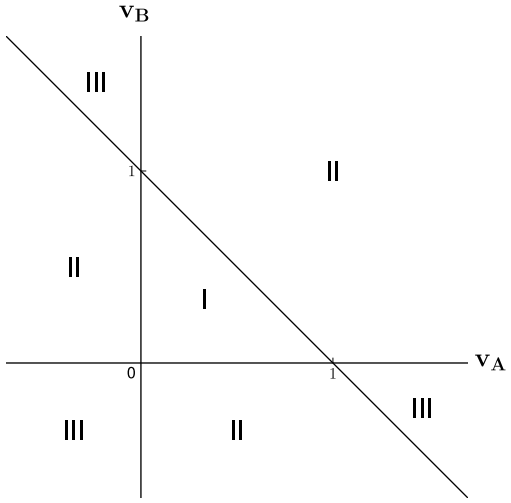

Figure 3.1: Different regions of the parameter space of the v_α, plotted in the v_A-v_B plane.

The term $\sum_\alpha \xi_\alpha \, N_\alpha \, (N + N_{\alpha+2} - N_{\alpha+1} + 1)/2$ is independent of the configuration, and may be ignored in the canonical ensemble with the N_α fixed.

It will be convenient to consider the fundamental parameters of the model, in addition to the particle numbers N_α of each species, to be the v_α rather than the fields ξ_α, as the v_α are more directly related to the physical behavior of the model. We divide the space of these parameters into three regions; see Figure 3.1, plotted in terms of v_A and v_B, as these fix v_C by (3.8). In region I, $v_\alpha > 0$ for all α. In regions II and III, $v_\alpha < 0$ for one or two values of α, respectively. In the standard model $v_A = v_B = v_C = 1/3$.

We see from (3.6) that each of the v_α determines the energetically preferred alignment of the two other particle species $\alpha \pm 1$. Effectively there is a contribution of $3\, v_\alpha/N$ to the energy every time any pair of particles of species $\alpha + 1$ and $\alpha + 2$ are not cyclically aligned, that is, whenever a particle of type $\alpha + 2$ precedes one of type $\alpha + 1$. If for example $v_A > 0$, a pair of B and C particles will have a lower energy arranged as $B \cdots C$ than as $C \cdots B$. If $v_A < 0$ the preferred arrangement is reversed, and the configuration $C \cdots B$ will have a lower energy than the usual cyclic ordering $B \cdots C$. This determines the ground states of the system, when $\beta \to \infty$, as described in Appendix B.1.

Background

The standard ABC model was introduced by Evans et al [32, 33] and in the form we use by Clincy et al [14]. This model was originally considered on the ring, i.e. with the boundary conditions periodic rather than closed, by specifying a dynamics consisting of asymmetric nearest neighbor exchanges between particles of different species. The stationary state of this dynamical system on the ring is generally not an equilibrium one. Its properties have been studied extensively in [32] and in [8, 9, 11, 26, 39]. In the special case that the number of particles of each species is the same the stationary state of the model defined on the ring is a canonical Gibbs measure with the energy given by (3.6), with $v_\alpha = 1/3$ for all α. The stationary state of the dynamical model defined on the interval, or equivalently on a ring with exchanges across one bond blocked, is always the canonical Gibbs measure regardless of the number of particles of each species and is identical to that on the ring for equal N_α.

The equilibrium properties of the standard ABC model on the interval were obtained exactly in [5], see also [7]. In particular it was shown there that (in the thermodynamic limit) the system has a unique state (density profiles) whenever the average densities $N_\alpha/N = r_\alpha$ are not all equal to 1/3, i.e. $r_\alpha \neq v_\alpha$ for some α. When $r_\alpha = 1/3$ the system undergoes a second order transition at $\beta = \beta_c = 2\pi\sqrt{3}$ from a uniform density profile to a periodic profile [11]. There are thus for $\beta > \beta_c$ a continuum of phases (density profiles) specified by a rotation angle θ. The results we derive here for the case when the v_α are not all equal to 1/3 are more restricted. They suggest however that the phase diagram for general v_α is qualitatively similar to that of the standard ABC model, with a phase transition only at $r_\alpha = v_\alpha$.

The outline of the rest of the chapter is as follows. In Section 3.2 we discuss general properties of the macroscopic system in the scaling limit. Section 3.3 describes basic properties of the solutions of the Euler-Lagrange equations. Special cases are considered in Sections 3.4 and 3.5 for different values of the parameters. In Appendix B.1 we discuss properties of the microscopic model specified by (3.2). Appendix B.2 discusses the connection between the generalized ABC model and the Lotka-Volterra family of ODE systems, and in Appendix B.3 we discuss some restrictions on solutions of the

Euler-Lagrange equations for the case $r_\alpha \neq v_\alpha$ for some α, with the v_α in region I.

3.2 Scaling limit

The main goal of this chapter is to study the phase diagram of the equilibrium system with energy (3.2) when N becomes macroscopic. For this we consider the scaling limit in which

$$N \to \infty, \qquad N_\alpha/N \to r_\alpha, \qquad i/N \to x \in [0,1], \tag{3.9}$$

so that r_α is the average density of the particle species α. In this limit the state of the system is described by density profiles $\rho_\alpha(x)$, $\alpha = A, B, C$, where $\rho_\alpha(x)$ represents the density of particles of type α at a position x. These density profiles satisfy the constraints

$$0 \leq \rho_\alpha(x) \leq 1, \qquad \int_0^1 \mathrm{d}x\, \rho_\alpha(x) = r_\alpha, \qquad \sum_\alpha \rho_\alpha(x) = 1. \tag{3.10}$$

The free energy (multiplied by β) $\mathcal{F}(\{\rho\})$ associated to the canonical ensemble measure (3.4), see [5, 8], is given by

$$\mathcal{F}(\{\rho\}) = \beta \mathcal{E}(\{\rho\}) - \mathcal{S}(\{\rho\}) \tag{3.11}$$

where $\mathcal{E}(\{\rho\})$ and $\mathcal{S}(\{\rho\})$ are the energy per site and entropy per site in the scaling limit:

$$\mathcal{E}(\{\rho\}) = \sum_\alpha \int_0^1 \mathrm{d}x \left(\int_0^1 \mathrm{d}y\, \Theta(y-x) \rho_\alpha(x) \rho_{\alpha+2}(y) + x\, \xi_\alpha\, \rho_\alpha(x) \right) \tag{3.12}$$

$$\mathcal{S}(\{\rho\}) = -\sum_\alpha \int_0^1 \mathrm{d}x\, \rho_\alpha(x) \log \rho_\alpha(x). \tag{3.13}$$

As in the microscopic case, we can use the constraints (3.10) to rewrite the free energy in a form analogous to (3.6),

$$\begin{aligned} \mathcal{F}(\{\rho\}) = \beta \sum_\alpha \int_0^1 \mathrm{d}x \int_0^1 \mathrm{d}y\, \Theta(y-x)\, 3\, v_{\alpha+1}\, \rho_\alpha(x) \rho_{\alpha+2}(y) \\ + \sum_\alpha \int_0^1 \mathrm{d}x\, \rho_\alpha(x) \log \rho_\alpha(x) + F, \end{aligned} \tag{3.14}$$

where the constant $F = \sum_\alpha \xi_\alpha r_\alpha (1 + r_{\alpha+2} - r_{\alpha+1})/2$ is independent of the profiles $\rho_\alpha(x)$.

The functional $\mathcal{F}(\{\rho\})$ is the large deviation functional giving probabilities in the $N \to \infty$ limit [5, 8, 14]; that is, the probability of the profile $\rho_\alpha(x)$ is proportional to $\exp\left(-N\mathcal{F}(\{\rho\})\right)$. The typical equilibrium density profiles for the macroscopic model are thus those that minimize the free energy. There will be a coexistence of phases when the minimizer is not unique. To study this we have to consider solutions of the Euler-Lagrange equations (ELE) associated to the stationary points of (3.11).

Let $\mathcal{F}_\alpha(x) = \delta\mathcal{F}/\delta\rho_\alpha(x)$ be the variational derivative of $\mathcal{F}$ taken as though all of the ρ_α are independent. Applying the constraints (3.10) leads to the ELE

$$\mathcal{F}_A - \mathcal{F}_C = \text{constant}, \qquad \mathcal{F}_B - \mathcal{F}_C = \text{constant}, \tag{3.15}$$

where the $\mathcal{F}_\alpha$ from (3.14) are

$$\begin{aligned}\mathcal{F}_\alpha(x) = 1 + \log\rho_\alpha(x) + 3\beta v_{\alpha+1} r_{\alpha+2} \\ -3\beta\int_0^x \mathrm{d}y\,(v_{\alpha+1}\rho_{\alpha+2}(y) - v_{\alpha+2}\rho_{\alpha+1}(y)).\end{aligned} \tag{3.16}$$

It is easy to show that these $\mathcal{F}_\alpha$ satisfy

$$\sum_\alpha \rho_\alpha(x)\frac{\partial\mathcal{F}_\alpha}{\partial x}(x) = 0, \tag{3.17}$$

which with (3.15) implies that $\mathcal{F}_\alpha(x)$ is constant for all α. Then from (3.16) the ELE are given by

$$\rho_\alpha(x) = \rho_\alpha(0)\exp\left(3\beta\int_0^x \mathrm{d}y\,(v_{\alpha+1}\rho_{\alpha+2}(y) - v_{\alpha+2}\rho_{\alpha+1}(y))\right), \tag{3.18}$$

which may be evaluated at $x = 1$ to yield the boundary conditions

$$\rho_\alpha(1) = \rho_\alpha(0)\, e^{3\beta(v_{\alpha+1}r_{\alpha+2} - v_{\alpha+2}r_{\alpha+1})}. \tag{3.19}$$

Equivalently, one may also write the ELE in differential form as

$$\frac{\mathrm{d}\rho_\alpha}{\mathrm{d}x} = 3\beta\rho_\alpha\left(v_{\alpha+1}\rho_{\alpha+2} - v_{\alpha+2}\rho_{\alpha+1}\right). \tag{3.20}$$

The ELE are to be solved subject to (3.10).

Examining the ELE (3.20) one finds that there exist two constants of the motion,

$$\sum_\alpha \rho_\alpha(x) = 1, \tag{3.21}$$

and

$$K = \prod_{\alpha} \rho_{\alpha}^{v_\alpha}(x). \tag{3.22}$$

To study solutions of the ELE we eliminate ρ_C using (3.21), so that the solutions give trajectories in the ρ_A-ρ_B plane, and more specifically in the triangle

$$\rho_A, \rho_B \geq 0, \qquad \rho_A + \rho_B \leq 1. \tag{3.23}$$

Any such trajectory lies within a level set of K; as we will see below, when the v_α lie in region I such a level set is either the single point $\rho_\alpha = v_\alpha$ or a simple closed curve encircling this point. When the v_α lie in regions II and III the level curve is an open curve joining two vertices of the triangle. A solution of the ELE satisfying the boundary conditions (3.19), or equivalently the constraint $\int_0^1 \rho_\alpha(x)\, dx = r_\alpha$, is obtained by choosing first a value of K and then a portion of the trajectory labeled by K which is traversed in time one. See Figures 3.2 and 3.3 for typical level sets and trajectories.

In the special case where $r_\alpha = v_\alpha$ the macroscopic free energy is rotation invariant (see Appendix B.1 for details on the analogous result for the microscopic system). To verify this we consider rotated profiles

$$\tilde{\rho}_\alpha(x) = \begin{cases} \rho_\alpha(x - z) & \text{if } x \geq z \\ \rho_\alpha(x + (1 - z)) & \text{if } x \leq z \end{cases}. \tag{3.24}$$

The entropy is clearly unchanged by the rotation, $\mathcal{S}(\{\tilde{\rho}\}) = \mathcal{S}(\{\rho\})$, while the difference in energy, computed from (3.14), is

$$\begin{aligned} \mathcal{E}(\{\tilde{\rho}\}) - \mathcal{E}(\{\rho\}) &= 3 \sum_{\alpha} \int_{1-z}^{1} \mathrm{d}x \int_{0}^{1-z} \mathrm{d}y \; v_{\alpha+1} \left(\rho_\alpha(x) \rho_{\alpha+2}(y) - \rho_\alpha(y) \rho_{\alpha+2}(x) \right) \\ &= 3 \sum_{\alpha} \int_{1-z}^{1} \mathrm{d}x \; v_{\alpha+1} \left(\rho_\alpha(x)\, r_{\alpha+2} - r_\alpha\, \rho_{\alpha+2}(x) \right) = 0, \end{aligned} \tag{3.25}$$

where we have used $r_\alpha = v_\alpha$ and $\int_0^1 \mathrm{d}x \; \rho_\alpha(x) = r_\alpha$. As we shall see this case, which generalizes the $r_\alpha = 1/3$ case in the standard ABC model, plays a special role in the phase diagram.

It was proven in [5, Section 10] for the standard ABC model that solutions of the ELE always exist, and that the minimizer of the free energy must be given by one of the solutions. The same result holds for the generalized ABC model, with no modification of

the proof required. The fundamental question is then whether or not there is a unique minimizer. This question was answered completely for the standard ABC model in [5], and we believe that the direct generalization of the behavior in that case should hold for the general model. We state this here as a conjecture, although it is partially established in [5] and in the remainder of this chapter; the statement depends upon a critical temperature $T_c = \beta_c^{-1}$, where

$$\beta_c = \frac{2\pi}{3\sqrt{v_A v_B v_C}}. \tag{3.26}$$

Conjecture 3.2.1. Solutions of the ELE. *(a) If the v_α lie in region I and $r_\alpha = v_\alpha$ for $\alpha = A, B, C$ then there exist (i) the constant solution $\rho_\alpha(x) = v_\alpha$, $0 \le x \le 1$, (ii) for $\beta > n\,\beta_c$, $n = 1, 2, \ldots$, a unique solution corresponding to a trajectory which traverses one of the level sets of K exactly n times, which we refer to as a type n solution, and (iii) no other solutions. The minimizer of the free energy is, for $\beta \le \beta_c$, the (unique) constant solution and, for $\beta > \beta_c$, the type 1 solution. At β_c there is a second order phase transition from the homogeneous phase to the phase segregated, heterogeneous phase.*

(b) For values of the v_α and r_α other than those discussed in (a) there exists for every β a unique solution minimizing the free energy.

Statement (a.i) here is a trivial observation, and the existence portion of (a.ii) will be established in Section 3.4. Beyond this, as we will discuss below, we can prove all or part of this conjecture for some special values of the parameters besides the standard case, $v_\alpha = 1/3$ for all α, for which the conjecture has been proven in full. In particular we can prove uniqueness of the solution of the ELE when $\beta < 4\pi/3$. This follows from the result in [5] that for such β the standard ABC model free energy functional is globally convex on the space of density functions satisfying (3.10). As the addition of external fields only adds terms that are linear in the particle densities to the standard ABC free energy (see (3.12)), the second variation of (3.11) with respect to the density functions is the same as that of the standard model. Thus for $\beta < 4\pi/3$ the free energy for the generalized ABC model with external fields is also globally convex, implying that there is a unique solution of the ELE, which must be the minimizer of the free

energy. For $r_\alpha = v_\alpha$ this is just the constant solution $\rho_\alpha(x) = v_\alpha$, $0 \le x \le 1$. For other values of the r_α there is for $\beta < 4\pi/3$ a unique segment of a unique $K = K(\beta; \underline{r})$ trajectory which minimizes $\mathcal{F}$.

For $\beta \ge 4\pi/3$ and $r_\alpha = v_\alpha$ (so that the v_α are in region I), we have the following additional results:

(i) Conjecture 3.2.1(a) is proven when, for some α, $v_\alpha = 1/2$ and $v_{\alpha+1} = v_{\alpha+2} = 1/4$, and checked numerically in other cases.

(ii) The constant solution is linearly stable for $\beta \le \beta_c$ and unstable for $\beta > \beta_c$.

(iii) Nonconstant minimizers are always of type 1.

(iv) For small enough K, or equivalently, for large enough β, the type 1 solution is unique for every β.

When $r_\alpha \ne v_\alpha$ for some α we prove uniqueness for the cases when one of the v_α is zero and the other two have opposite signs, and when one of the v_α is one.

In the next section we describe general properties of the solutions of the ELE. The case $r_\alpha = v_\alpha$ (with the v_α in region I) is discussed in detail in Section 3.4, while the special cases when $r_\alpha \ne v_\alpha$ are considered in Section 3.5.

3.3 General properties of solutions of the ELE

The trajectories of the densities $\rho_\alpha(x)$ that are solutions of the ELE may be obtained by studying the level sets of the constant of the motion K (3.22), as described in Section 3.2. To do this let us define a line in the ρ_A-ρ_B plane passing through the point (v_A, v_B) by setting

$$\rho_B = v_B + m\,(\rho_A - v_A)\,, \tag{3.27}$$

with m an arbitrary constant. The change in $\log K$ as ρ_A is varied along the line (3.27) can be manipulated using (3.10) to yield

$$\begin{aligned} \frac{\mathrm{d}\log K}{\mathrm{d}\rho_A} &= \left(\frac{v_A}{\rho_A} - \frac{v_C}{\rho_C}\right) + m\left(\frac{v_B}{\rho_B} - \frac{v_C}{\rho_C}\right) \\ &= \left[1 + \frac{\rho_A}{\rho_C}\left(m^2 + 2m + 1\right) + \frac{\rho_A}{\rho_B}m^2\right]\left(\frac{v_A}{\rho_A} - 1\right). \end{aligned} \tag{3.28}$$

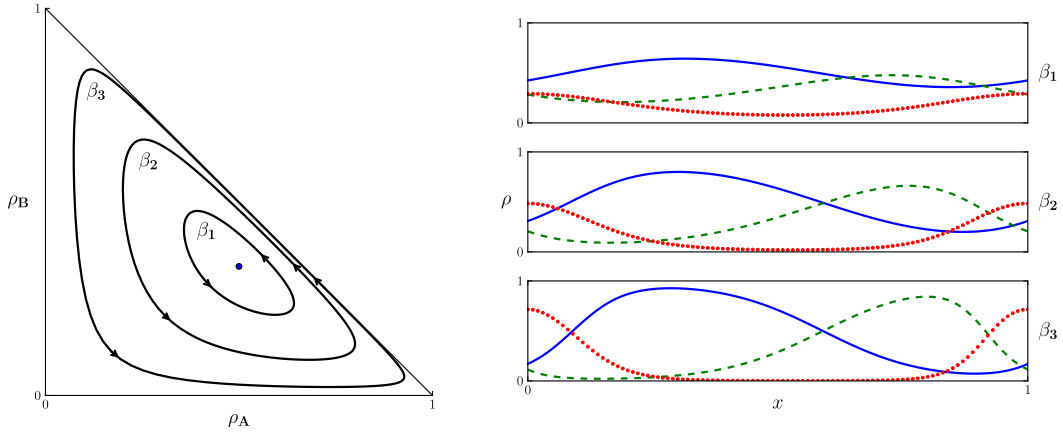

Figure 3.2: Plots of ρ_A (solid), ρ_B (dashed), and ρ_C (dotted) and their corresponding trajectories in the ρ_A-ρ_B plane. See description under Region I, Case 1.

Thus K is monotone increasing for $\rho_A < v_A$ and decreasing for $\rho_A > v_A$. A similar result holds for ρ_B and v_B. The shape of the level sets of K, and thus also the trajectories of the densities, depends upon which region the v_α lie in; compare Figures 3.2 and 3.3. We now give more details.

Region I

It follows from (3.28) that in region I K achieves its maximum value at the center point (v_A, v_B), where

$$K\big|_{\rho_\alpha = v_\alpha} = K_{\max} = \prod_\alpha v_\alpha^{v_\alpha}, \tag{3.29}$$

and decreases monotonically as one moves along any straight line in the (ρ_A, ρ_B) plane starting from the center. K approaches its minimum value, $K_{\min} = 0$, on the boundaries of the triangle (3.23) where one or more of the particle densities goes to zero. As K is continuous in ρ_A, ρ_B inside the triangle, this implies that the level sets of K in this case consist of a single point at the center (v_A, v_B) and closed curves surrounding the center point.

As the level curves of K are closed, nonconstant solutions $\rho_\alpha(x)$ of the ELE must be portions of periodic functions of x. When the period τ is greater (less) than 1, this corresponds to the trajectory of the densities making less (more) than one full rotation around the center point. We will refer to solutions with $n - 1 < 1/\tau \leq n$, for

n an integer, as type n solutions. For example, a solution that does not make one full rotation would be labeled as type 1, while a solution making exactly three rotations around the center would be labeled as type 3. This is consistent with the terminology used in Conjecture 3.2.1(a). The constant solution of the ELE is not assigned a type.

Trajectories of the particle densities satisfying the ELE for a given set of v_α depend upon the choice of the r_α. For the v_α in region I there are two cases to consider: (1) $r_\alpha = v_\alpha$ for all α, (2) $r_\alpha \neq v_\alpha$ for some α.

Case 1: $r_\alpha = v_\alpha$. In this case the model is rotation invariant, and one has $\rho_\alpha(1) = \rho_\alpha(0)$ for all α. Here both constant and nonconstant solutions of the ELE are possible. The constant solution is given by $\rho_\alpha(x) = v_\alpha$, $0 \leq x \leq 1$, as noted above. As $\rho_\alpha(1) = \rho_\alpha(0)$, see (3.19), nonconstant solutions must have an integer number of periods in the interval $x \in [0, 1]$, corresponding to the number of times the trajectory orbits the center. Note that as one moves along the interval in x that the maxima (and minima) of the particle densities proceed in cyclic order, that is, after species α reaches its maximum (minimum) density, the next species to achieve its maximum (minimum) density is $\alpha + 1$.

Example numerical solutions of the ELE in this case and their corresponding trajectories with $v_A = 1/2$, $v_B = 1/3$, $v_C = 1/6$, and $r_\alpha = v_\alpha$ for all α, are shown in Figure 3.2. In this plot the inverse temperatures $\beta_1 = 13$, $\beta_2 = 15$, and $\beta_3 = 20$, all larger than β_c, which has value 4π for this choice of the v_α. The trajectories lie along lines of constant K, with $K_1 \approx .349$, $K_2 \approx .291$, and $K_3 \approx .189$ for the solutions at β_1, β_2, and β_3 respectively. Arrows indicate the flow along the trajectory as x increases, and the point (v_A, v_B) is marked by a dot. For this case $K_{\max} \approx .364$.

Case 2: $r_\alpha \neq v_\alpha$. Here there is no rotation invariance and the densities at opposite ends of the interval are not the same, $\rho_\alpha(1) \neq \rho_\alpha(0)$ for some α, see (3.19). In this case only nonconstant solutions of the ELE are possible at finite temperatures, i.e. for$\beta > 0$. These solutions will be portions of the periodic solutions described in Case 1. In contrast to the $r_\alpha = v_\alpha$ case, however, solutions of type n do not exist for arbitrarily large values of n; there is some cutoff $n_{\max} \geq 2$, which depends on the difference between the r_α and the v_α, above which type n solutions, $n \geq n_{\max}$, do not exist. This is because the average value of each density ρ_α around one full orbit of the center is v_α, so as n

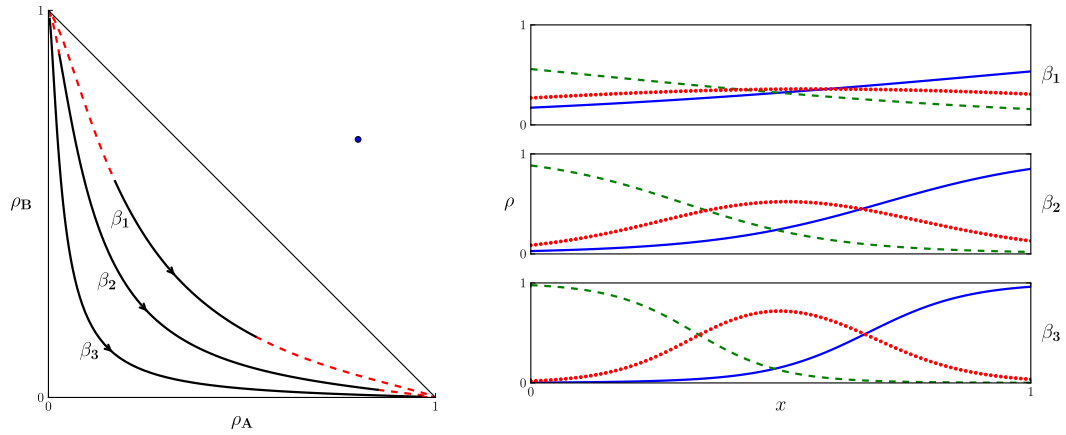

Figure 3.3: Plots of ρ_A (solid), ρ_B (dashed), and ρ_C (dotted) and their corresponding trajectories in the ρ_A-ρ_B plane. See description under Regions II and III.

becomes large the average density for the full profile r_α is steadily driven towards v_α. See Appendix B.3 for more details.

Regions II and III

When the v_α lie in regions II and III, the point (v_A, v_B) lies outside the triangle (3.23). Thus by (3.28) the level sets of K inside the triangle cannot be closed curves, as when the v_α are in region I. Let us consider the value of K along one of the boundaries of the triangle, where $\rho_\alpha = 0$ for some α. If v_α is less than zero, K will be infinite along this boundary. If v_α is zero K will be finite, and if v_α is larger than zero K will be zero. On the vertices where two boundaries meet, with K equal to zero along one and infinite along the other, the value of K at the vertex is not well defined, depending on the way in which the limit is taken. Thus when the v_α lie in regions II and III, lines of constant K for K finite and nonzero will be curves terminating on the vertices of the triangle where boundaries along which K is infinite and zero meet. When the v_α lie on the boundaries between different regions, e.g. for the special values of the v_α considered in Section 3.5, the level sets of K will be curves with ends terminating on either the edges or the vertices of the triangle. Solutions of the ELE are therefore nonconstant at finite temperatures and are not periodic.

Additionally, one may easily see by considering the ELE (3.20) that when one or two

of the v_α are negative, the density of one particle species will monotonically increase in x, and another species will monotonically decrease. If for example $v_A < 0$ while $v_B, v_C > 0$, ρ_B will be monotonically increasing and ρ_C will be monotonically decreasing. Note that if the v_α lie in region II, as x increases from 0 to 1 the maxima and minima of the particle densities proceed in cyclic order, as for region I systems, but when the v_α lie in region III the order is *reversed*. That is, in region III a maximum (minimum) density of species α is followed by a maximum (minimum) of species $\alpha + 2$.

Example numerical solutions and the corresponding trajectory of the densities with $v_A = 4/5$, $v_B = 2/3$, $v_C = -7/15$, $r_A = r_B = r_C = 1/3$, are plotted in Figure 3.3. In this figure $\beta_1 = 1$, $\beta_2 = 3$, and $\beta_3 = 5$. The trajectories lie along lines of constant K, with $K_1 \approx .306$, $K_2 \approx .167$, and $K_3 \approx .066$ for the solutions at β_1, β_2, and β_3 respectively. Portions of the level curves not traversed by the solutions are marked with dashed lines. Arrows indicate the flow along the trajectory, and the point (v_A, v_B) is marked by a dot.

3.4 The case $r_\alpha = v_\alpha$

If $r_\alpha = v_\alpha$ for all α (so that we are necessarily in region I) then as already noted the constant solution $\rho_\alpha(x) = v_\alpha$, $0 \le x \le 1$, is always a solution of the ELE, and other solutions are given by traversing, exactly n times for a type n solution, one of the simple closed curves which is a level set of K. We show in Section 3.4.2 that the constant solution cannot minimize the free energy when $\beta > \beta_c$, and in Section 3.4.3 that no type n solution with $n \ge 2$ can minimize the free energy. Thus the existence of a unique minimizer as described in Conjecture 3.2.1(a) would be established if we could show that no non-constant solution can exist for $\beta < \beta_c$ and that for $\beta > \beta_c$ there is a unique type 1 solution, exactly what is proven in [5] for $v_\alpha = 1/3$ for all α.

Now under a change of scale $t = \beta x$ the ELE (3.20) become

$$\frac{\mathrm{d}\rho_\alpha}{\mathrm{d}t} = 3\rho_\alpha \left(v_{\alpha+1}\rho_{\alpha+2} - v_{\alpha+2}\rho_{\alpha+1} \right), \tag{3.30}$$

and type 1 solutions of (3.20) correspond to solutions of (3.30) which have period β, the inverse of the temperature. The period $\tau(K)$ of the solution of (3.30) is easily seen

to be a continuous function of K for $0 < K \leq K_{\max}$; a perturbative calculation as in [5] shows that $\lim_{K \nearrow K_{\max}} \tau(K) = \beta_c$ as K and we establish in Section 3.4.4 that $\lim_{K \searrow 0} \tau(K) = \infty$. The existence portion of Conjecture 3.2.1(a.ii) follows immediately from these observations. If one could show that the period of the solution of (3.30) is a monotonically decreasing function of K for $0 < K \leq K_{\max}$ then uniqueness would be established. However, (3.30) is for arbitrary v_α a generic member of the generalized Lotka-Volterra family of quadratic centers [66] (for details on the correspondence between (3.30) and a standard parametrization of the Lotka-Volterra family, see Appendix B.2), and monotonicity of the period as a function of orbit size is for this family an open question [66]. In terms of the parameters used in (3.30), monotonicity was established in [5] when all v_α are 1/3, and below we establish monotonicity when, for some α, $v_\alpha = 1/2$ and $v_{\alpha+1} = v_{\alpha+2} = 1/4$. Finally, monotonicity at sufficiently low temperature (or equivalently, small K) follows, for any v_α, from the correspondence established in Appendix B.2 and the results of [66].

3.4.1 $v_\alpha = 1/2$, $v_{\alpha+1} = v_{\alpha+2} = 1/4$

When the v_α lie in region I and two of them are equal, say $v_A = v_B = \gamma$ with $0 < \gamma < 1/2$, one may find explicitly an autonomous evolution equation for the third. We begin with the expression

$$K = \rho_A(x)^\gamma \rho_B(x)^\gamma \rho_C(x)^{1-2\gamma}, \tag{3.31}$$

which together with (3.10) may be used to obtain the densities ρ_A and ρ_B in terms of ρ_C:

$$\rho_A(x) = \frac{1}{2}\left(1 - \rho_C(x) \pm \sqrt{(1-\rho_C(x))^2 - 4K^{1/\gamma}\rho_C(x)^{-\lambda}}\right), \tag{3.32}$$

$$\rho_B(x) = \frac{1}{2}\left(1 - \rho_C(x) \mp \sqrt{(1-\rho_C(x))^2 - 4K^{1/\gamma}\rho_C(x)^{-\lambda}}\right). \tag{3.33}$$

where $\lambda = (1-2\gamma)/\gamma$. With (3.32) the reparameterized ELE (3.30) for ρ_C is

$$\begin{aligned} \rho_C'(t) &= 3\gamma\rho_C(t)\left(\rho_B(t) - \rho_A(t)\right) \\ &= 3\gamma\rho_C(t)\left(\pm\sqrt{(1-\rho_C(t))^2 - 4K^{1/\gamma}\rho_C(x)^{-\lambda}}\right). \end{aligned} \tag{3.34}$$

Squaring (3.34) we have

$$\frac{9\gamma^2}{2}\rho_C'(t)^2 + U_K(\rho_C(t)) = 0, \tag{3.35}$$

with

$$U_K(\rho) = \frac{9}{32}\left(4K^{1/\gamma}\rho_C(x)^{2-\lambda} - \rho^2\,(1-\rho)^2\right). \tag{3.36}$$

This is the equation for a zero energy particle of mass 1 confined in a potential well. The zeros of the potential correspond to the turning points for the particle,

With $\gamma = 1/4$ and thus $\lambda = 2$ the potential becomes quartic. The zeros of U_K are then

$$\frac{1}{2} \pm \rho_0, \qquad \rho_0 = \sqrt{\frac{1}{4} - 2K^2}. \tag{3.37}$$

Note that in this case $K_{max} = 1/2\sqrt{2}$, so $0 < \rho_0 < 1/2$. The period $\tau(K)$ of the type 1 solution $\rho(t)$ may now be directly calculated, yielding

$$\begin{aligned}\tau(K) &= \int_{1/2-\rho_0}^{1/2+\rho_0} \mathrm{d}\rho \frac{2}{\sqrt{-2\,U_K(\rho)}} \\ &= \frac{16/3}{\sqrt{1/2-\rho_0^2}-\rho_0} F\left(\frac{\pi}{2}, -\frac{4\rho_0\sqrt{1/2-\rho_0^2}}{\left(\sqrt{1/2-\rho_0^2}-\rho_0\right)^2}\right).\end{aligned} \tag{3.38}$$

Here $F(\pi/2, \cdot)$ is the complete elliptic integral the first kind. The period (3.38) is a monotonically decreasing function of K, with (as expected) $\lim_{K\nearrow K_{max}}(\tau(K)) = 8\sqrt{2}\pi/4 = \beta_c$ and $\lim_{K\searrow 0}\tau(K) = \infty$. Thus for all $\beta > \beta_c$ there is a unique value of K for which $\tau(K) = \beta$ and hence a unique type 1 solution of the ELE, and there is no type 1 solution for $\beta < \beta_c$.

3.4.2 Linear stability of the constant solution for $\beta < \beta_c$

We will now consider the linear stability of the constant solution $\rho_\alpha(x) = v_\alpha$, $0 \le x \le 1$. Let us define two bounded continuous functions $\phi_A(x)$, $\phi_B(x)$, satisfying

$$\int_0^1 \mathrm{d}x\ \phi_A(x) = \int_0^1 \mathrm{d}x\ \phi_B(x) = 0, \tag{3.39}$$

and perturb the constant solution as

$$(\rho_A, \rho_B, \rho_C) \to (v_A + \epsilon\,\phi_A, v_B + \epsilon\,\phi_B, v_C - \epsilon\,(\phi_A + \phi_B)) \tag{3.40}$$

for some fixed ϵ very small. Under this perturbation all the terms in the free energy linear in ϵ cancel. The order ϵ^2 contribution to the entropy is

$$\frac{1}{2}\int_0^1 \mathrm{d}x \ \left[\frac{1}{r_A}\phi_A^2(x)+\frac{1}{r_B}\phi_B^2(x)+\frac{1}{r_C}(\phi_A(x)+\phi_B(x))^2\right]. \tag{3.41}$$

The energy due to interaction with the external fields is linear in the densities, so the ϵ^2 term for the energy is due entirely to the asymmetric mean field ABC interaction,

$$\begin{aligned}\beta\int_0^1 \mathrm{d}x\int_0^1 \mathrm{d}y\ \Theta(y-x)\Big[&-\phi_A(x)(\phi_A(y)+\phi_B(y))+\phi_B(x)\phi_A(y)\\ &-(\phi_A(x)+\phi_B(x))\phi_B(y)\Big]\\ &=3\beta\int_0^1 \mathrm{d}x\int_0^1 \mathrm{d}y\ \Theta(y-x)\,\phi_B(x)\phi_A(y).\end{aligned} \tag{3.42}$$

Now expanding $\phi_A(x)$ and $\phi_B(x)$ in a Fourier series as

$$\phi_A(x)=\sum_{n=1}^{\infty}(a_n\sin(2\pi nx)+b_n\cos(2\pi nx)), \tag{3.43}$$

$$\phi_B(x)=\sum_{n=1}^{\infty}(c_n\sin(2\pi nx)+d_n\cos(2\pi nx)), \tag{3.44}$$

we see that the second variation of the free energy functional around the constant solution is given by

$$\begin{aligned}\sum_{n=1}^{\infty}\Bigg[&\frac{v_A+v_C}{v_Av_C}(a_n^2+b_n^2)+\frac{v_B+v_C}{v_Bv_C}(c_n^2+d_n^2)\\ &+\frac{2}{v_C}(a_nc_n+b_nd_n)-\frac{3\beta}{\pi n}(b_nc_n-a_nd_n)\Bigg].\end{aligned} \tag{3.45}$$

If we write $u_n=(a_n,\ b_n,\ c_n,\ d_n)$, the second variation can be expressed in matrix form as $\sum_{n=1}^{\infty} u_n\,M\,u_n^T/\,(v_Av_Bv_C)$, where

$$M=\begin{bmatrix} v_B(1-v_B) & 0 & v_Av_B & 3\beta/(2\pi n)\\ 0 & v_B(1-v_B) & -3\beta/(2\pi n) & v_Av_B\\ v_Av_B & 3\beta/(2\pi n) & v_A(1-v_A) & 0\\ 3\beta/(2\pi n) & v_Av_B & 0 & v_A(1-v_A)\end{bmatrix}. \tag{3.46}$$

The eigenvalues of M are

$$\begin{aligned}\lambda_{\pm}=\frac{1}{2}\Bigg[&v_A(1-v_A)+v_B(1-v_B)\\ &\pm\sqrt{(v_A(1-v_A)+v_B(1-v_B))^2-4\left(v_Av_Bv_C-\left(\frac{3\beta}{2\pi n}\right)^2\right)}\Bigg],\end{aligned} \tag{3.47}$$

each with degeneracy 2. Thus for $\beta \leq \beta_c = 2\pi/(3\sqrt{v_A v_B v_C})$ the matrix M is positive definite, so the second variation of the free energy around the constant solution is also positive and the constant solution is a local minimum. At lower temperatures, $\beta > \beta_c$, the smallest eigenvalue λ_- becomes negative, so in this regime the constant solution can no longer be the minimizer of the free energy.

3.4.3 Solutions of type $n \geq 2$

In this section we will show that solutions of the ELE for $r_\alpha = v_\alpha$ with two or more full periods in $x \in [0, 1]$ can never minimize the free energy.

Consider a set of profiles $\{\rho\}$, not necessarily solutions of the ELE but satisfying the constraints (3.10). Then for any integer $n \geq 2$ we define the set of profiles $\{\hat{\rho}_n\}$ by

$$\hat{\rho}_{n,\alpha}(x) = \rho_\alpha(nx - j) \quad \text{for } \frac{j}{n} \leq x \leq \frac{j+1}{n}, \quad j = 0, ..., n-1. \tag{3.48}$$

That is, we obtain the $\hat{\rho}_{n,\alpha}$ by shrinking the ρ_α horizontally by a factor of n and repeating these reduced profiles n times in the interval $[0, 1]$. We claim then that

$$\mathcal{S}(\{\hat{\rho}_n\}) = \mathcal{S}(\{\rho\}), \tag{3.49}$$

$$\mathcal{E}(\{\hat{\rho}_n\}) = \frac{1}{n}\mathcal{E}(\{\rho\}) + \left(1 - \frac{1}{n}\right)\mathcal{E}(\{r\}), \tag{3.50}$$

where $\mathcal{E}(\{r\}) = \sum_\alpha v_\alpha v_{\alpha+2}/2$ is the energy of the constant solution $\rho_\alpha(x) = v_\alpha$.

The proof proceeds by direct calculation. First let us consider the entropy of the new profiles,

$$\begin{aligned} \mathcal{S}(\{\hat{\rho}_n\}) &= -\sum_\alpha \sum_{j=0}^{n-1} \int_{j/n}^{(j+1)/n} \mathrm{d}x\, \hat{\rho}_{n,\alpha}(x) \log \hat{\rho}_{n,\alpha}(x) \\ &= -\sum_\alpha \sum_{j=0}^{n-1} \frac{1}{n} \int_0^1 \mathrm{d}\tilde{x}\, \rho_\alpha(\tilde{x}) \log \rho_\alpha(\tilde{x}) = \mathcal{S}(\{\rho\}). \end{aligned} \tag{3.51}$$

Here we have used a change of variables with $x = (\tilde{x} + j)/n$. The calculation of the

energy proceeds similarly. Using the same change of variables

$$\begin{aligned}
\mathcal{E}(\{\hat{\rho}_n\}) &= \sum_\alpha \Bigg\{ \sum_{j,k=0}^{n-1} \frac{1}{n^2} \int_0^1 \mathrm{d}\tilde{x} \int_0^1 \mathrm{d}\tilde{y}\, \Theta\Big(\frac{\tilde{y}+k-\tilde{x}-j}{n}\Big)\, \rho_\alpha(\tilde{x})\rho_{\alpha+2}(\tilde{y}) \\
&\qquad + \sum_{j=0}^{n-1} \frac{1}{n} \int_0^1 \mathrm{d}\tilde{x}\, \xi_\alpha \frac{\tilde{x}+j}{n} \rho_\alpha(\tilde{x}) \Bigg\} \\
&= \sum_\alpha \Bigg\{ \sum_{j=0}^{n-1} \frac{1}{n^2} \int_0^1 \mathrm{d}\tilde{x} \int_0^1 \mathrm{d}\tilde{y}\, \Theta(\tilde{y}-\tilde{x})\, \rho_\alpha(\tilde{x})\rho_{\alpha+2}(\tilde{y}) \\
&\qquad + \sum_{0\le j<k\le n-1} \frac{1}{n^2} \int_0^1 \mathrm{d}\tilde{x} \int_0^1 \mathrm{d}\tilde{y}\, \rho_\alpha(\tilde{x})\rho_{\alpha+2}(\tilde{y}) + \frac{1}{n} \int_0^1 \mathrm{d}\tilde{x}\, \tilde{x}\, \xi_\alpha \rho_\alpha(\tilde{x}) \Bigg\} \\
&= \frac{1}{n}\mathcal{E}(\{\rho\}) + \Big(1-\frac{1}{n}\Big)\, \mathcal{E}(\{r\}), \qquad (3.52)
\end{aligned}$$

as there are $n(n-1)/2$ pairs of indices with $0 \le j < k \le n-1$, and $\sum_\alpha \xi_\alpha r_\alpha = 0$, as $r_\alpha = v_\alpha$ implies $\xi_\alpha = r_{\alpha+2} - r_{\alpha+1}$.

Now there are two cases to consider. If $\mathcal{E}(\{\rho\}) < \mathcal{E}(\{r\})$, then by (3.52) $\mathcal{E}(\{\hat{\rho}_n\}) > \mathcal{E}(\{\rho\})$, thus the original profiles ρ_α have a lower free energy and the $\hat{\rho}_{n,\alpha}$ cannot be minimizers. If instead $\mathcal{E}(\{\rho\}) \ge \mathcal{E}(\{r\})$, then $\mathcal{E}(\{\hat{\rho}_n\}) > \mathcal{E}(\{r\})$ as well, and as long as ρ_α is not the constant solution $\mathcal{S}(\{r\}) > \mathcal{S}(\{\hat{\rho}_n\})$. Then $\mathcal{F}(\{r\}) < \mathcal{F}(\{\hat{\rho}_n\})$, so again the $\hat{\rho}_{n,\alpha}$ are not minimizers. A type n solution of the ELE at an inverse temperature β is of the form $\hat{\rho}_{n,\alpha}$, where ρ_α is a type 1 solution at an inverse temperature β/n. Thus no type n solution for $n \ge 2$ can minimize the free energy.

3.4.4 K-β relation

It follows from the result of Section 3.4.3 that when $r_\alpha = v_\alpha$ a minimizer of the free energy must be either the constant solution of the ELE or a type 1 solution. Let $K(\beta)$ denote the value of K for the minimizer at temperature β; if several minimizers exist then we choose one of them arbitrarily to define $K(\beta)$. Of course, if $K(\beta) < K_{\max}$ then $\tau(K(\beta)) = \beta$. If $\tau(K)$ is monotonic then $K(\beta)$ will be the inverse of the function $\tau(K)$ and must be continuous, since $\tau(K)$ is, but we cannot show this and thus cannot rule out the possibility that $K(\beta)$ may be discontinuous. However, we do show here that $K(\beta)$ must be monotonic decreasing.

We begin with the integral form (3.18) of the ELE:

$$\log \rho_\alpha(x) = \log \rho_\alpha(0) + 3\beta \int_0^x \mathrm{d}y \, (v_{\alpha+1}\rho_{\alpha+2}(y) - v_{\alpha+2}\rho_{\alpha+1}(y)). \tag{3.53}$$

Substituting this into the entropy (3.13) and using $\int_0^1 \rho_\alpha(x)\,dx = r_\alpha$ gives

$$\begin{aligned}
\sum_\alpha r_\alpha \log \rho_\alpha(0) &= -3\beta \sum_\alpha \int_0^1 \mathrm{d}x \int_0^x \mathrm{d}y \; \rho_\alpha(x) \, (v_{\alpha+1}\rho_{\alpha+2}(y) - v_{\alpha+2}\rho_{\alpha+1}(y)) \\
&\qquad - \mathcal{S}(\{\rho\}) \\
&= 6\beta \sum_\alpha \int_0^1 \mathrm{d}x \int_0^1 \mathrm{d}y \; \Theta(y-x) v_{\alpha+1}\rho_\alpha(x)\rho_{\alpha+2}(y) \\
&\qquad - \mathcal{S}(\{\rho\}) - 3\beta \sum_\alpha v_\alpha r_{\alpha+1} r_{\alpha+2} \\
&= 2\beta \mathcal{E}(\{\rho\}) - \mathcal{S}(\{\rho\}) - 2\beta \mathcal{E}(\{r\}),
\end{aligned} \tag{3.54}$$

where $\mathcal{E}(\{r\}) = 3\sum_\alpha v_\alpha r_{\alpha+1} r_{\alpha+2}/2 + F$ (see (3.14)) is the energy of the constant profile $\rho_\alpha(x) = r_\alpha$ (which is not a solution of the ELE unless $r_\alpha = v_\alpha$). (3.54) is a general relation which holds for all profiles $\{\rho\}$ satisfying the ELE, i.e. for all stationary points of $\mathcal{F}(\{\rho\})$, whether or not $r_\alpha = v_\alpha$.

Now suppose that $r_\alpha = v_\alpha$ for all α. Then if $\{\rho\} = \{\rho^{(\beta)}\}$ is the minimizing solution of the ELE corresponding to $K(\beta)$, (3.54) becomes

$$\log K(\beta) = 2\beta \mathcal{E}(\{\rho^{(\beta)}\}) - \mathcal{S}(\{\rho^{(\beta)}\}) - 2\beta \mathcal{E}(\{r\}), \tag{3.55}$$

where now $\mathcal{E}(\{r\}) = \mathcal{E}(\{\rho^{(0)}\}) = 9v_A v_B v_C/2 + F$. For $\beta_2 > \beta_1$ we subtract the corresponding equations (3.55) and rearrange terms to obtain

$$\begin{aligned}
\log \frac{K(\beta_2)}{K(\beta_1)} &= 2\big(\mathcal{F}_{\beta_2}(\{\rho^{(\beta_2)}\}) - \mathcal{F}_{\beta_2}(\{\rho^{(\beta_1)}\})\big) + \big(\mathcal{S}(\{\rho^{(\beta_2)}\}) - \mathcal{S}(\{\rho^{(\beta_1)}\})\big) \\
&\qquad + 2(\beta_2 - \beta_1)\big(\mathcal{E}(\{\rho^{(\beta_1)}\}) - \mathcal{E}(\{\rho^{(0)}\})\big).
\end{aligned} \tag{3.56}$$

where we have indicated the explicit β dependence in (3.11) by writing $\mathcal{F}_\beta$. But it follows from simple general thermodynamic arguments that both $\mathcal{S}(\{\rho^{(\beta)}\})$ and $\mathcal{E}(\{\rho^{(\beta)}\})$ are monotonic decreasing functions of β, and since $\rho^{(\beta_2)}$ minimizes $\mathcal{F}_{\beta_2}$ all three terms on the right side of (3.56) are nonpositive. This establishes the monotonicity of $K(\beta)$.

One may also see that when β is large, $K(\beta)$ must be small. For from (3.55) we have

$$\frac{\log K(\beta)}{\beta} = 2\left(\mathcal{E}(\{\rho^{(\beta)}\}) - \mathcal{E}(\{r\})\right) + \beta^{-1}\mathcal{S}(\{\rho^{(\beta)}\}); \tag{3.57}$$

since the energy and entropy are bounded functions and $\mathcal{E}(\{\rho^{(\beta)}\})$ is decreasing in β the right hand side of (3.57) approaches a finite value as $\beta \nearrow \infty$. In fact, one can show that $\lim_{\beta\nearrow\infty} \mathcal{E}(\{\rho^{(\beta)}\})$ is the ground state energy per particle $3v_Av_Bv_C + F$ (see Appendix B.1), so that asymptotically $\log K(\beta) \sim -(3/2)v_Av_Bv_C\beta$.

3.5 Special cases when $r_\alpha \neq v_\alpha$

For certain values of the r_α and v_α when $r_\alpha \neq v_\alpha$, we are able to prove Conjecture 3.2.1(b). There are two such special cases. In the first case, one of the v_α is zero and $v_{\alpha\pm1}$ have opposite signs (i.e., one of $v_{\alpha\pm1}$ must be greater than one). In this case, the v_α lie in fact on the *boundary* between regions II and III. In the second case one of the v_α is one. We will present the proof of Conjecture 3.2.1(b) for these cases in the sections below.

3.5.1 $v_\alpha = 0$, $v_{\alpha\pm1} > 1$

For definiteness let us take $v_C = 0$, $v_B > 1$. On the orbit with conserved quantity K we have $\rho_A(x)^{v_A}\rho_B(x)^{1-v_A} = K$ and so

$$\rho_A(x) = K^{1/v_A}\rho_B(x)^\gamma, \qquad \rho_B(x) = K^{-1/(v_A-1)}\rho_A(x)^{1/\gamma}, \tag{3.58}$$

where $\gamma = (v_A - 1)/v_A$ satisfies $\gamma > 1$. Thus the profiles satisfy

$$\rho_A' = 3\beta\rho_A(v_B\rho_C) = 3\beta(1-v_A)\rho_A(1-\rho_A - K^{1/(1-v_A)}\rho_A^{1/\gamma}) \equiv f_K(\rho_A), \tag{3.59}$$

$$\rho_B' = 3\beta\rho_B(-v_A\rho_C) = -3\beta v_A\rho_B(1-\rho_B - K^{1/v_A}\rho_B^\gamma) \equiv g_K(\rho_B). \tag{3.60}$$

Note that if $K^* > K$ then

$$f_K(\rho) > f_{K^*}(\rho) > 0 \qquad \text{and} \qquad g_{K^*}(\rho) > g_K(\rho) > 0. \tag{3.61}$$

Now consider two profiles $\rho_\alpha(x)$ and $\rho^*_\alpha(x)$ satisfying the ELE which have different starting values: $(\rho_A(0), \rho_B(0)) \neq (\rho^*_A(0), \rho^*_B(0))$; we claim that the corresponding averages are not equal: $(r_A, r_B) \neq (r^*_A, r^*_B)$. We denote the corresponding conserved quantities by K and K^* and consider several cases.

Case 1: $K = K^*$**.** Without loss of generality we take $\rho_A^*(0) > \rho_A(0)$ and hence by (3.58) also $\rho_B^*(0) > \rho_B(0)$. Since $\rho_\alpha(x)$ and $\rho_\alpha^*(x)$, $\alpha = A, B$, satisfy the same differential equation which by (3.61) has a strictly negative right hand side we have $\rho_\alpha(x) > \rho_\alpha^*(x)$ for all x and so

$$r_A^* > r_A \qquad \text{and} \qquad r_B^* > r_B. \tag{3.62}$$

Case 2: $\rho_A^*(0) = \rho_A(0)$**.** Now without loss of generality we may take $K^* > K$ and so by (3.58) we have $\rho_B^*(0) > \rho_B(0)$. Thus by (3.60) and (3.61) we have that $\rho_B^*(x) > \rho_B(x)$, and by (3.59) and (3.61) that $\rho_A(x) > \rho_A^*(x)$ for $0 < x \leq 1$, and so

$$r_A^* < r_A \qquad \text{and} \qquad r_B^* > r_B. \tag{3.63}$$

The general case: Since we have dealt with the possibility $K^* = K$ in Case 1 we may take $K^* > K$. The case $\rho_A^*(0) = \rho_A(0)$ has been considered in Case 2. If $\rho_A^*(0) > \rho_A(0)$ we introduce a profile ρ_α^{**} with $\rho_A^{**}(0) = \rho_A^*(0)$ and $K^{**} = K$; then by Cases 1 and 2 we have

$$r_B^* > r_B^{**} > r_B. \tag{3.64}$$

If instead $\rho_A^*(0) < \rho_A(0)$ we argue similarly, introducing a profile ρ_α^{**} with $\rho_A^{**}(0) = \rho_A(0)$ and $K^{**} = K^*$, obtaining

$$r_A > r_A^{**} > r_A^*. \tag{3.65}$$

Thus the solution of the ELE must be unique.

The $v_C = 0$, $v_B < 0$, $v_A = 1 - v_B > 1$ case may be argued very similarly, but making use of comparisons between the values of the densities at the end of the interval $\rho_\alpha(1)$ rather than the initial values $\rho_\alpha(0)$, $\alpha = A, B$. Otherwise the argument proceeds identically to the case above, so we will omit the full derivation here.

3.5.2 $v_\alpha = 1$

When one of the $v_\alpha = 1$ it is possible to solve the ELE exactly. Let us assume $v_A = 1$ and v_B, v_C are not zero, a trivial case, so the v_α lie in region II. The ELE for ρ_A and

ρ_B become

$$\begin{aligned}\frac{\mathrm{d}\rho_A}{\mathrm{d}x} &= 3\beta v_B\,\rho_A(\rho_B+\rho_C)\\ &= 3\beta v_B\,\rho_A(1-\rho_A), \qquad (3.66)\\ \frac{\mathrm{d}\rho_B}{\mathrm{d}x} &= 3\beta\rho_B(v_C\,\rho_A-\rho_C)\\ &= -3\beta\,\rho_B(1-\rho_B)+3\beta(1-v_B)\rho_A\,\rho_B. \qquad (3.67)\end{aligned}$$

The equation for ρ_A may easily be solved to obtain

$$\rho_A(x)=\frac{1}{1+c_A\,e^{-3\beta v_B\,x}}, \qquad (3.68)$$

where $c_A = 1/\rho_A(0) - 1$. Using (3.68) one may then solve for the density ρ_B,

$$\rho_B(x)=c_A\left(c_A+e^{3\beta v_B\,x}\right)^{\frac{1-v_B}{v_B}}\,\frac{1}{(1+c_A)^{1/v_B}+c_A\,c_B\,e^{3\beta v_B\,x}}, \qquad (3.69)$$

with the constant

$$c_B = (1+c_A)^{1/v_B}\left(\frac{1}{(1+c_A)\rho_B(0)}-\frac{1}{c_A}\right)$$

To show that the solution is unique, we must demonstrate that there is only one choice of the initial values $\rho_\alpha(0)$ which will yield a particular set of average densities r_α at a given β. This may be seen directly from the density profiles (3.68), (3.69), which depend simply on c_A and c_B. It is easy to see that

$$\frac{\mathrm{d}\rho_A(x)}{\mathrm{d}c_A}<0, \qquad \frac{\mathrm{d}\rho_B(x)}{\mathrm{d}c_B}<0, \qquad (3.70)$$

and as $\mathrm{d}c_A/\mathrm{d}\rho_A(0) < 0$, $\mathrm{d}c_B/\mathrm{d}\rho_B(0) < 0$, we have

$$\frac{\mathrm{d}r_A}{\mathrm{d}\rho_A(0)}>0, \qquad \frac{\mathrm{d}r_B}{\mathrm{d}\rho_B(0)}>0. \qquad (3.71)$$

Thus there is a unique solution of the ELE, given by (3.68), (3.69), for all β. The average density of the profiles is given by

$$\begin{aligned}r_A &= \frac{1}{3\beta v_B}\log\frac{e^{c_A}+e^{3\beta v_B}}{1+e^{c_A}}, \qquad (3.72)\\ r_B &= 1-\frac{1}{3\beta}\log\frac{\left(e^{c_A}+e^{3\beta v_B}\right)^{1/v_B}+e^{3\beta+c_A}\,c_B}{(1+e^{c_A})^{1/v_B}+e^{c_A}\,c_B}, \qquad (3.73)\\ r_C &= 1-r_A-r_B. \qquad (3.74)\end{aligned}$$

In principle one may invert equations (3.72), (3.73) to write the solutions in terms of the average densities r_A and r_B rather than $\rho_A(0)$ and $\rho_B(0)$.

Chapter 4

The inverse Ising problem

4.1 Introduction

In this chapter we investigate the problem of inferring the interactions between a set of Ising spins given their correlations. As a first step in describing this so-called inverse Ising problem, we review the standard or "forward" Ising problem, i.e. the computation of Ising model observables (correlations, etc.) given the form of the interactions.

Here we are interested in the Ising model consisting of a finite number N of binary random variables or spins η_i, labeled from 1 to N, which take values $\eta_i \in \{0, 1\}$. The spins interact via a set of local fields or chemical potentials $\{h_i\}$ and pairwise couplings $\{J_{ij}\}$. For convenience we refer to the set of all the fields and couplings as $\mathbf{J} = \{\{h_i\}, \{J_{ij}\}\}$. The Hamiltonian is then

$$H_{\mathbf{J}}(\underline{\eta}) = -\sum_i h_i \eta_i - \sum_{j>i} J_{ij} \eta_i \eta_j, \tag{4.1}$$

where

$$\underline{\eta} = \{\eta_1, \eta_2, \ldots, \eta_N\} \tag{4.2}$$

specifies the configuration of the system. Equilibrium properties of the Ising spin system are described by the Gibbs measure

$$\mu_{\mathbf{J}}(\underline{\eta}) = \frac{e^{-H_{\mathbf{J}}(\underline{\eta})}}{Z}, \tag{4.3}$$

which specifies the probability of each configuration $\underline{\eta}$. Here Z is the partition function, a normalizing factor obtained by summing the numerator of (4.3) over the set of all configurations. In (4.3) and throughout this chapter we choose units such that $k_B T = 1$; the temperature will not play a role in our discussion.

In principle, we can compute any equilibrium observable of interest by taking an average with respect to the Gibbs measure, or via simulation. This is the forward Ising problem. In particular, we will be interested in the correlations

$$p_i \equiv \langle \eta_i \rangle_{\mathbf{J}} = \sum_{\underline{\eta}} \eta_i \frac{e^{-H_{\mathbf{J}}(\underline{\eta})}}{Z}, \qquad p_{ij} \equiv \langle \eta_i \eta_j \rangle_{\mathbf{J}} = \sum_{\underline{\eta}} \eta_i \eta_j \frac{e^{-H_{\mathbf{J}}(\underline{\eta})}}{Z}. \tag{4.4}$$

As with the couplings and fields, we refer to the set of all one- and two-point correlations as $\mathbf{p} = \{\{p_i\}, \{p_{ij}\}\}$ for convenience. Practically speaking, for a large system it becomes impossible to explicitly compute quantities such as (4.4). In this case, Monte Carlo simulations are helpful. One first introduces dynamics, such as spin flips with rates given by the popular Metropolis algorithm, chosen such that the steady state of the dynamics is given by the Gibbs measure. Averages of observables taken over a long simulation will then yield the same results as averages over (4.3).

The inverse Ising problem consists of inverting the map from interactions to observables given by (4.3). In other words, given a set correlations (or other observables), we must find the Ising model which reproduces the correlations. This problem arises, for example, if we would like to use the Ising model as a phenomenological model to describe the behavior of some experimental system. To fit an Ising model to data, we must solve the inverse problem.

As a simple phenomenological model for complex systems, the Ising model has several attractive characteristics. First, the Ising model with local fields and pairwise couplings (4.1) is the maximum entropy model which is capable of reproducing a set of observed one- and two-point correlations (4.4). It has been argued for statistical inference problems that, in the absence of information which would lead us to select a particular model, the maximum entropy model consistent with the data should be favored, because it is the least constrained model which successfully describes the system [30]. This is a natural choice; the probability distribution which maximizes the entropy of a closed system is the equilibrium distribution.

Additionally, in the study of complex systems, one common goal is to understand how the collective behavior of a complex network of heterogeneous components, which may be quantified in terms of correlations between the components, emerges from the

structure of their interactions. This includes, for example, making a distinction between a correlation caused by direct interaction between components and one that is a result of network effects. The Ising model provides a simple, natural framework for examining such questions [16].

Indeed, the Ising model has proved useful for studying the correlated firing patterns of networks of neurons [15, 24, 56, 59], as well as the structure of proteins and protein-protein interactions [60, 67]. In each case, the Ising model has been employed as a simplified model of a vastly more complicated system, whose real dynamics would be difficult or impossible to model directly. While we present the analysis of data obtained from real neuronal networks, we will not be concerned with the physical interpretation of the Ising model applied to any particular experimental system. Rather, we focus on the method of solution.

The inverse Ising problem can be stated as follows. Let us assume that the system which we would like to investigate consists of N components, each of which may be in one of two different states. Experimental data takes the form of a sequence of B measurements of the configuration $\underline{\eta}^{(k)}$, $k = 1, \ldots, B$. From this data we define the empirical measure

$$\mu_{\text{ex}}(\underline{\eta}) = \frac{1}{B}\sum_{k=1}^{B} \delta(\underline{\eta}, \underline{\eta}^{(k)}), \tag{4.5}$$

where δ is the Kronecker delta function. Using (4.5) we find the emperical correlations,

$$p_i^* = \frac{1}{B}\sum_{k=1}^{B} \eta_i^{(k)}, \qquad p_{ij}^* = \frac{1}{B}\sum_{k=1}^{B} \eta_i^{(k)}\eta_j^{(k)}. \tag{4.6}$$

The inverse problem is solved when we obtain the set of fields $\{h_i^*\}$ and couplings $\{J_{ij}^*\}$ for which

$$p_i = \langle \eta_i \rangle_{\mathbf{J}^*} = p_i^*, \qquad p_{ij} = \langle \eta_i \eta_j \rangle_{\mathbf{J}^*} = p_{ij}^*. \tag{4.7}$$

Unlike the forward problem, a direct approach to the solution is not immediately clear.

Maximum likelihood estimation, a fundamental method of statistical inference, provides one method of solution of the inverse problem. The approach is as follows. Using the general Ising model with pairwise interactions, we compute via (4.3) the probability or *likelihood* of observing the collection of experimental data $\{\underline{\eta}^{(k)}\}$ as a function of the

interactions $\mathbf{J}$:

$$\mathcal{L}(\{\underline{\eta}^{(k)}\}|\mathbf{J}) = \prod_{k=1}^{B} \frac{e^{-H_{\mathbf{J}}(\underline{\eta}^{(k)})}}{Z}. \tag{4.8}$$

For convenience, we compute the logarithm of the likelihood, divided by the number of data points B,

$$\hat{\mathcal{L}}(\{\underline{\eta}^{(k)}\}|\mathbf{J}) = -\log Z + \sum_i p_i^* h_i + \sum_{j>i} p_{ij}^* J_{ij}. \tag{4.9}$$

The couplings and fields $\mathbf{J}$ which maximize the likelihood (or equivalently, the average log-likelihood (4.9)) then satisfy

$$\frac{\partial \hat{\mathcal{L}}}{\partial h_i} = \langle \eta_i \rangle_{\mathbf{J}} - p_i^* = 0, \qquad \frac{\partial \hat{\mathcal{L}}}{\partial J_{ij}} = \langle \eta_i \eta_j \rangle_{\mathbf{J}} - p_{ij}^* = 0. \tag{4.10}$$

Thus we see that the $\mathbf{J} = \mathbf{J}^*$ which maximize the likelihood of the experimental data, if they exist and are finite, also reproduce the experimentally measured one- and two-point correlations.

Equivalently, one can think of the average log-likelihood (4.9) as the negative of the cross-entropy S^* between the empirical measure and that of the Ising model (4.3) [17],

$$\begin{aligned} S^*(\{\underline{\eta}^{(k)}\}, \mathbf{J}) &= -\sum_{\underline{\eta}} \mu_{\text{ex}}(\underline{\eta}) \log \mu_{\text{ex}}(\underline{\eta}) + D_{\text{KL}}(\mu_{\text{ex}} || \mu_{\mathbf{J}}) \\ &= \log Z - \sum_i p_i^* h_i - \sum_{j>i} p_{ij}^* J_{ij}, \end{aligned} \tag{4.11}$$

where $D_{\text{KL}}(\mu_{\text{ex}}||\mu_{\mathbf{J}})$ is the Kullback-Leibler divergence between μ_{ex} and $\mu_{\mathbf{J}}$,

$$D_{\text{KL}}(\mu_{\text{ex}}||\mu_{\mathbf{J}}) = -\sum_{\underline{\eta}} \mu_{\text{ex}}(\underline{\eta}) \log \frac{\mu_{\mathbf{J}}(\underline{\eta})}{\mu_{\text{ex}}(\underline{\eta})}. \tag{4.12}$$

The Kullback-Leibler divergence is a measure of distance between two probability measures. Hence the maximum likelihood solution $\mathbf{J}^*$ also minimizes the "distance" between the empirical measure and (4.3), as measured by the KL divergence. Note that, because the one- and two-point correlations of the Ising model with interactions $\mathbf{J}^*$ match those obtained from data, as shown in (4.10), the cross-entropy S^* (4.11) is equivalent to the standard entropy of the Ising model when $\mathbf{J} = \mathbf{J}^*$.

Do the interactions $\mathbf{J}^*$ maximizing (4.9) exist, and if so, are they unique? A set of arbitrarily specified correlations may not be realizable (i.e. there may not exist any

probability measure which yields the specified correlations). See [18, 35, 36] for a discussion of this problem. Since we assume that the correlations come from an empirical measure (4.5), they are realizable, but it may not be obvious that local fields and pairwise couplings are enough to specify the desired correlations. To establish existence and uniqueness of the solution, consider the matrix of second derivatives of the cross-entropy

$$\begin{aligned}\chi &= \begin{pmatrix} \frac{\partial^2 S^*}{\partial h_i \partial h_{i'}} & \frac{\partial^2 S^*}{\partial h_i \partial J_{k'l'}} \\ \frac{\partial^2 S^*}{\partial h_{i'} \partial J_{kl}} & \frac{\partial^2 S^*}{\partial J_{kl} \partial J_{k'l'}} \end{pmatrix} \\ &= \begin{pmatrix} \langle \eta_i \, \eta_{i'} \rangle_{\mathbf{J}} - \langle \eta_i \rangle_{\mathbf{J}} \langle \eta_{i'} \rangle_{\mathbf{J}} & \langle \eta_i \, \eta_{k'} \, \eta_{l'} \rangle_{\mathbf{J}} - \langle \eta_i \rangle_{\mathbf{J}} \langle \eta_{k'} \, \eta_{l'} \rangle_{\mathbf{J}} \\ \langle \eta_{i'} \, \eta_k \, \eta_l \rangle_{\mathbf{J}} - \langle \eta_{i'} \rangle_{\mathbf{J}} \langle \eta_k \, \eta_l \rangle_{\mathbf{J}} & \langle \eta_k \, \eta_l \, \eta_{k'} \, \eta_{l'} \rangle_{\mathbf{J}} - \langle \eta_k \, \eta_l \rangle_{\mathbf{J}} \langle \eta_{k'} \, \eta_{l'} \rangle_{\mathbf{J}} \end{pmatrix}. \end{aligned} \tag{4.13}$$

In the typical language of the Ising model, (4.13) is the susceptibility matrix, which gives the response of each one- and two-point correlation p_i and p_{kl} to an infinitesimal change in one of the fields $h_{i'}$ or couplings $J_{k'l'}$. The matrix χ is the covariance matrix for the set of single spin variables η_i and pairs $\eta_i \eta_j$, thus it is nonnegative. If χ has zero modes, a small regularization term

$$\frac{\gamma}{2} \left(\sum_i h_i^2 + \sum_{j>i} J_{ij}^2 \right) \tag{4.14}$$

can be added to (4.11) to ensure that the Hessian (4.13) is positive definite [17]. With such an addition the cross-entropy is strictly convex, which establishes the existence and uniqueness of the solution to the (regularized) inverse problem.

Minimization of (4.11) provides a method by which the desired $\mathbf{J}^*$ may be obtained. However, this equation has no analytical solution for more than a couple of spins, and, because the number of terms in the partition function scales exponentially with the system size, direct numerical minimization is precluded for large systems with $N \gtrsim 20$.

Typical methods of solving the inference problem include the Boltzmann learning method, which involves iterative Monte Carlo simulations followed by small updates to the interaction parameters [1]. This method can be very slow for large systems, though recent advances have notably improved the speed [12, 27, 65]. Other methods such as iterative scaling algorithms [47, 62], pseudo-likelihood approximation [4, 50], various perturbative expansions [15, 51, 54, 58] and mean field (or Gaussian model)

approximations [28] have also been developed which attempt to solve the Inverse Ising problem in certain limits. Such approximations are often computationally simple, but suffer from a limited range of validity.

In this Chapter we review a statistical mechanical approach to the inverse Ising problem [16, 17] based on a selective cluster expansion which improves upon mean field methods. Moreover it avoids overfitting the data by selecting only clusters with significant contributions to the inverse problem, minimizing the impact of finite sampling noise. The outline is as follows. In Section 4.2 we present the selective cluster expansion (SCE) algorithm, developed by Cocco and Monasson, which gives an approximate solution to the inverse Ising problem. Section 4.3 details some algorithmic and numerical improvements of the cluster algorithm, which have collectively allowed for the application of this algorithm to much larger data sets, and have improved the speed of the algorithm significantly. Numerical tests of the algorithm on real data from recordings of neuronal networks are detailed in Section 4.4.

4.2 Selective cluster expansion algorithm

When an exact computation of the partition function is out of reach, and interactions are strong such that high temperature expansions are not helpful, an accurate estimate of the interactions which solve the inverse Ising problem can be obtained through cluster expansions. Cluster expansions have a rich history in statistical mechanics, *e.g.* the virial expansion in the theory of liquids or cluster variational methods [48].

The recently proposed selective cluster expansion algorithm of Cocco and Monasson [16, 17] makes use of an assumption about the properties of the inverse of the susceptibility matrix, χ^{-1}, to efficiently generate an approximate solution to the inverse Ising inference problem. The inverse susceptibility gives the response of the inferred interactions to a small change in the correlations $\mathbf{p}^*$. χ^{-1} is typically much sparser and shorter range than χ (see for example results for the Ising model with nearest-neighbor interactions, reported in [17]), implying that most interactions inferred from a given set of data depend strongly on only a small set of correlations. Thus an estimate of the

interactions for the entire system can be constructed by solving the inference problem on small subsets (clusters) of spins and combining the results. The SCE gives such an estimate by recursively solving the inverse Ising problem on small clusters of spins, selecting the clusters which give significant information about the underlying interaction graph according to their contribution to the entropy S of the inferred Ising model, and building from these a new set of clusters to analyze. At the end of this cluster expansion procedure, an estimate of the entropy and of the interactions for the full system is produced based on the values inferred on each cluster.

We note that the assumption that χ^{-1} is sparse and short-ranged does not necessarily hold in all cases. However, in applications to real data this is precisely the case which we are most interested in, as the inferred network of interactions will be stable under small changes in the experimental measurements. If, on the other hand, the inverse susceptibility matrix is dense with many large entries, even small perturbations such as the inclusion or exclusion of a single spin in the system could significantly affect the inferred interactions. As typical experiments involve observations of only small subsets of a much larger system, global sensitivity to small changes of the components of the system would render the inferred Ising model physically meaningless, even if the inverse problem is technically well-posed [17].

Let S_Γ denote the entropy of the Ising model defined just on a subset $\Gamma = \{i_1, i_2, \ldots\}$ of the full set of spins, which reproduces the one- and two-point correlations obtained from data for this subset. The entropy S of the inferred Ising model on the full system of N spins can then be expanded formally as a sum of individual contributions from each of the $2^N - 1$ nonempty subsets,

$$S = \sum_\Gamma \Delta S_\Gamma, \qquad \Delta S_\Gamma = S_\Gamma - \sum_{\Gamma' \subset \Gamma} \Delta S_{\Gamma'} \,. \tag{4.15}$$

The cluster entropy ΔS_Γ, defined recursively in (4.15), measures the contribution of the cluster Γ to the total entropy. It is calculated by substracting the cluster entropies of all subsets of Γ from S_Γ. Each cluster entropy depends only upon the correlations between the spins in that cluster, and for small clusters it is easy to compute numerically. The contribution of each cluster to the interactions, which we denote $\Delta \mathbf{J}_\Gamma$, is defined

analogously and computed at the same time as the cluster entropy. The elements of $\mathbf{J}_\Gamma$ are the couplings and fields which minimize the cross entropy S^* restricted to the cluster Γ.

As an example, the entropy of a single-spin cluster is, using (4.15) with $N = 1$,

$$\Delta S^{(1)}_{(i)}(p^*_i) \equiv S^{(1)}_{(i)} = -p^*_i \log p^*_i - (1 - p^*_i) \log(1 - p^*_i). \tag{4.16}$$

The contribution to the field of a single-spin cluster is

$$\Delta h^{(1)}_i \equiv h^{(1)}_i = -\frac{\partial S^{(1)}_{(i)}}{\partial p^*_i} = \log\left(\frac{p^*_i}{1 - p^*_i}\right). \tag{4.17}$$

The entropy of a two spin subsystem $\{i, j\}$ is

$$\begin{aligned} S^{(2)}_{(i,j)}(p^*_i, p^*_j, p^*_{ij}) = &- p^*_{ij} \log p^*_{ij} - (p^*_i - p^*_{ij}) \log (p^*_i - p^*_{ij}) \\ &- (p^*_j - p^*_{ij}) \log (p^*_j - p^*_{ij}) \\ &- (1 - p^*_i - p^*_j + p^*_{ij}) \log (1 - p^*_i - p^*_j + p^*_{ij}) \end{aligned} \tag{4.18}$$

Using again (4.15) with $N = 2$, we obtain $\Delta S_{(i,j)} = S_{(i,j)} - \Delta S_{(i)} - \Delta S_{(j)}$, which measures the loss in entropy when imposing the constraint $\langle \eta_i \, \eta_j \rangle = p^*_{ij}$ to a system of two spins with fixed magnetizations, $\langle \eta_i \rangle = p^*_i$, $\langle \eta_j \rangle = p^*_j$. The contribution to the field of the two spin cluster is

$$\Delta h^{(2)}_i = \log\left(\frac{p^*_i - p^*_{ij}}{1 - p^*_i - p^*_j + p^*_{ij}}\right) - \Delta h^{(1)}_i, \tag{4.19}$$

and the contribution to the coupling is

$$\begin{aligned} \Delta J^{(2)}_{ij} &\equiv J^{(2)}_{ij} \\ &= \log p^*_{ij} - \log (p^*_i - p^*_{ij}) - \log (p^*_j - p^*_{ij}) + \log (1 - p^*_i - p^*_j + p^*_{ij}) \,. \end{aligned} \tag{4.20}$$

It is difficult to write the entropy analytically for clusters of more than two spins, but S_Γ can be computed numerically as the minimum of the cross-entropy (4.11). This involves calculating Z, a sum over an exponential number of spin configurations. In practice this limits the size of the clusters which we can consider to those with $\lesssim 20$ spins.

A recursive use of (4.15) allows us to obtain ΔS_Γ for larger and larger clusters Γ (see also the pseudocode of Algorithm 1). It is important to note that the form of ΔS_Γ is

such that the sum of the cluster entropies of a cluster Γ and all of its subsets is just the total entropy of the cluster, S_Γ. The analogous result also holds for $\Delta\mathbf{J}$. This means in particular that by construction the sum over all clusters for the full system of N spins yields the exact entropy S and interactions $\mathbf{J}$.

It is also posible to perform the expansion of (4.15) in $S-S_0$, where S_0 is a "reference entropy" approximating S which we expand around. As with S, the reference entropy S_0 should be computable on all subsets of the system, and should depend only on the one- and two-point correlations of the spins in the subsets. Again, by the construction rule (4.15) and independent of the functional form of S_0, summing over all the clusters will give back the exact value of $S-S_0$ for the full system. We will show in applications to neural data (see Section 4.4) that it can be useful to consider an expansion $S-S_{\mathrm{G}}$ rather than S alone, using a Gaussian approximation as a reference entropy S_0. In some cases the expansion of $S-S_{\mathrm{G}}$ converges much faster than the expansion of S alone. We describe the Gaussian approximation in more detail in Appendix C.3.

The cluster entropy measures a cluster's contribution to the total entropy, which could not be gained from its sub-clusters taken separately. Intuitively, we expect that clusters with small $|\Delta S_\Gamma|$ contribute little new information about the underlying interaction graph which is not revealed by any of their subsets. For example, it is easy to see from the form of ΔS for a two-spin cluster that, if the spins are independent, the cluster entropy will be zero as the entropy of the pair of spins is simply equal to the sum of the single spin entropies. It has also been shown [16, 17] that small cluster entropies have a universal distribution, reflecting fluctuations in the experimentally observed correlations due to finite sampling (see Appendix C.2). Cluster entropies that are nonzero due to real interactions between the constituent spins also tend to decrease in magnitude as the cluster size becomes large, decaying exponentially in the size of the shortest closed interaction path between the spins in the cluster. In the SCE therefore all clusters which have $|\Delta S_\Gamma|$ smaller than a fixed threshold T are discarded. Selecting only those clusters which have cluster entropies larger than a chosen threshold helps to avoid the overfitting of noisy data.

Clearly, it is not possible to compute all of the 2^N-1 cluster entropies, corresponding

to all the nonempty subsets of the full set of spins, even for rather small systems. To make the algorithm computationally feasible we must have a method for truncating the cluster expansion. This is implemented in the SCE by a recursive construction rule for the clusters included in the expansion (see the pseudocode of Algorithm 2). We begin with the computation of the cluster entropies for all N clusters of size $k = 1$. The contribution of each cluster to the interactions is also recorded for later use. Each subsequent step follows the same pattern. First, clusters with $|\Delta S_\Gamma| < T$ are removed. We then include in the next step of the expansion all clusters which are unions of two of the remaining clusters of size k, $\Gamma' = \Gamma_1 \cup \Gamma_2$, such that the new cluster Γ' contains $k + 1$ spins.

The expansion naturally terminates when no more new clusters can be formed. This approach prevents a combinatorial explosion of the number of clusters considered in the expansion. It is also consistent with the idea of exploring paths of strong interactions in the interaction graph, as new clusters are built up from smaller clusters which have already been found to have significant interactions and which share many spins in common. Final estimates for the entropy and the interactions are obtained by adding up all of the ΔS_Γ and $\Delta \mathbf{J}_\Gamma$.

4.2.1 Pseudocode of the cluster algorithm

In this section we present pseudocodes useful for the practical implementation of the inference algorithm, following [16].

The principal routine of the cluster algorithm is the iterative computation of the cluster entropy, given in Algorithm 1. When the routine to compute the entropies of various clusters is called several times a substantial speed-up can be achieved by memorizing the entropies ΔS_Γ of every cluster. In Section 4.3 we will discuss how to calculate the subset entropy S_Γ in more detail.

The core of the inference algorithm is the recursive building-up and selection of new clusters, described in Algorithm 2. The threshold T, which establishes which clusters will be kept in the expansion, is a parameter which is fixed in each run of the selective cluster algorithm. The choice of the optimal threshold T^* is discussed in Section 4.2.2.

Algorithm 1 Computation of cluster-entropy ΔS_Γ

Require: Γ (of size K), $\mathbf{p}^*$, routine to calculate S and S_0

$\Delta S_\Gamma \leftarrow S_\Gamma - S_{0,\Gamma}$

for SIZE $= K-1$ **to** 1 **do**

for every Γ' with SIZE spins in Γ **do**

$\Delta S_\Gamma \leftarrow \Delta S_\Gamma - \Delta S_{\Gamma'}$

end for

end for

Output: ΔS_Γ

4.2.2 Convergence and choice of the optimal threshold T^*

In the following we describe the practical procedure for applying the inference algorithm to a set of data.

If we wish to use an inferred Ising model to make predictions, it is best to take into account the estimated statistical fluctuations of the empirical correlations so as to avoid overfitting (i.e. fitting the model to greater precision than is justified by the data), rather than generating as close a fit as possible to the empirical correlations $\mathbf{p}^*$. It is generally observed that models which are adjusted to fit experimental data too closely give poorer predictions of the experimental system's future behavior (for an excellent discussion, see [28, Chapter 7]). As such, when applying the SCE algorithm to data we search for an "optimal" value of the threshold, which we denote T^*, where the difference between the correlations of the inferred Ising model and the empirical correlations is of the same order as the expected fluctuations of the empirical correlations due to finite sampling, see Appendix C.2.

Because we do not know *a priori* the optimal value of the threshold T^* we run the algorithm at different values of the threshold following the iterative heuristic below:

- Start with a large value of the threshold T, typically $T = 1$, at which only single-spin clusters are selected.
- Infer the fields and the couplings at that threshold.

Algorithm 2 Selective Cluster Expansion

Require: N, T, S_0, routine to calculate ΔS_Γ from $\mathbf{p}^*$

LIST $\leftarrow \emptyset$ {All selected clusters}

SIZE $\leftarrow 1$

LIST(1) $\leftarrow (1) \cup (2) \cup \ldots \cup (N)$ {Clusters of SIZE=1}

repeat {Building-up of clusters with one more spin}

LIST $\leftarrow$ LIST $\cup$ LIST(SIZE) {Store current clusters}

LIST(SIZE+1) $\leftarrow \emptyset$

for every pair $\Gamma_1, \Gamma_2 \in$ LIST(SIZE) **do**

$\Gamma_I \leftarrow \Gamma_1 \cap \Gamma_2$ {Spins belonging to Γ_1 and to Γ_2}

$\Gamma_U \leftarrow \Gamma_1 \cup \Gamma_2$ {Spins belonging to Γ_1 or to Γ_2}

if Γ_I contains (SIZE-1) spins **and** $|\Delta S_{\Gamma_U}| > T$ **then**

LIST(SIZE+1) $\leftarrow$ LIST(SIZE+1) $\cup \Gamma_U$ {add Γ_U to list of selected clusters}

end if

end for

SIZE $\leftarrow$ SIZE+1

until LIST(SIZE) $= \emptyset$

$S \leftarrow S_0$, $J \leftarrow -\frac{d}{d\mathbf{p}^*} S_0$ {Calculation of S, $\mathbf{J}$}

for $\Gamma \in$ LIST **do**

$S \leftarrow S + \Delta S_\Gamma$, $\mathbf{J} \leftarrow \mathbf{J} - \frac{d}{d\mathbf{p}^*} \Delta S_\Gamma$

end for

Output: S, $\mathbf{J}$ and LIST of clusters

- If the number of selected clusters has changed with respect to the previous value of the threshold, run a Monte Carlo simulation of the inferred Ising model to check the reconstruction of the correlations. From the Monte Carlo simulation we obtain reconstructed correlations $\mathbf{p}^{\rm rec}$ and calculate the relative errors on the reconstructed averages and connected correlations $c_{ij}^{\rm rec} = p_{ij}^{\rm rec} - p_i^{\rm rec}\, p_j^{\rm rec}$ with respect to their statistical fluctuations due to finite sampling,

$$\epsilon_p = \left(\frac{1}{N} \sum_i \frac{(p_i^{\rm rec} - p_i^*)^2}{(\delta p_i^*)^2} \right)^{\frac{1}{2}}, \quad \epsilon_c = \left(\frac{2}{N\,(N-1)} \sum_{i<j} \frac{(c_{ij}^{\rm rec} - c_{ij}^*)^2}{(\delta c_{ij}^*)^2} \right)^{\frac{1}{2}}. \tag{4.21}$$

  The denominators in (4.21) measure the typical fluctuations of the data expected at thermal equilibrium, see (C.13), (C.16), and

$$\delta c_{ij}^* \approx \delta p_{ij}^* + p_i^* \delta p_j^* + p_j^* \delta p_i^* \,. \tag{4.22}$$

- Iterate this procedure by lowering the threshold T and stopping when the errors $\epsilon_p \simeq 1$, $\epsilon_c \simeq 1$. The corresponding value of the threshold is the optimal threshold T^*.

Note that T^* is chosen as the first value of the threshold such that $\epsilon_p \simeq 1, \epsilon_c \simeq 1$ in order to reconstruct the data with the simplest possible network of interactions. Decreasing the threshold more than is necessary to fit the one- and two-point correlations is undesirable not only because the complicated structure of interactions due to overfitting will not necessarily correspond well with the underlying interaction network, but also because progressively lower values of the threshold increase the computational difficulty of the inference problem. We note however that there is no risk of overfitting data which has been perfectly sampled. In this case, as there is no sampling noise, one is justified in fitting the model to the data as tightly as is practically possible.

4.3 Numerical methods

In this section we review some of the computational challenges of the algorithm and numerical methods for running the algorithm efficiently.

The primary computational bottleneck of the selective cluster expansion algorithm is the repeated solution of the inverse Ising problem and the computation of the entropy on each K-spin cluster in the expansion, which is used to calculate the cluster entropy (see Algorithm 1).

For each cluster Γ the partition function of the K-spin system restricted to Γ,

$$Z_\Gamma(\mathbf{J}) = \sum_{\{\eta_i=0,1;\, i\in\Gamma\}} \exp\left(\sum_{i\in\Gamma} h_i\,\eta_i + \sum_{j>i;\ i,j\in\Gamma} J_{ij}\,\eta_i\,\eta_j\right), \tag{4.23}$$

can be computed in time $\propto 2^K$. Then one has to find the most likely set of $\{J_{ij}\}$ and $\{h_i\}$ for each cluster given the experimental data, that is, we must solve the convex optimization problem

$$\min_{\mathbf{J}}\left(S^*_\Gamma(\mathbf{p}^*,\mathbf{J}) = \log Z_\Gamma(\mathbf{J}) - \sum_{i\in\Gamma} h_i\,p^*_i - \sum_{j>i;\,i,j\in\Gamma} J_{ij}\,p^*_{ij}\right). \tag{4.24}$$

No analytical solution exists for clusters of more than a few spins. As a single run of the cluster expansion algorithm may include thousands or even millions of clusters, it is critically important that the optimization problem (4.24) be solved as quickly as possible.

Given a starting value for the $\mathbf{J}$, we employ a hybrid approach which combines the standard optimization techniques of gradient descent and Newton's method to step progressively closer to the minimum. Gradient descent steps are chosen along the direction of steepest descent, while Newton's method specifies a step direction towards the minimum of a local quadratic approximation of S^*. When far from the minimum, we use gradient descent for its computational simplicity and numerical stability. Once the $\mathbf{J}$ are determined to be close to the values which solve (4.24), we switch to Newton's method, which requires more computational resources but has a much better rate of convergence near the minimum [44].

A careful choice of the initial conditions is also essential for obtaining a fast solution with minimal computational effort. We begin the optimization problem with an initial guess for $\mathbf{J}$ based upon the assumption that the couplings and fields minimizing S^* will be similar to those that were found for smaller clusters containing the same sites. That

is, we assume

$$\Delta \mathbf{J}_\Gamma \approx 0, \tag{4.25}$$

which implies

$$\mathbf{J}_\Gamma \approx \sum_{\Gamma' \subset \Gamma} \Delta \mathbf{J}_{\Gamma'}. \tag{4.26}$$

In many cases the initial guess (4.26) works very well, and the optimization routine may find the minimum with just a single step. Just including this choice for the initial interactions can cut the total running time of the algorithm in half.

As described in Section 4.1, we may regularize the interactions $\mathbf{J}$, and in particular the couplings $\{J_{ij}\}$, by adding a penalty term to S^* for each coupling which is nonzero. Regularization is useful for controlling large couplings that arise from noise or undersampling of the experimental system, as well as ensuring the convexity of the susceptibility χ, so that the inference problem has a unique solution at a finite value of the couplings. Common choices of the penalty are based on the L_1-norm

$$\gamma \sum_{j>i} |J_{ij}| \tag{4.27}$$

or the L_2-norm

$$\gamma \sum_{j>i} J_{ij}^2. \tag{4.28}$$

Such terms are natural in the context of Bayesian inference. The addition of (4.27) to S^* is equivalent to assuming a Laplacian prior distribution for the couplings, while the L_2-norm penalty (4.28) corresponds to a Gaussian prior. In this framework the regularization strength γ is proportional to $1/B$, so that in the limit of perfect sampling the regularization strength goes to zero.

Use of the L_1-norm penalty makes the optimization problem more difficult, as the function to be minimized is no longer smooth. In particular, in this case the gradient of S^* is undefined when any of the couplings $J_{ij} = 0$. To overcome the lack of differentiability of S^* we use a modified version of the projected scaled sub-gradient method of [55]. This method makes use of the sub-gradient, a generalization of the gradient which is well-defined even when some couplings are zero. It also allows couplings to be set exactly to zero during the step process, unlike a typical gradient descent or Newton's

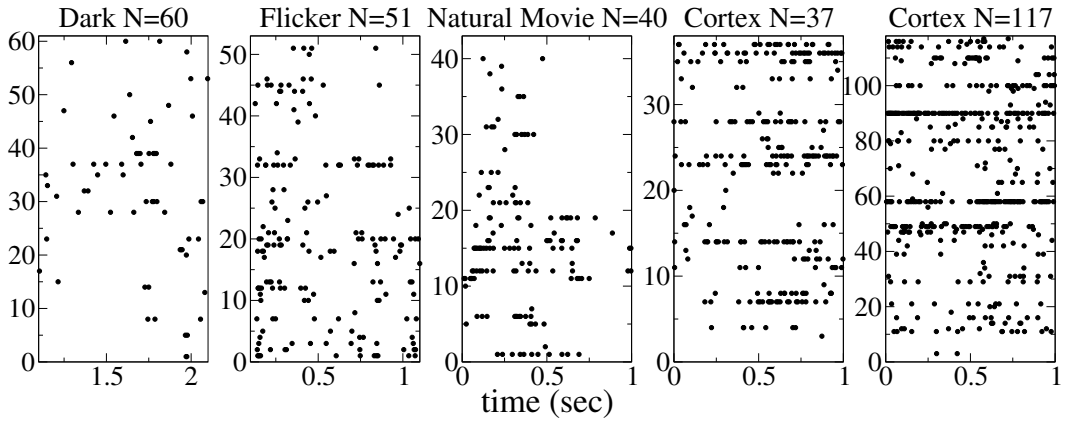

Figure 4.1: Raster plot of spike train data from recordings of neuron populations: in the retina in dark conditions ($N = 60$ cells) and with a random flickering stimulus ($N = 51$ cells), data by M. Meister; in the retina with a natural movie stimulus ($N = 40$ cells), data by M. Berry; in the prefrontal cortex of a rat ($N = 37$ cells), data by A. Peyrache and F. Battaglia; in the medial prefrontal cortex of a rat ($N = 117$ cells), data by G. Buzsáki and S. Fujisawa. Recordings last for 30 minutes – 1 hour, here we plot only 1 s of the recording. One can translate the continuous time data in the raster plot into binary patterns of activity by arranging the time interval into bins of size Δt and recording whether or not each neuron spikes within each time bin. The probability p_i that a neuron i spikes in a time window of size Δt is the number of windows in which the neuron i is active divided by the total number of time windows. The probability p_{ij} that two neurons i, j are active in the same time window is given by the number of time windows in which both the neurons are active divided by the total number of time windows.

method step. Despite these additional complexities the optimization problem including the L_1-norm penalty can be solved with similar speed and accuracy as in the L_2-norm regularized or unregularized case.

4.4 Applications to real data

As an example of potential applications of the Selective Cluster Expansion algorithm (SCE) we have re-analyzed, following [15], several sets of real data from multielectrode recordings of collections of neurons. We examine *in vitro* recordings of salamander retinal ganglion cells:

- A 4450 second recording of 51 ganglion cells in a retina illuminated with randomly

flickering bright squares [57]. The recording is made with a multielectrode array on a surface of about 1 mm^2, and approximately 20% of the ganglion cells on that surface are recorded.

- A 2000 second recording of the spontaneous activity of 60 cells of the same retina as above observed in total darkness, of which 32 cells are common to the recording with randomly flickering stimulus [57].

- A recording of 40 cells in a salamander retina presented with a 120 second natural movie repeated 20 times. This recording is much denser; approximately 90% of the ganglion cells on the analyzed surface are recorded [56].

We also study several *in vivo* recordings of neurons in the medial prefrontal cortex of a rat during a working memory task:

- A 1500 second recording of 37 cells with tetrodes, each consisting of of four electrodes, which record both superficial and deep layers of the medial prefrontal cortex [49].

- A 2800 second recording of 117 cells with silicon probes which record both superficial and deep layers of the medial prefrontal cortex [25].

Fig. 4.1 shows the neural activity in the first second of recordings of the different data sets. The data presented here is in the form of spike trains – a list of all of the times at which a particular neuron fired – for each neuron observed in the experiment. To translate this continuous-time data into a binary form, consistent with the Ising model, we first divide the total time interval of a recording of the activity into small time bins of size Δt. The activity is then represented by set of binary variables $\eta_i^{(k)}$, where $k = 1, \ldots, B$ labels the time bin and $i = 1, \ldots, N$ is a label which refers to a particular neuron. In the data we consider N spans a few decades (30 to 120). If in bin k neuron i has spiked at least once then we set $\eta_i^{(k)} = 1$, otherwise $\eta_i^{(k)} = 0$. Empirical correlations are then computed as described in Section 4.1.

Spiking frequencies and pairwise correlations (i.e. one- and two-point correlations) for a fixed time window are shown in Fig. 4.4 and Fig. 4.5, along with fits from the

inferred Ising model. We observe from these figures that in cortical data the frequency of the activity is higher, and in particular some cells spike very rapidly. The retinal recordings are stationary in the sense that that the spiking frequencies and pairwise correlations of the data do not change over time, at least on the time scale of 120 seconds in the recording with a natural movie stimulus. The cortical data sets, however, are nonstationary. In particular some cells are active only in part of the recording of the 117 cells in medial prefrontal cortex. Note that in the analysis we present here data are considered to be stationary and the time dependence is not explicitly taken into account.

For each data set, the values of the correlation indices

$$CI_{ij} = \frac{p^*_{ij}}{p^*_i\, p^*_j} \tag{4.29}$$

give some indication of the strength of the interactions between the spins. Neglecting all other spins in the system, the approximation

$$J^{(2)}_{ij} = \log CI_{ij} = \log \frac{p^*_{ij}}{p^*_i\, p^*_j} \tag{4.30}$$

is close to the real coupling J^*_{ij}, assuming that network effects are minor and that the coupling is weak. Histograms of the correlation indices for pairs of spins in each data set are presented in Figs. 4.8 and 4.9, along with the best inferred value of the couplings. Here one can see that the correlation indices for the $N = 37$ Cortical data set (CA) are particularly small, implying that the interactions are weak and the inference problem is easier. When the correlation indices are large the magnitude of the couplings will be also be larger. In this case the convergence of the SCE and the optimal expansion variable (*i.e.* $S - S_{\rm G}$ or S with no reference entropy) will depend on the structure of the interactions. We explore this point in more detail below.

4.4.1 Performance of the algorithm for retinal data

We show the behavior of the reconstruction errors ϵ_p and ϵ_c as a function of the threshold T on the retinal data in Fig. 4.2 for the expansion of $S - S_{\rm G}$. Results on the convergence of the algorithm and on the value of the inferred entropy are summarized in Table 4.1

for the different procedures tested, including expansions without the reference entropy. These results include the value of the optimal threshold T^*, as well as size of the largest cluster in the expansion $K_{\max}$, the total number of clusters processed $N_{\rm tot}$, the total number of clusters selected at $N_{\rm sel}$, and the inferred value of the entropy S, all evaluated at T^*.

As shown in the figures and in the table a Gaussian approximation reference entropy S_G is helpful for the inference problem when the SCE is applied to retinal data. The threshold T^* is lower for the expansion of S alone, implying an increase in the number of processed clusters and a larger value for $K_{\max}$. For the flickering stimulus (Fl) the procedure without reference entropy did not converge even at a low value of the threshold. Here small couplings, which would have been obtained through the Gaussian couplings in the expansion of $S - S_{\rm G}$, are important for the proper reconstruction of the correlations. Decreasing the threshold enough to fit many small couplings drives the SCE algorithm to consider very large clusters ($K_{\max} = 17$ at the smallest value of T tested), which slows the algorithm considerably.

We have also studied the inference problem on subsets of the full data sets described above. As shown in the right column of Fig. 4.2, the value of the theshold T^* and the maximum cluster size $K_{\max}$ for large subsets of spins are of the same order of magnitude as for the full set. Moreover the number of clusters selected increases approximately linearly with the system size. This property was related in [16, 17] to the *locality* of the coupling-susceptibility χ^{-1}, and was shown to hold on artificial data of unidimensional and bidimensional Ising models.

4.4.2 Performance of the algorithm for cortical data

As expected from the small values of the correlation indices the SCE applied to the cortical recording of $N = 37$ neurons (CA) works very well for expansions both with and without the Gaussian reference entropy. Indeed, the expansion converges already at just $K_{\max} = 2$ with the reference entropy, and $K_{\max} = 4$ without it. For the cortical recording of $N = 117$ cells we have tested the performance of the algorithm with time bins of size $\Delta t = 5$ ms (C5) and $\Delta t = 20$ ms (CB). In both cases the convergence of

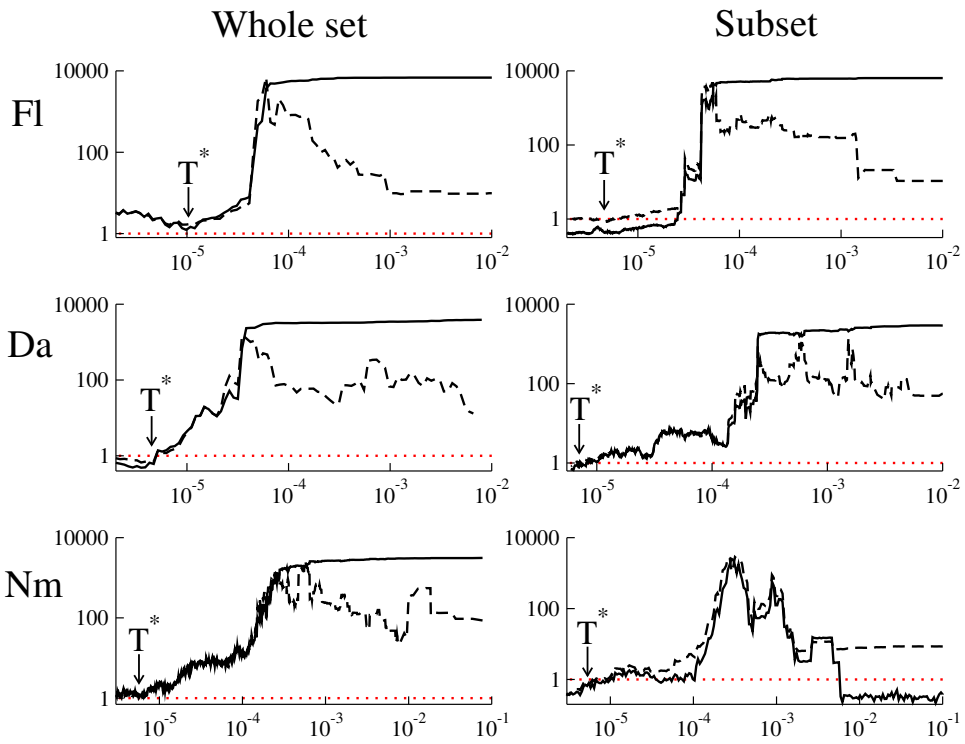

Figure 4.2: Performance of the SCE of $S - S_{\mathrm{G}}$ with L_2 norm regularization on retinal data as a function of the threshold T. The reconstruction errors ϵ_p (solid) and ϵ_c (dashed) (4.21) are computed from Monte Carlo simulations. The value $\epsilon = 1$ is indicated by a red dotted line, and the selected optimal threshold T^* is marked in each plot with an arrow. Fl : flickering stimulus, left whole set of 51 cells, right subset of 32 cells; Da : dark, left whole set of 60 cells, right subset of 32 cells; Nm : natural movie stimulus, left whole set of 40 cells, right subset of 20 cells.

Retinal data							
		Fl 51	Fl 32	Da 60	Da 32	Nm 40	Nm 20
	T^*	9.8×10^{-6}	6.5×10^{-6}	3.5×10^{-6}	6.0×10^{-6}	5.6×10^{-6}	3.7×10^{-5}
$S - S_{\mathrm{G}}$	$K_{\max}$	6	7	11	8	9	5
L_2 norm	N_{tot}	1.1×10^4	4700	7.6×10^4	9200	6.8×10^4	930
	N_{sel}	1450	840	1.0×10^4	1700	1.0×10^4	190
	T^*	6.2×10^{-6}	6.7×10^{-6}	5.0×10^{-6}	8.2×10^{-6}	6.6×10^{-6}	3.5×10^{-5}
$S - S_{\mathrm{G}}$	$K_{\max}$	7	7	9	8	9	5
L_1 norm	N_{tot}	1.5×10^4	4500	5.1×10^4	7300	5.8×10^4	940
	N_{sel}	2000	830	7500	1400	8500	190
	T^*	$< 6.0 \times 10^{-7}$	1.2×10^{-6}	2.7×10^{-6}	6.1×10^{-6}	1.1×10^{-6}	6.4×10^{-6}
S	$K_{\max}$	> 17	9	11	9	15	7
L_1 norm	N_{tot}	$> 3.0 \times 10^5$	3.8×10^4	3.1×10^5	2.6×10^4	1.7×10^6	5900
	N_{sel}	$> 3.2 \times 10^4$	6400	3.3×10^4	4100	2.4×10^5	1300
Same for all	S	3.5	2.2	4.6	2.5	3.7	1.9

Table 4.1: Convergence of the Selective Cluster Expansion on retinal data. In cases where the algorithm did not easily converge, bounds on the minimum or maximum quantities necessary to obtain a good fit to the data are given, determined by the lowest value of the threshold considered.

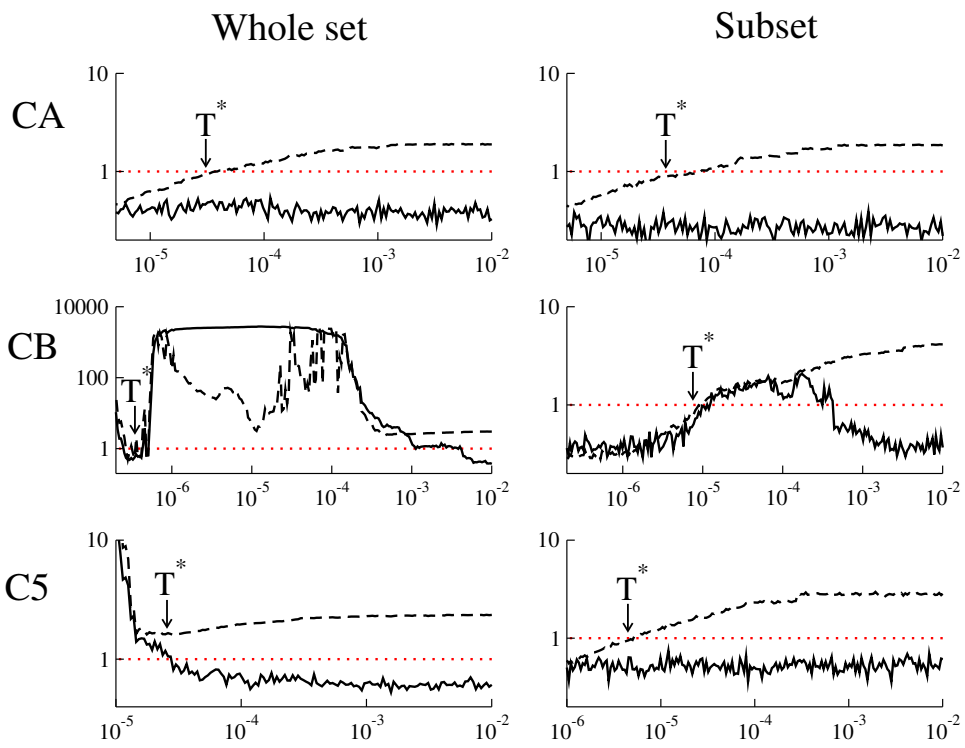

Figure 4.3: Performance of the SCE of S with L_1 norm regularization on cortical data as a function of the threshold T. The reconstruction errors ϵ_p (solid) and ϵ_c (dashed) (4.21) are computed from Monte Carlo simulations. The value $\epsilon = 1$ is indicated by a red dotted line, and the selected optimal threshold T^* is marked in each plot with an arrow. CA : cortex recording of 37 cells; CB : cortex recording of 117 cells analyzed with a time bin of 20 ms; C5 : cortex recording of 117 cells analyzed with a time bin of 5 ms.

Cortical data							
		CA 37	CA 20	CB 117	CB 30	C5 117	C5 30
	T^*	7.8×10^{-6}	7.8×10^{-6}	$< 8.0 \times 10^{-8}$	1.0×10^{-5}	$< 5.0 \times 10^{-8}$	5.3×10^{-6}
$S - S_{\mathrm{G}}$	$K_{\max}$	2	3	> 11	4	> 8	3
L_2 norm	N_{tot}	910	230	$> 5.6 \times 10^5$	940	$> 2.1 \times 10^5$	570
	N_{sel}	91	32	$> 2.3 \times 10^4$	110	$> 5.4 \times 10^4$	64
	T^*	7.8×10^{-6}	7.8×10^{-6}	$< 8.0 \times 10^{-8}$	9.9×10^{-6}	$< 5.0 \times 10^{-8}$	7.8×10^{-6}
$S - S_{\mathrm{G}}$	$K_{\max}$	3	3	> 10	4	> 8	3
L_1 norm	N_{tot}	920	230	$> 5.4 \times 10^5$	920	$> 2.0 \times 10^5$	530
	N_{sel}	93	32	$> 2.2 \times 10^4$	110	$> 5.2 \times 10^4$	55
	T^*	3.4×10^{-5}	5.7×10^{-5}	2.5×10^{-7}	2.9×10^{-5}	2.0×10^{-5}	4.8×10^{-6}
S	$K_{\max}$	4	3	10	4	4	3
L_1 norm	N_{tot}	1300	270	4.4×10^6	5000	1.6×10^4	1200
	N_{sel}	140	40	1.7×10^5	580	630	140
Same for all	S	6.6	3.8	14.7	3.3	5.9	1.2

Table 4.2: Convergence of the Selective Cluster Expansion on cortical data. In cases where the algorithm did not easily converge, bounds on the minimum or maximum quantities necessary to obtain a good fit to the data are given, determined by the lowest value of the threshold considered.

the algorithm was faster in without the reference entropy (see Table 4.2). Expansions of $S - S_G$ converged very slowly, and the relative errors ϵ_p, ϵ_c did not approach one at a threshold $T \approx 10^{-7}$.

The poor performance of the expansion of $S - S_{\mathrm{G}}$ for cortical data, and the success of the expansion in S alone, is in stark contrast with the analysis of retinal recordings. This phenomenon is related to the fact that the interaction network which is capable of fitting the cortical data is relatively dilute and with a few large couplings, for which the Gaussian result is a poor approximation. The presence of a reference entropy makes reconstructing the empirical correlations more difficult in this case, as the inferred interaction network is then fully connected (even if many of these couplings are small).

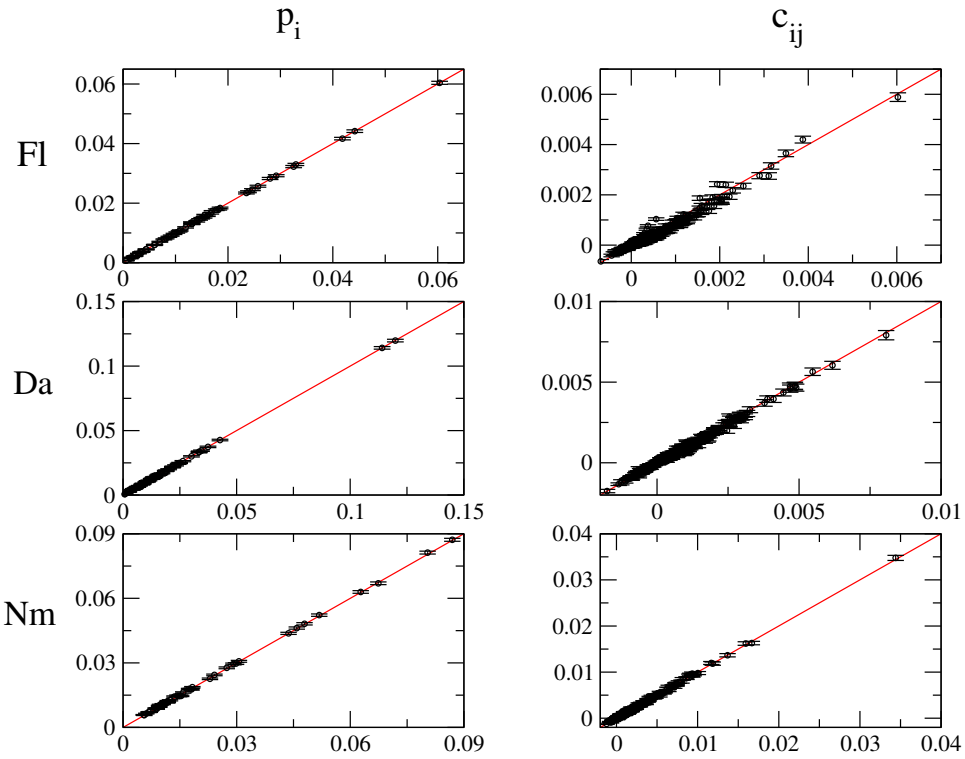

Figure 4.4: Spiking frequencies p_i^{rec} and connected correlations c_{ij}^{rec} for retinal data sets calculated from a Monte Carlo simulation of the inferred Ising model (vertical) versus the experimental values p_i^*, c_{ij}^* (horizontal). The error bars are given by the statistical fluctuations δp_i^*, δc_{ij}^*.

4.4.3 Reconstruction of the one- and two-point correlations

The spiking probabilities and connected correlations obtained from Monte Carlo simulations with the inferred parameters at T^* are close to those obtained from experiments, as shown in Fig. 4.4 and Fig. 4.5. Indeed the conditions $\epsilon_c \simeq 1$, $\epsilon_p \simeq 1$ specify that the difference between the inferred and empirical correlations is approximately the same as the statistical uncertainty of the empirical correlations due to sampling a finite number of configurations. We find that the reconstruction of the $\mathbf{p}^*$ is equally good for all different choices of the reference entropy and regularization, provided of course that they reach a threshold T^* at which ϵ_c, $\epsilon_p \simeq 1$.

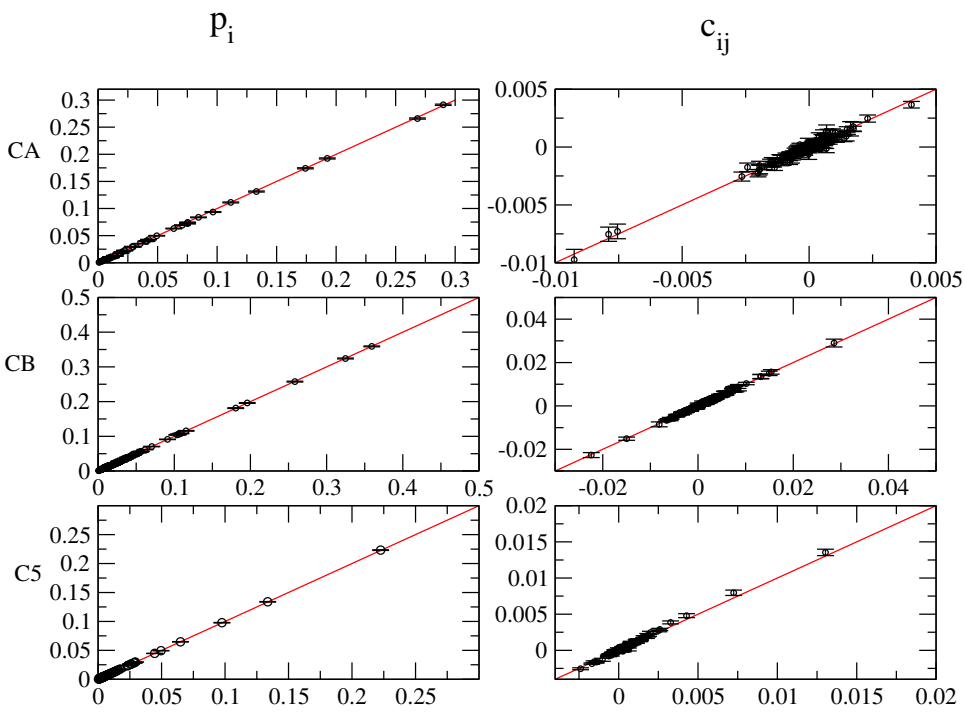

Figure 4.5: Spiking frequencies p_i^{rec} and connected correlations c_{ij}^{rec} for retinal data sets calculated from a Monte Carlo simulation of the inferred Ising model (vertical) versus the experimental values p_i^*, c_{ij}^* (horizontal). The error bars are given by the statistical fluctuations δp_i^*, δc_{ij}^*.

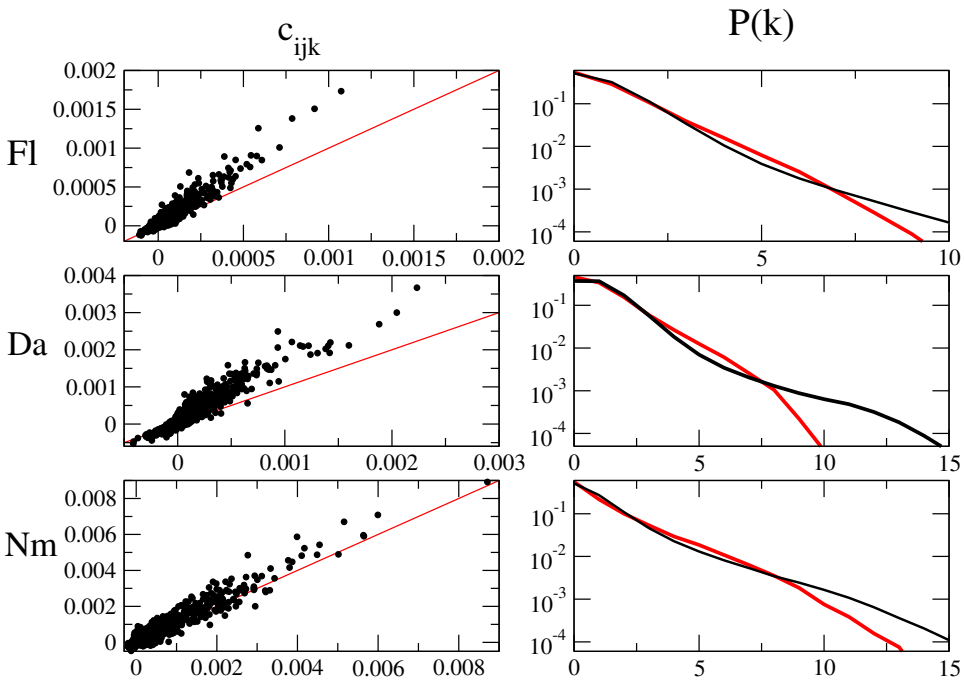

Figure 4.6: Reconstructed three-cell connected correlations $c^{\rm rec}_{ijk}$ (vertical), and probability $P^{\rm rec}(k)$ that k cells spike in the same time bin (black), versus the experimental ones c^{*}_{ijk} (horizontal) and $P^{*}(k)$ (red) from retina recordings. The reconstructed values are obtained from a Monte Carlo simulation of the inferred Ising model at T^{*}.

4.4.4 Reconstruction of three-cell correlations and multi-neuron firing frequencies

We have verified that the three-cell connected correlations c_{ijk} and the multi-neuron firing frequencies (i.e. the probability $P(k)$ that k cells spike in the same bin) are also quite well reproduced by the inferred Ising model, as shown in Figs. 4.6 and 4.7. Note that for the cortical recording of 37 cells (CA) and of 117 cells analyzed with $\Delta t =$ 5 ms (C5) the connected three-cell correlations are in most cases so small that it is difficult to separate them from the sampling noise. We have therefore also plotted the correlations p_{ijk}, which is the probability that the three cells spike in the same time bin, in Fig. 4.7. We emphasize that, unlike the reconstruction of the one- and two-point correlations, there are no *a priori* reasons that the Ising model should also reconstruct the higher moments of the experimental distribution, because it is not the true model

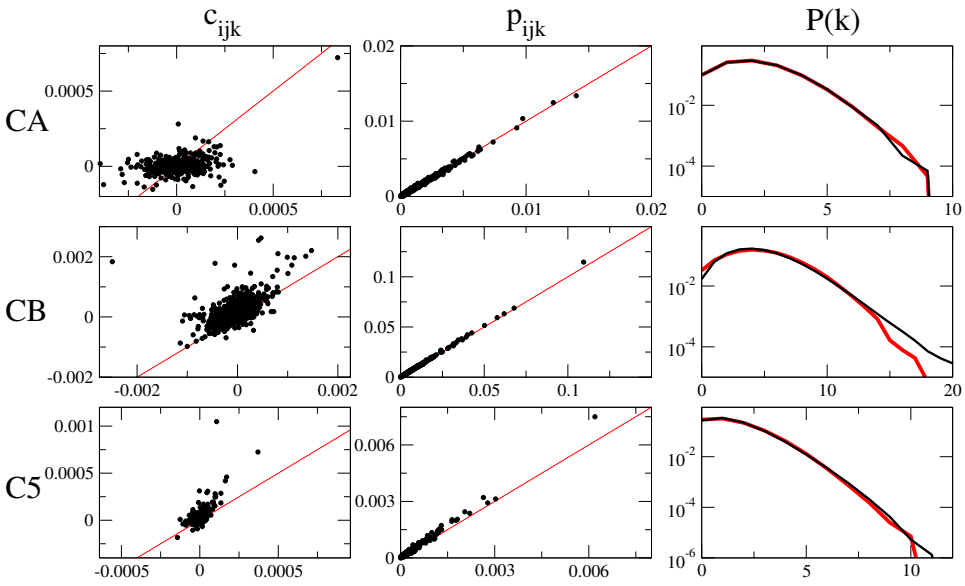

Figure 4.7: Reconstructed three-cell correlations $p^{\rm rec}_{ijk}$ and connected correlations $c^{\rm rec}_{ijk}$ (vertical), and probability $P^{\rm rec}(k)$ that k cells spike in the same time bin (black), versus the experimental ones p^{*}_{ijk}, c^{*}_{ijk} (horizontal) and $P^{*}(k)$ (red) from cortex recordings. The reconstructed values are obtained from a Monte Carlo simulation of the inferred Ising model at T^{*}.

which has generated the data, and these measurements are not used as constraints in the inference. Nevertheless this model seems to reproduce fairly well the statistics of the data, at least for the c_{ijk} and the $P(k)$.

Intuitively the reason for such success could be simply due to the fact that the number of effective configurations the system explores is 2^S, which should be compared with the number of parameters $N\,(N+1)/2$ that we use to fit the distribution (see discussion in [15]). In principle any model with a number of parameters similar to the effective number of configurations could be equally good. For the data sets we have analyzed with $N \leq 60$, (see Tables 4.1 and 4.2) we have that $N\,(N+1)/2 > 2^S$. For larger systems with more than one hundred cells, the exponential growth of 2^S with N, due to the fact that $S \propto N$, will be difficult to compensate with the increase of the number of parameters $\propto N^2$. For the recording of 117 cortical neurons with time bins of size 5 ms we have $S = 5.9$ so $2^S < N\,(N+1)/2$, but for 20 ms for we obtain $N\,(N+1)/2 = 6900$ while $2^S = 2.6 \times 10^4$. Even here the reconstruction of the higher moments is still quite good. This could indicate that the Ising model, which is the

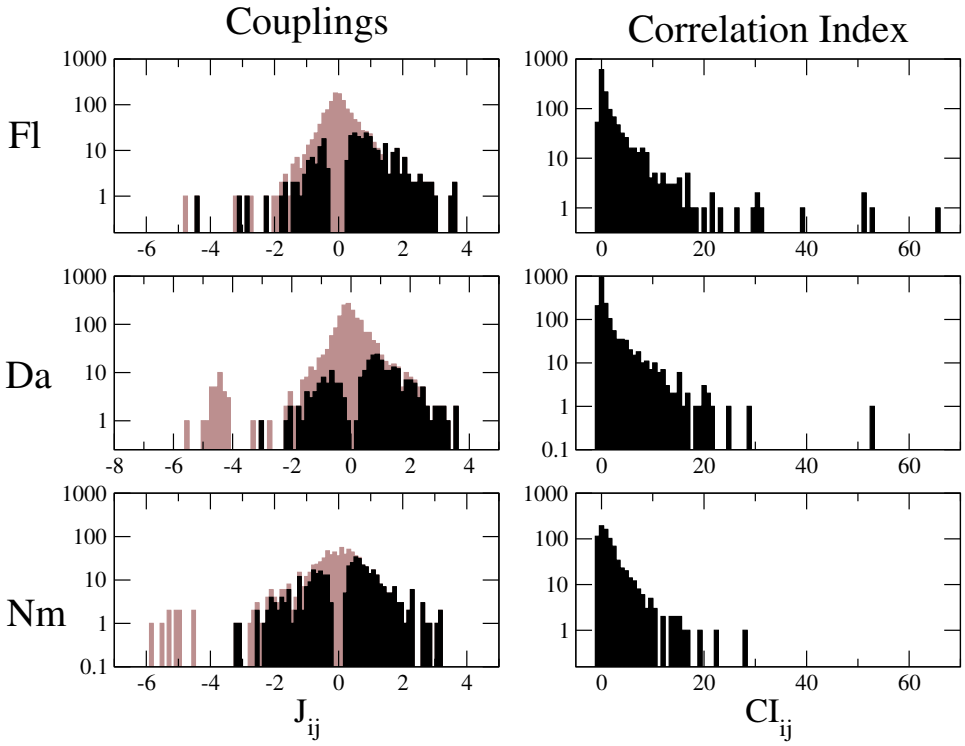

Figure 4.8: Histogram of couplings for retinal data, compared to the histogram of correlation indices. Reliable couplings are marked in black, and unreliable couplings are marked in brown.

maximal entropy model, is really a good model for the neural activity.

4.4.5 Reliability of inferred couplings

Uncertainties in the inferred interactions δJ_{ij} due to finite sampling can be computed from (C.18) (see Appendix C.2 for a brief derivation). Fig. 4.8 and Fig. 4.9 show the the histogram of couplings in which we distinguish *reliable* couplings, for which $|J_{ij}|/\delta J_{ij} > 3$, from *unreliable* couplings, which are compatible with zero within the error bars. As expected, because of the sampling fluctuations there are many unreliable couplings (particularly small couplings), but it is important to note that these may still be necessary to accurately reproduce the correlations. Large reliable couplings generally correspond to large correlation indices, but the converse is not necessarily true.

As shown in Fig. 4.8 correlation indices are large in the retinal data and many couplings have large values, with magnitudes up to $|J_{ij}| \approx 4$. The histogram of couplings

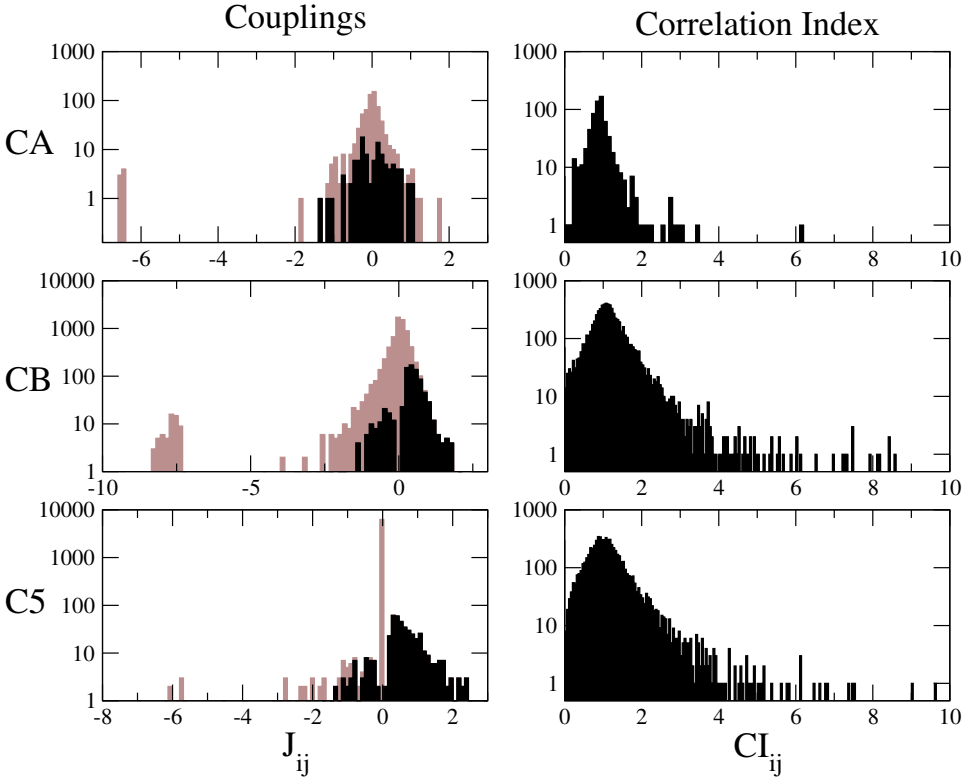

Figure 4.9: Histogram of couplings for cortical data, compared to the histogram of correlation indices. Reliable couplings are marked in black, and unreliable couplings are marked in brown.

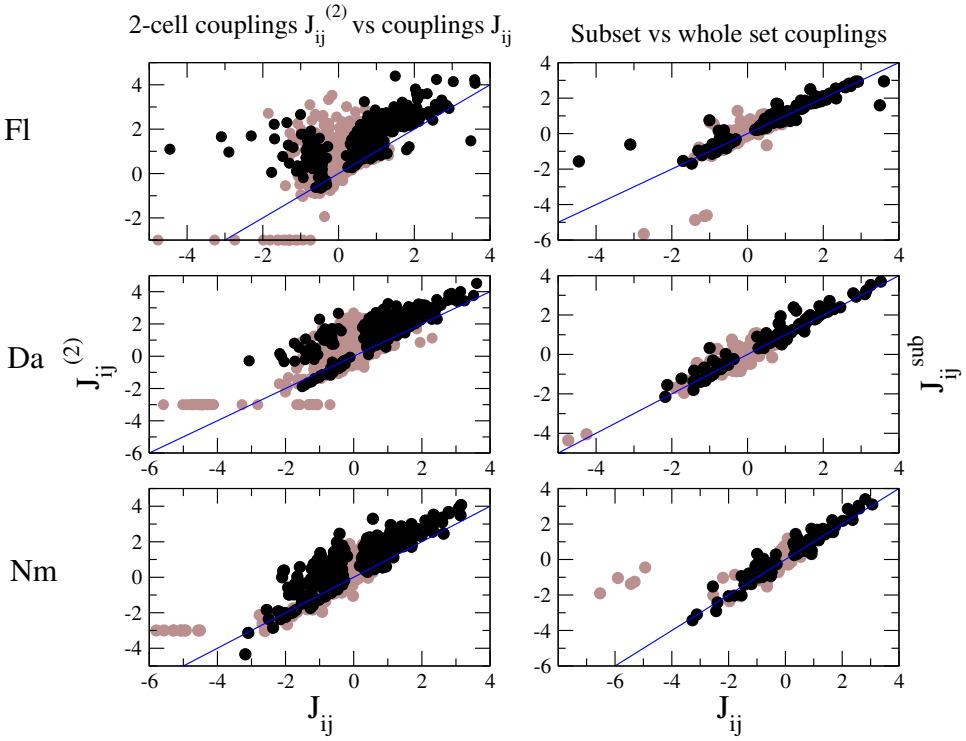

Figure 4.10: Left: two-spin couplings $J^{(2)}$ versus couplings, right: couplings inferred from a subset of cells versus couplings inferred from the whole set. Reliable couplings are marked in black, and unreliable couplings are marked in brown.

is similar for the different data sets. Fig. 4.9 shows that the correlation indices and inferred couplings for the cortical data tend to be smaller. For both data sets there are some large negative couplings, but these are mostly unreliable.

4.4.6 Network effects: comparison with correlation index and with inferred couplings on a subset of data

We investigate the importance of the network effects in the inference by comparing the couplings inferred via SCE with the two-spin couplings $J^{(2)}_{ij}$ (4.30) given by the logarithm of the correlation index, and by comparing the couplings obtained for a full set of data to those obtained when only considering a subset of the whole system. As shown in Fig. 4.10 for retinal data the inferred couplings are generally different from two-spin couplings, indicating that network effects are important. Thus the structure of

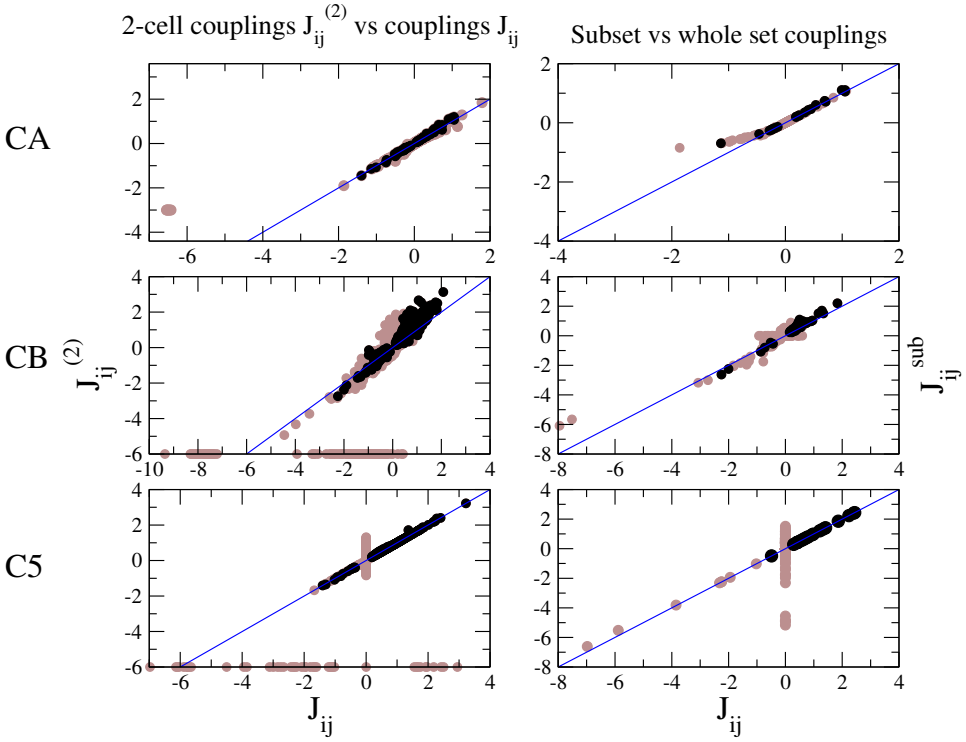

Figure 4.11: Left: two-spin couplings $J^{(2)}$ versus couplings, right: couplings inferred from a subset of cells versus couplings inferred from the whole set. Reliable couplings are marked in black, and unreliable couplings are marked in brown.

the interactions is not a simple reflection structure of the structure of the correlations; a procedure such as the SCE is necessary to disentangle couplings from correlations.

As shown in Fig. 4.10 (right) most of the couplings inferred for the subsets of cells are similar to the ones inferred for the whole set, though some couplings may change in magnitude. The fact that many couplings are similar implies that the inverse susceptibility is local, and therefore each coupling can be inferred from the knowledge of the correlations in a local "neighborhood." Couplings only change if a spin in the neighborhood is removed.

As shown in Fig. 4.11, the correlation indices and the couplings for the 37 cell cortical recording (CA) are very are similar because not only is the interaction network sparse, but also the correlation length is small. The couplings calcuated on a subset are also similar to the ones for the whole set. For the cortical data of 117 cells with $\Delta t = 5$ ms, only some two spin clusters are enough to infer the couplings in the cluster expansion. Neverthless it is important to select the right ones rather than simply including all the two spin clusters in the inference procedure. The inclusion of all the two spin clusters would yield a fully connected interaction graph, much denser than the observed network of couplings, which does not reproduce the observed correlations. Typically the large couplings $J_{ij}^{(2)}$ correspond to real interactions, while the correlations leading to smaller $J_{ij}^{(2)}$ reflect network effects rather than direct interactions. In the cortical data overall network effects are much less pronounced.

4.5 Discussion

In this Chapter we have presented the inverse Ising problem and described one method of solution, the selective cluster expansion (SCE) of the entropy. We have also briefly described numerical and algorithmic methods which improve upon the original implementation of the SCE algorithm [16, 17]. As demonstrated in Section 4.4, we are able to infer an Ising model which accurately reproduces the correlations obtained from a set of experimental data even when the size of the system is large (the maximum we consider being $N = 117$ spins).

Despite the success of the SCE algorithm, there are some limitations which slow down the algorithm particularly in the case of large data sets and which could be improved. First, when a large number of clusters are selected the construction rule for new clusters becomes a time limiting step. This can happen, for example, when considering very low values of the threshold, particularly in the expansion of S without the reference entropy S_{G}. Second, the necessity of using a Monte Carlo simulation to test how well the correlations are reconstructed at each value of the threshold is a drawback, making practical implementation of the algorithm more cumbersome. Some theoretical arguments to estimate the optimal threshold or an approximation in the direct problem could be used to speed up the algorithm, expecially when N is large, and where the thermalization of Monte Carlo simulation can be slow. Future work on the SCE method should attempt to address these issues, and to provide theoretical guarantees for the convergence of the algorithm, which are currently lacking.

As shown in Section 4.4.4, there is evidence that the Ising model with pairwise interactions is in fact able to reproduce features of the data beyond the one- and two-point correlations, even though these features do not appear as constraints in the inference problem. The reason why the maximum entropy approach is successful in this case, and in related applications, is still an open question, and one that merits further research.

Bibliography

[1] D. Ackley, G. Hinton, and T. Sejnowski. A learning algorithm for Boltzmann machines. *Cognitive Science*, 9(1):147–169, 1985.

[2] E. Andjel, M. Bramson, and T. Liggett. Shocks in the asymmetric exclusion process. *Probability Theory and Related Fields*, 78(2):231–247, 1988.

[3] H. Au-Yang and J. H. H. Perk. The Many Faces of the Chiral Potts Model. *arXiv.org*, q-alg, Sept. 1996.

[4] E. Aurell and M. Ekeberg. Inverse Ising inference using all the data. *Physical Review Letters*, 108(9):090201, 2012.

[5] A. Ayyer, E. A. Carlen, J. L. Lebowitz, P. K. Mohanty, D. Mukamel, and E. R. Speer. Phase diagram of the ABC model on an interval. *Journal of Statistical Physics*, 137(5):1166–1204, 2009.

[6] J. Barton and S. Cocco. Accepted.

[7] J. Barton, J. L. Lebowitz, and E. R. Speer. The grand canonical ABC model: a reflection asymmetric mean-field Potts model. *Journal of Physics A: Mathematical and Theoretical*, 44:065005, 2011.

[8] L. Bertini, N. Cancrini, and G. Posta. On the Dynamical Behavior of the ABC Model. *Journal of Statistical Physics*, 144(6):1284–1307, Aug. 2011.

[9] L. Bertini, A. De Sole, D. Gabrielli, G. Jona-Lasinio, and C. Landim. Towards a nonequilibrium thermodynamics: a self-contained macroscopic description of driven diffusive systems. *Journal of Statistical Physics*, 135(5):857–872, 2009.

[10] R. A. Blythe and M. R. Evans. Nonequilibrium steady states of matrix-product form: a solver's guide. *Journal of Physics A: Mathematical and Theoretical*, 40:R333, 2007.

[11] T. Bodineau, B. Derrida, V. Lecomte, and F. van Wijland. Long Range Correlations and Phase Transitions in Non-equilibrium Diffusive Systems. *Journal of Statistical Physics*, 133(6):1013–1031, Nov. 2008.

[12] T. Broderick, M. Dudik, G. Tkačik, R. E. Schapire, and W. Bialek. Faster solutions of the inverse pairwise Ising problem. *arXiv.org*, q-bio.QM, Dec. 2007.

[13] A. Campa, T. Dauxois, and S. Ruffo. Statistical mechanics and dynamics of solvable models with long-range interactions. *Physics Reports*, 2009.

[14] M. Clincy, B. Derrida, and M. R. Evans. Phase transition in the ABC model. *Physical Review E*, 2003.

[15] S. Cocco, S. Leibler, and R. Monasson. Neuronal couplings between retinal ganglion cells inferred by efficient inverse statistical physics methods. *Proceedings of the National Academy of Sciences*, 106(33):14058–14062, 2009.

[16] S. Cocco and R. Monasson. Adaptive Cluster Expansion for Inferring Boltzmann Machines with Noisy Data. *Physical Review Letters*, 106(9), Mar. 2011.

[17] S. Cocco and R. Monasson. Adaptive Cluster Expansion for the Inverse Ising Problem: Convergence, Algorithm and Tests. *Journal of Statistical Physics*, 147(2):252–314, Mar. 2012.

[18] O. Costin and J. L. Lebowitz. On the construction of particle distributions with specified single and pair densities. *The Journal of Physical Chemistry B*, 108(51):19614–19618, 2004.

[19] T. M. Cover and J. A. Thomas. *Elements of Information Theory*. John Wiley & Sons, July 2006.

[20] B. Derrida. An exactly soluble non-equilibrium system: the asymmetric simple exclusion process. *Physics Reports*, 301(1):65–83, 1998.

[21] B. Derrida. Non-equilibrium steady states: fluctuations and large deviations of the density and of the current. *Journal of Statistical Mechanics: Theory and Experiment*, 2007:P07023, 2007.

[22] B. Derrida, M. R. Evans, V. Hakim, and V. Pasquier. Exact solution of a 1D asymmetric exclusion model using a matrix formulation. *Journal of Physics A: Mathematical and General*, 26:1493, 1993.

[23] B. Derrida, S. Janowsky, J. L. Lebowitz, and E. R. Speer. Exact solution of the totally asymmetric simple exclusion process: shock profiles. *Journal of Statistical Physics*, 73(5):813–842, 1993.

[24] G. D. Field and E. J. Chichilnisky. Information processing in the primate retina: circuitry and coding. *Annual Review of Neuroscience*, 30:1–30, 2007.

[25] S. Fujisawa, A. Amarasingham, M. T. Harrison, and G. Buzsáki. Behavior-dependent short-term assembly dynamics in the medial prefrontal cortex. *Nature Neuroscience*, 11(7):823–833, 2008.

[26] C. Furtlehner and G. Fayolle. Stochastic dynamics of discrete curves and multi-type exclusion processes. *Journal of Statistical Physics*, 2007.

[27] E. Ganmor, R. Segev, and E. Schneidman. The architecture of functional interaction networks in the retina. *The Journal of Neuroscience*, 31(8):3044–3054, 2011.

[28] T. Hastie, R. Tibshirani, and J. H. Friedman. *The Elements of Statistical Learning.* Data Mining, Inference, and Prediction. Springer Verlag, 2009.

[29] D. A. Huse. Simple three-state model with infinitely many phases. *Physical Review B*, 1981.

[30] E. T. Jaynes. On the rationale of maximum-entropy methods. *Proceedings of the IEEE*, 1982.

[31] Y. Kafri, D. Biron, M. R. Evans, and D. Mukamel. Slow coarsening in a class of driven systems. *The European Physical Journal B-Condensed Matter and Complex Systems*, 16(4):669–676, 2000.

[32] Y. Kafri, M. R. Evans, H. M. Koduvely, and D. Mukamel. Phase separation and coarsening in one-dimensional driven diffusive systems: Local dynamics leading to long-range Hamiltonians. *Physical Review E*, 1998.

[33] Y. Kafri, M. R. Evans, H. M. Koduvely, and D. Mukamel. Phase separation in one-dimensional driven diffusive systems. *Physical Review Letters*, 1998.

[34] S. Klumpp and R. Lipowsky. Traffic of molecular motors through tube-like compartments. *Journal of Statistical Physics*, 113(1):233–268, 2003.

[35] T. Kuna, J. L. Lebowitz, and E. R. Speer. Realizability of Point Processes. *Journal of Statistical Physics*, 129(3):417–439, Sept. 2007.

[36] T. Kuna, J. L. Lebowitz, and E. R. Speer. Necessary and sufficient conditions for realizability of point processes. *The Annals of Applied Probability*, 21(4):1253–1281, 2011.

[37] R. Lahiri, M. Barma, and S. Ramaswamy. Strong phase separation in a model of sedimenting lattices. *Physical Review E*, 61(2):1648–1658, 2000.

[38] R. Lahiri and S. Ramaswamy. Are steadily moving crystals unstable? *Physical Review Letters*, 79(6):1150–1153, 1997.

[39] A. Lederhendler, O. Cohen, and D. Mukamel. Phase diagram of the ABC model with nonconserving processes. *Journal of Statistical Mechanics: Theory and Experiment*, 2010:P11016, 2010.

[40] A. Lederhendler and D. Mukamel. Long-range correlations and ensemble inequivalence in a generalized ABC model. *Physical Review Letters*, 2010.

[41] C. T. MacDonald, J. H. Gibbs, and A. C. Pipkin. Kinetics of biopolymerization on nucleic acid templates. *Biopolymers*, 6(1):1–25, Jan. 1968.

[42] L. Mittag and M. Stephen. Mean-field theory of the many component Potts model. *Journal of Physics A: Mathematical, Nuclear and General*, 7:L109, 1974.

[43] D. Mukamel. Notes on the Statistical Mechanics of Systems with Long-Range Interactions. *arXiv.org*, cond-mat.stat-mech, May 2009.

[44] J. Nocedal and S. J. Wright. *Numerical Optimization*. Springer Verlag, 2006.

[45] M. Opper and D. Saad. *Advanced Mean Field Methods*. Theory and Practice. MIT Press, Feb. 2001.

[46] S. Ostlund. Incommensurate and commensurate phases in asymmetric clock models. *Physical Review B*, 1981.

[47] S. Pajevic. PLoS Computational Biology: Efficient Network Reconstruction from Dynamical Cascades Identifies Small-World Topology of Neuronal Avalanches. *PLoS Computational Biology*, 2009.

[48] A. Pelizzola. Cluster variation method in statistical physics and probabilistic graphical models. *Journal of Physics A: Mathematical and General*, 38(33):R309–R339, Aug. 2005.

[49] A. Peyrache, M. Khamassi, K. Benchenane, S. I. Wiener, and F. P. Battaglia. Replay of rule-learning related neural patterns in the prefrontal cortex during sleep. *Nature Neuroscience*, 12(7):919–926, May 2009.

[50] P. Ravikumar, M. J. Wainwright, and J. D. Lafferty. High-dimensional Ising model selection using 1-regularized logistic regression. *The Annals of Statistics*, 38(3):1287–1319, 2010.

[51] F. Ricci-Tersenghi. The Bethe approximation for solving the inverse Ising problem: a comparison with other inference methods. *arXiv.org*, cond-mat.dis-nn, Dec. 2011.

[52] S. Sandow and G. Schuetz. On Uq [SU (2)]-symmetric driven diffusion. *Europhysics Letters*, 26:7, 1994.

[53] A. Schadschneider. Statistical physics of traffic flow. *Physica A: Statistical Mechanics and its Applications*, 285(1):101–120, 2000.

[54] M. T. Schaub and S. R. Schultz. The Ising decoder: reading out the activity of large neural ensembles. *Journal of Computational Neuroscience*, 32(1):101–118, June 2011.

[55] M. Schmidt, G. Fung, and R. Rosales. Fast optimization methods for l1 regularization: A comparative study and two new approaches. *Machine Learning: ECML 2007*, pages 286–297, 2007.

[56] E. Schneidman, M. J. Berry II, R. Segev, and W. Bialek. Weak pairwise correlations imply strongly correlated network states in a neural population. *Nature*, 2006.

[57] M. Schnitzer and M. Meister. Multineuronal firing patterns in the signal from eye to brain. *Neuron*, 37(3):499–511, 2003.

[58] V. Sessak and R. Monasson. Small-correlation expansions for the inverse Ising problem. *Journal of Physics A: Mathematical and Theoretical*, 42:055001, 2009.

[59] J. Shlens, G. D. Field, J. Gauthier, M. I. Grivich, D. Petrusca, A. Sher, A. Litke, and E. Chichilnisky. The structure of multi-neuron firing patterns in primate retina. *The Journal of Neuroscience*, 26(32):8254–8266, 2006.

[60] M. Socolich, S. W. Lockless, W. P. Russ, H. Lee, K. H. Gardner, and R. Ranganathan. Evolutionary information for specifying a protein fold. *Nature*, 437(7058):512–518, Sept. 2005.

[61] J. P. Straley and M. E. Fisher. Three-state Potts model and anomalous tricritical points. *Journal of Physics A: Mathematical, Nuclear and General*, 6:1310, 1973.

[62] A. Tang, D. Jackson, J. Hobbs, W. Chen, J. L. Smith, H. Patel, A. Prieto, D. Petrusca, M. I. Grivich, and A. Sher. A maximum entropy model applied to spatial and temporal correlations from cortical networks in vitro. *The Journal of Neuroscience*, 28(2):505–518, 2008.

[63] A. Tarantola. Inverse problem theory and methods for model parameter estimation: SIAM. *Society for Industrial and Applied Mathematics*, 3600:19104–12688, 2005.

[64] D. J. Thouless, P. W. Anderson, and R. G. Palmer. Solution of'solvable model of a spin glass'. *Philosophical Magazine*, 35(3):593–601, 1977.

[65] G. Tkačik, E. Schneidman, M. J. Berry II, and W. Bialek. Ising models for networks of real neurons. *arXiv.org*, q-bio.NC, Nov. 2006.

[66] J. Villadelprat. The period function of the generalized Lotka-Volterra centers. *Journal of Mathematical Analysis and Applications*, 2008.

[67] M. Weigt, R. A. White, H. Szurmant, J. A. Hoch, and T. Hwa. Identification of direct residue contacts in protein–protein interaction by message passing. *Proceedings of the National Academy of Sciences*, 106(1):67–72, 2009.

Appendix A

Appendices for Chapter 2

A.1 Proof of Theorem 2.4.1(b)

We begin by giving an alternate form of the boundary conditions (2.28). With (2.14) and (2.16) these become

$$\lambda_\alpha - \lambda_{\alpha+1} = \log\big(y_K(t_\alpha - \beta)\big) - \log\big(y_K(t_\alpha + \beta - \tau_K/3)\big). \tag{A.1}$$

From (2.9) and (2.14), $(\log y_K(t))' = [y_K(t+\tau_K/3) - y_K(t-\tau_K/3)]/2$, so that

$$\lambda_\alpha - \lambda_{\alpha+1} = \frac{1}{2}\int_{t_\alpha+\beta-\tau_K/3}^{t_\alpha-\beta} \left[y_K\left(t+\frac{\tau_K}{3}\right) - y_K\left(t-\frac{\tau_K}{3}\right)\right]\, dt. \tag{A.2}$$

The solution of (A.2) which also satisfies $\sum_\alpha \lambda_\alpha = 0$ is

$$\lambda_\alpha = \frac{1}{2}\int_{s_\alpha-(\tau_K/6-\beta)}^{s_\alpha+(\tau_K/6-\beta)} \left(\frac{1}{3} - y_K(t)\right)\, dt, \tag{A.3}$$

where $s_\alpha = t_\alpha + \tau_K/2$. The form (A.3) is convenient when $2\beta \le \tau_K/3$; if $2\beta \ge \tau_K/3$ we may rewrite this as

$$\lambda_\alpha = \frac{1}{2}\int_{s_\alpha-(\beta-\tau_K/6)}^{s_\alpha+(\beta-\tau_K/6)} \left(y_K(t) - \frac{1}{3}\right)\, dt. \tag{A.4}$$

The representations (A.3) and (A.4) are useful because they translate the boundary conditions for the grand canonical model into a form similar to the condition (2.17) in the canonical model.

We need also to recall from [5] some further properties of the function $y_K(t)$ and its definite integrals

$$Y(K,s,\delta) = \int_{s-\delta}^{s+\delta} y_K(t)\, dt \quad \text{and} \quad W(K,s,\delta) = \int_{s-\delta}^{s+\delta} y_K\left(t+\frac{\tau_K}{3}\right)\, dt. \tag{A.5}$$

Note that from (2.17),

$$r_\alpha = \frac{1}{2\beta} Y(K, t_\alpha, \beta) \tag{A.6}$$

and that from (2.16),

$$\lambda_\alpha \;=\; \frac{\delta}{3} - \frac{1}{2}Y(K, s_\alpha, \delta) = \frac{\delta}{3} - \frac{1}{2}W(K, s_{\alpha+1}, \delta), \tag{A.7}$$

for $\delta = \tau_K/6 - \beta \geq 0$, while for $\delta' = -\delta > 0$,

$$\lambda_\alpha \;=\; \frac{1}{2}Y(K, s_\alpha, \delta') - \frac{\delta'}{3} = \frac{1}{2}W(K, s_{\alpha+1}, \delta') - \frac{\delta'}{3}. \tag{A.8}$$

Proposition A.1.1. *For $0 < K < 1/27$:*

(a) (i) $y_K(t)$ is even and τ_K-periodic (and hence also symmetric about $t = \tau_K/2$), takes its minimum value at $t = 0$, is strictly increasing on $[0, \tau_K/2]$, and takes its maximum value at $t = \tau_K/2$. Moreover, (ii) $y_K(t - \tau_K/3) + y_K(t) + y_K(t + \tau_k/3) = 1$ for all t.

(b) The minimum value $a = a(K) = y_K(0)$ of y_K is an increasing function of K satisfying $0 < a(K) < 1/3$. The maximum value $b = b(K) = y_K(\tau_K/2)$ is $b = [2 - a - \sqrt{4a - 3a^2}]/2$, and $y_K(\tau/6) = (1 - b)/2$, $y_K(\tau/3) = (1 - a)/2$.

(c) (i) For fixed K and δ, with $0 < \delta < \tau_K/2$, the function $Y(K, t, \delta)$ shares with $y_K(t)$ the properties listed in (a.i). Moreover, (ii)

$$Y(K, t - \tau_K/3, \delta) + Y(K, t, \delta) + Y(K, t + \tau_k/3, \delta) = 2\delta. \tag{A.9}$$

(d) For $0 < \delta < \tau_k/2$, $Y(K, 0, \delta)$ is strictly decreasing, and $W(K, \tau_k/6, \delta)$ strictly increasing, in K.

Finally, for $0 < K_2 < K_1 < 1/27$:

(e) (i) For any t_0 the curves $y_{K_1}(t_0 + t)$ and $y_{K_2}(t)$ intersect exactly once in the interval $0 \leq t \leq \tau_{K_2}/2$, and (ii) $y_{K_2}(t) < y_{K_1}(t)$ and $y_{K_2}(\tau_{K_2}/2 - t) > y_{K_1}(\tau_{K_1}/2 - t)$ for $0 \leq t \leq \tau_{K_1}/6$.

Proof. These results either appear in [5] or are immediate consequences of results appearing there. For (a) and (b) see Section 5.2 of [5] and in particular Remark 5.1(a); for (c.i) see Remark 5.3(b). (c.ii) follows from (a.ii). The first statement of (d) follows from the fact that $Y(K, 0, \delta)$ is continuous in K and, for $0 < \delta < \tau_k/2$, approaches $2\delta/3$ as $K \nearrow 1/27$ and 0 as $K \searrow 0$, together with Theorem 6.1 of [5] which, if one takes there $r_A = r_C$, asserts that for given r_B with $0 < r_B < 1/3$ there is at most one value of

K satisfying (A.6). The second statement of (d) is verified similarly. Finally, (e.i) is a special case of Lemma 6.2(a) of [5] and (e.ii) then follows from (e.i) and the inequalities $y_{K_2}(0) < y_{K_1}(0)$, $y_{K_2}(\tau_{K_1}/6) < y_{K_2}(\tau_{K_2}/6) < y_{K_1}(\tau_{K_1}/6)$, $y_{K_2}(\tau_{K_2}/2) > y_{K_1}(\tau_{K_1}/2)$, and $y_{K_2}(\tau_{K_2}/2 - \tau_{K_1}/6) > y_{K_2}(\tau_{K_2}/3) > y_{K_1}(\tau_{K_1}/3)$, easily obtained from the properties given in (a) and (b). □

We now turn to the proof of Theorem 2.4.1(b). We know (see the remarks at the beginning of Section 2.4) that there is at least one minimizer and that every minimizer satisfies the ELE (2.27), (2.28). Thus the conclusion of the theorem will follow from:

Lemma A.1.2. *If λ_A, λ_B, and λ_C are not all equal then:*

(a) No solution of (2.27), (2.28) *of type n, $n \geq 2$, can minimize $\hat{\mathcal{F}}$.*

(b) At most one solution of (2.27), (2.28) *of type 1 exists.*

Remark A.1.3. In proving Lemma A.1.2 we need not consider either the constant solution of the ELE or nonconstant solutions for which $2\beta = (n-2)\beta_c/3$, both of which satisfy (2.28) only when all the λ_α are equal. We may also suppose, without loss of generality, that

$$\lambda_A \leq \lambda_C \leq \lambda_B, \quad \text{with } \lambda_A < \lambda_C \text{ or } \lambda_C < \lambda_B. \tag{A.10}$$

If $\delta = \tau_K/6 - \beta > 0$ it then follows from (A.7) that $Y(K, s_B, \delta) \leq Y(K, s_C, \delta) \leq Y(K, s_A, \delta)$ and then from Proposition A.1.1(c.i) (see Figure A.1, which displays graphically the qualitative properties of $Y(K, s, \delta)$ implied there) that $0 \leq s_B \leq \tau_K/6$, so that $\tau_K/2 \leq t_B \leq 2\tau_K/3$ and hence, from Proposition A.1.1(c.i) and (A.6), that $r_A \leq r_C \leq r_B$. If $\lambda_A < \lambda_C$ then $s_B > 0$, $t_B > \tau_K/2$, and $r_A < r_C$; similarly $r_C < r_B$, if $\lambda_C < \lambda_B$. Similarly, if $\tau_K/6 < \beta < \tau_K/2$ then (now using (A.8)) $\tau_K/2 \leq s_B \leq 2\tau_K/3$ and $r_B \leq r_C \leq r_A$, again with strict inequality for two of the λ_α implying the corresponding inequality for the r_α.

Proof of Lemma A.1.2(a): Consider some type n solution $\rho(x)$, $n \geq 2$, of (2.27), (2.28); $\rho(x)$ has the form (2.14) with $2\beta > \tau_K/3$. We need to find a profile $\tilde{\rho}(x)$ with $\hat{\mathcal{F}}(\{\tilde{\rho}\}) < \hat{\mathcal{F}}(\{\rho\})$. There are three subcases:

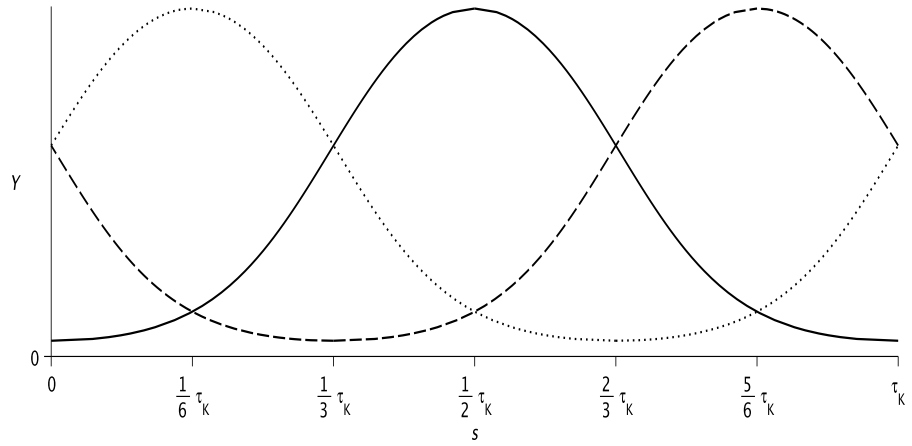

Figure A.1: Plots showing qualitative features of $Y(K, s, \delta)$ (solid), $Y(K, s+\tau_K/3, \delta)$ (dotted), and $Y(K, s-\tau_K/3, \delta)$ (dashed) for $0 < \delta < \tau_K/2$, based on Proposition A.1.1(c.1).

Case (a.i) $2\beta > \tau_K$**.** In this case it was shown in [5] that there is a *rearrangement* $\tilde{\rho}(x)$ of $\rho(x)$ with $\mathcal{F}(\{\tilde{\rho}\}) < \mathcal{F}(\{\rho\})$. This rearrangement does not change the mean densities r_α and hence also $\hat{\mathcal{F}}(\{\tilde{\rho}\}) < \hat{\mathcal{F}}(\{\rho\})$.

Case (a.ii) $2\beta = \tau_K$**.** In this case the solution $\rho(x)$ has mean densities $r_\alpha = 1/3$, so that $\sum \lambda_\alpha r_\alpha = 0$. From the description of the curve Γ in Section 2.4.1 it follows that for some $z > 0$ there exists a minimizer $\tilde{\rho}(x)$ of $\hat{\mathcal{F}}^{(\beta,0)}$ with mean densities $\tilde{r}_\alpha = 1/3 + z\lambda_\alpha$, so that $\sum \lambda_\alpha \tilde{r}_\alpha > 0$. But then

$$\hat{\mathcal{F}}^{(\beta,\lambda)}(\{\rho\}) = \hat{\mathcal{F}}^{(\beta,0)}(\{\rho\}) > \hat{\mathcal{F}}^{(\beta,0)}(\{\tilde{\rho}\}) > \hat{\mathcal{F}}^{(\beta,\lambda)}(\{\tilde{\rho}\}). \tag{A.11}$$

Case (a.iii) $\tau_K > 2\beta > \tau_K/3$**.** By Remark A.1.3, $r_B \le r_C \le r_A$, with $r_B < r_C$ if $\lambda_C < \lambda_B$ and $r_C < r_A$ if $\lambda_A < \lambda_C$. Consider now the profile $\tilde{\rho}$ with $\tilde{\rho}_\alpha(x) = \rho_{\alpha+1}(x)$. The canonical free energy functional satisfies $\mathcal{F}(\{\tilde{\rho}\}) = \mathcal{F}(\{\rho\})$ and so

$$\begin{aligned}\hat{\mathcal{F}}(\{\tilde{\rho}\}) - \hat{\mathcal{F}}(\{\rho\}) &= \sum_\alpha \lambda_\alpha r_\alpha - \sum_\alpha \lambda_\alpha r_{\alpha+1} \\ &= (\lambda_A - \lambda_C)(r_A - r_B) + (\lambda_B - \lambda_C)(r_B - r_C) < 0. \end{aligned} \tag{A.12}$$

□

The next result, the key to the proof of Lemma A.1.2(b), gives certain monotonicity properties of $Y(K, s, \delta)$ and $W(K, s, \delta)$.

Lemma A.1.4. *If K, s, and δ satisfy $0 < K < 1/27$ and $0 \le s, \delta \le \tau_K/6$, then:*

(a) For fixed K and s the function $2\delta/3 - Y(K,s,\delta)$ (respectively $2\delta/3 - W(K,s,\delta)$) is strictly increasing (respectively strictly decreasing) in δ;

(b) For fixed K and δ the functions $Y(K,s,\delta)$ and $W(K,s,\delta)$ are strictly increasing in s;

(c) For fixed s and δ the function $Y(K,s,\delta)$ (respectively $W(K,s,\delta)$) is strictly increasing (respectively strictly decreasing) in K.

Proof. (a) We rely throughout on Proposition A.1.1(a,b). From $0 \le s+\delta \le \tau_K/3$ and $-\tau_K/6 \le s-\delta \le \tau_K/6$ it follows that $y_K(s+\delta) \le (1-a)/2$ and $y_K(s-\delta) \le (1-b)/2$. Then from (A.5),

$$\frac{d}{d\delta}\left[\frac{2\delta}{3} - Y(K,s,\delta)\right] = \frac{2}{3} - y_K(s+\delta) - y_K(s-\delta) \ge \frac{a+b}{2} - \frac{1}{3} > 0, \tag{A.13}$$

as is easily verified from $b = [2 - a - \sqrt{4a - 3a^2}]/2$ with $0 < a < 1/3$. To show that $(d/d\delta)(2\delta/3 - W(K,s,\delta)) < 0$ it suffices similarly to verify that

$$z(K,s,\delta) := y_K\left(s + \frac{\tau_K}{3} + \delta\right) + y_K\left(s + \frac{\tau_K}{3} - \delta\right) > \frac{2}{3}. \tag{A.14}$$

Because y_K is even and τ_K-periodic, z is invariant under $(s,\delta) \to (s',\delta')$ with $s' = \tau_K/6 - \delta$, $\delta' = \tau_K/6 - s$, so that it suffices to verify (A.14) for $s + \delta \le \tau_K/6$, and since under this condition both terms in $z(K,s,\delta)$ are increasing in s it suffices to consider $s = 0$. But because y_K is even,

$$\begin{aligned} z(K,0,\delta) &= \frac{1}{2}\Big[y_K\left(\frac{\tau_K}{3} + \delta\right) + y_K\left(-\frac{\tau_K}{3} + \delta\right) \\ &\qquad + y_K\left(-\frac{\tau_K}{3} - \delta\right) + y_K\left(\frac{\tau_K}{3} - \delta\right)\Big] \\ &= 1 - \frac{1}{2}\left[y_K(\delta) + y_K(-\delta)\right] \ge \frac{1+b}{2} > 2/3. \end{aligned} \tag{A.15}$$

(b) See Proposition A.1.1(c).

(c) The proofs for Y and of W are similar and we check only Y. Suppose that $0 < K_2 < K_1 < 1/27$ and that for some $s_* \in [0, \tau_{K_1}/6]$,

$$Y(K_1, s_*, \delta) \le Y(K_2, s_*, \delta). \tag{A.16}$$

Then certainly $y_{K_1}(t_*) < y_{K_2}(t_*)$ for some $t_* \in [s_* - \delta, s_* + \delta]$, and since $y_{K_1}(0) > y_{K_2}(0)$, Proposition A.1.1(e.i) implies that $y_{K_1}(t) \le y_{K_2}(t)$ for $t \in [t_*, \tau_{K_1}/3]$. Then for $s \in [s_*, \tau_{K_1}/6]$,

$$\begin{aligned} &\frac{d}{ds}\left[Y(K_2, s, \delta) - Y(K_1, s, \delta)\right] \\ &\quad = \quad [y_{K_1}(s-\delta) - y_{K_2}(s-\delta)] + [y_{K_2}(s+\delta) - y_{K_1}(s+\delta)] \\ &\quad > \quad 0, \end{aligned} \tag{A.17}$$

since both terms on the right had side are positive. But for $0 \le \delta \le \tau_{K_1}/6$,

$$W(K_1, \tau_{K_1}/6, \delta) < W(K_2, \tau_{K_2}/6, \delta), \tag{A.18}$$

by Proposition A.1.1(e.ii), and so from Proposition A.1.1(a),

$$\begin{aligned} Y(K_1, \tau_{K_1}/6, \delta) &= \frac{1}{2}\int_{\tau_{K_1}/6-\delta}^{\tau_{K_1}/6+\delta} \left[y_{K_1}\left(t - \frac{\tau_{K_1}}{3}\right) + y_{K_1}(t)\right] dt \\ &= \frac{1}{2}\int_{\tau_{K_1}/6-\delta}^{\tau_{K_1}/6+\delta} \left[1 - y_{K_1}\left(t + \frac{\tau_{K_1}}{3}\right)\right] dt \\ &= \delta - \frac{1}{2}W(K_1, \tau_{K_1}/6, \delta) \\ &> \delta - \frac{1}{2}W(K_2, \tau_{K_2}/6, \delta) \\ &= Y(K_2, \tau_{K_2}/6, \delta) \\ &> Y(K_2, \tau_{K_1}/6, \delta) \end{aligned} \tag{A.19}$$

since $\tau_{K_1} < \tau_{K_2}$ (see Remark 2.2.1), contradicting (A.16) and (A.17). □

Proof of Lemma A.1.2(b): For type 1 solutions we have from (A.7) that

$$\lambda_B = \frac{\delta}{3} - \frac{1}{2}Y(K, s_B, \delta), \qquad \lambda_A = \frac{\delta}{3} - \frac{1}{2}W(K, s_B, \delta), \tag{A.20}$$

with $\delta = \tau_K/6 - \beta > 0$ and, by Remark A.1.3, $0 \le s_B \le \tau_K/6$. Thus the existence for some λ of two type 1 solutions would correspond to the existence of (K_1, s_1) and (K_2, s_2) with $0 < K_2 < K_1 < 1/27$ and $0 \le s_i \le \tau_{K_i}/6$, $i = 1, 2$, such that $2\delta_1/3 - Y(K_1, s_1, \delta_1) = 2\delta_2/3 - Y(K_2, s_2, \delta_2)$ and $2\delta_1/3 - W(K_1, s_1, \delta_1) = 2\delta_2/3 - W(K_2, s_2, \delta_2)$,

where $\delta_i = \tau_{K_i}/6 - \beta$ for $i = 1, 2$. Then from Lemma A.1.4(a,c),

$$\begin{aligned} \frac{2\delta_2}{3} - Y(K_2, s_2, \delta_2) &= \frac{2\delta_1}{3} - Y(K_1, s_1, \delta_1) \\ &< \frac{2\delta_1}{3} - Y(K_2, s_1, \delta_1) \\ &< \frac{2\delta_2}{3} - Y(K_2, s_1, \delta_2), \end{aligned} \tag{A.21}$$

so that Lemma A.1.4(b) implies that $s_1 < s_2$. But also

$$\begin{aligned} \frac{2\delta_2}{3} - W(K_2, s_2, \delta_2) &= \frac{2\delta_1}{3} - W(K_1, s_1, \delta_1) \\ &> \frac{2\delta_1}{3} - W(K_2, s_1, \delta_1) \\ &> \frac{2\delta_2}{3} - W(K_2, s_1, \delta_2), \end{aligned} \tag{A.22}$$

implying that $s_1 > s_2$, a contradiction. □

A.2 Reflection asymmetric interactions in a simple case

To give some idea of the importance of the asymmetry in the ABC model interactions, we present in this section a short analysis of the model with *nearest neighbor* interactions in one dimension.

For the system with asymmetric nearest neighbor terms only, the microscopic energy is given by

$$E_N(\underline{\zeta}) = \sum_{\alpha} \sum_{i=1}^{N} \left[\eta_\alpha(i)\eta_{\alpha+2}(i+1) + \frac{\lambda_\alpha}{2}(\eta_\alpha(i) + \eta_\alpha(i+1)) \right]. \tag{A.23}$$

We will take the convention that the sum of the chemical potentials is set to zero. We can use a transfer matrix to write the partition function for the system as

$$Z_N = \mathrm{tr}\left(T^N\right),$$

with

$$T = \begin{pmatrix} e^{-\beta\lambda_A} & e^{-\beta(\lambda_A+\lambda_B)/2} & e^{-\beta(1-\lambda_B/2)} \\ e^{-\beta(1+\lambda_A/2+\lambda_B/2)} & e^{-\beta\lambda_B} & e^{\beta\lambda_A/2} \\ e^{\beta\lambda_B/2} & e^{-\beta(1-\lambda_A/2)} & e^{\beta(\lambda_A+\lambda_B)} \end{pmatrix}.$$

At equal chemical potentials, the largest eigenvalue of T is $\lambda_+ = 2 + e^{-\beta}$, so the macroscopic free energy per particle in this case is

$$\mathcal{F} = \lim_{N\to\infty} -\frac{1}{\beta N}\log(Z_N) = -\frac{1}{\beta}\log(2+e^{-\beta}). \tag{A.24}$$

Nearest neighbor correlation functions can also be evaluated using the transfer matrix method. The AA nearest neighbor correlation function $\langle\eta_A(i)\eta_A(i+1)\rangle$ is given by

$$\langle\eta_A(i)\eta_A(i+1)\rangle = \lim_{N\to\infty}\frac{\mathrm{tr}\left(T^{N-1}ATA\right)}{\mathrm{tr}\left(T^N\right)} = \frac{1}{3\lambda_+}, \tag{A.25}$$

where A is the matrix

$$A = \begin{pmatrix} 1 & 0 & 0 \\ 0 & 0 & 0 \\ 0 & 0 & 0 \end{pmatrix}. \tag{A.26}$$

Similarly one may calculate

$$\langle\eta_A(i)\eta_B(i+1)\rangle = \lim_{N\to\infty}\frac{\mathrm{tr}\left(T^{N-1}ATB\right)}{\mathrm{tr}\left(T^N\right)} = \frac{1}{3\lambda_+}, \tag{A.27}$$

$$\langle\eta_A(i)\eta_C(i+1)\rangle = \lim_{N\to\infty}\frac{\mathrm{tr}\left(T^{N-1}ATC\right)}{\mathrm{tr}\left(T^N\right)} = \frac{1}{3(1+2e^{\beta})}. \tag{A.28}$$

These nearest neighbor correlation functions have very natural limits at high and low temperatures,

$$\lim_{\beta\to\infty}\langle\eta_A(i)\eta_A(i+1)\rangle = \frac{1}{6}, \qquad \lim_{\beta\to 0}\langle\eta_A(i)\eta_A(i+1)\rangle = \frac{1}{9}, \tag{A.29}$$

$$\lim_{\beta\to\infty}\langle\eta_A(i)\eta_B(i+1)\rangle = \frac{1}{6}, \qquad \lim_{\beta\to 0}\langle\eta_A(i)\eta_B(i+1)\rangle = \frac{1}{9}, \tag{A.30}$$

$$\lim_{\beta\to\infty}\langle\eta_A(i)\eta_C(i+1)\rangle = 0, \qquad \lim_{\beta\to 0}\langle\eta_A(i)\eta_C(i+1)\rangle = \frac{1}{9}. \tag{A.31}$$

At infinite temperature any arrangement of nearest neighbors is equally likely. At zero temperature, nearest neighbors must be of the same species, or of different species arranged in successive cyclic order: AA, AB, BB, BC, CC, or CA. Each pair is equally likely.

As we will see presently, the asymmetry of the ABC interaction is necessary for the formation of domains which proceed in cyclic order as $A\cdots AB\cdots BC\cdots CA$. Consider the model of (A.23), but with the nearest neighbor interactions symmetrized,

$$E_N(\underline{\zeta}) = \sum_{\alpha}\sum_{i=1}^{N}\left[\eta_\alpha(i)\left(\eta_{\alpha+1}(i+1)+\eta_{\alpha+2}(i+1)\right)+\frac{\lambda_\alpha}{2}(\eta_\alpha(i)+\eta_\alpha(i+1))\right]. \tag{A.32}$$

Using the conservation rule $\eta_A(i)+\eta_B(i)+\eta_C(i)=1$, this energy can then be rewritten as

$$E_N(\underline{\zeta}) = \frac{1}{2}\sum_{\alpha}\sum_{i=1}^{N}\left[1-\eta_\alpha(i)\eta_\alpha(i+1)+\frac{\lambda_\alpha}{2}(\eta_\alpha(i)+\eta_\alpha(i+1))\right]. \tag{A.33}$$

Taking the overall factor of $e^{-3\beta N/2}$ outside, the transfer matrix for this system is

$$T = \begin{pmatrix} e^{\beta(1/2-\lambda_A)} & e^{-\beta(\lambda_A+\lambda_B)/2} & e^{\beta\lambda_B/2} \\ e^{-\beta(\lambda_A+\lambda_B)/2} & e^{\beta(1/2-\lambda_B)} & e^{\beta\lambda_A/2} \\ e^{\beta\lambda_B/2} & e^{\beta\lambda_A/2} & e^{\beta(1/2+\lambda_A+\lambda_B)} \end{pmatrix}. \tag{A.34}$$

Its largest eigenvalue when all chemical potentials are zero is $\lambda_+ = 2+e^{\beta/2}$, with the two other eigenvalues $\lambda = e^{\beta/2}-1$ degenerate. Then the free energy per particle in the $N\to\infty$ limit is

$$\mathcal{F} = \lim_{N\to\infty} -\frac{1}{\beta N}\log(Z_N) = 3/2 - \frac{1}{\beta}\log(2+e^{\beta/2}). \tag{A.35}$$

Nearest neighbor correlation functions can be calculated as above for the asymmetric case. The result is

$$\langle\eta_A(i)\eta_A(i+1)\rangle = \lim_{N\to\infty}\frac{\mathrm{tr}\left(T^{N-1}ATA\right)}{\mathrm{tr}\left(T^N\right)} = \frac{1}{3}\left(1-\frac{2}{\lambda_+}\right), \tag{A.36}$$

$$\langle\eta_A(i)\eta_B(i+1)\rangle = \lim_{N\to\infty}\frac{\mathrm{tr}\left(T^{N-1}ATB\right)}{\mathrm{tr}\left(T^N\right)} = \frac{1}{3\lambda_+}, \tag{A.37}$$

$$\langle\eta_A(i)\eta_C(i+1)\rangle = \lim_{N\to\infty}\frac{\mathrm{tr}\left(T^{N-1}ATC\right)}{\mathrm{tr}\left(T^N\right)} = \frac{1}{3\lambda_+}. \tag{A.38}$$

In the high temperature limit, we again recover equal probability for any configuration of nearest neighbors. However in this case the correlations for nearest neighbor pairs of differing species are the same, regardless of their ordering. As the temperature goes towards zero, the correlations between nearest neighbor pairs of different species AB and AC go to zero, so one would expect to find large domains of particles of a single species. In contrast with the asymmetric case, there is no restriction on ordering of domains; a domain wall of the form AC is just as likely in this model as an AB boundary.

Appendix B

Appendices for Chapter 3

B.1 Properties of the microscopic system

Many of the properties of the canonical measure μ_β for the standard ABC model, described in [5, Sections 1 and 2], hold with relatively minor changes for the generalized model studied here. Below we discuss a few of the necessary modifications.

As in the standard ABC model, there is a certain nearest neighbor exchange dynamics which satisfies detailed balance with respect to the canonical Gibbs measure μ_β. In this dynamics a particle of type α at site i and a particle of type γ at site $i+1$ exchange places $\alpha\,\gamma \to \gamma\,\alpha$ with rate $q_{\alpha\gamma}$,

$$q_{\alpha\gamma} = \begin{cases} e^{-3\beta\, v_{\alpha+2}/N} & \text{if } \gamma = \alpha + 1 \\ 1 & \text{if } \gamma = \alpha - 1 \end{cases}, \tag{B.1}$$

where the v_α are as in (3.7). When the ξ_α are not all zero (i.e. the v_α are not all equal), the system no longer has cyclic symmetry in the particle types.

In analogy with what happens in the standard ABC model when $N_\alpha = N/3$ for all α, we have here a rotation invariant energy when $v_\alpha\, N = N_\alpha$ for all α (this is clearly only possible when the v_α lie in region I). That is, if one imagines connecting site N to site 1 and then rotating the configuration $\underline{\eta}$, the rotation leaves E unchanged. A simple way to check the rotation invariance is to consider moving a particle of type α from the end of the interval at site N to site 1, and translating all the other particles from sites i to $i+1$. The change in energy after this rotation is then $3\left(v_{\alpha+1}\, N_{\alpha+2} - v_{\alpha+2}\, N_{\alpha+1}\right)/N$, which vanishes for $v_\alpha\, N = N_\alpha$. Note that in this rotation invariant case the rates (B.1)

for a particle of type α at a site i and a particle of type γ at $i+1$ to exchange become

$$q_{\alpha\gamma} = \begin{cases} e^{-3\beta\, N_{\alpha+2}/N^2} & \text{if } \gamma = \alpha + 1 \\ \\ 1 & \text{if } \gamma = \alpha - 1 \end{cases}, \tag{B.2}$$

which satisfies the general condition on exchange rates derived in [32] for which detailed balance may hold on the ring.

We remark that the energy in this rotation invariant case may be constructed in a different way, beginning from the standard ABC model energy with $\xi_\alpha = 0$. If one wishes to write down an ABC-like energy that is explicitly rotation invariant, one way to achieve this is to take the standard ABC energy and average over starting the sum at each point of the lattice, i.e.

$$\tilde{E}(\underline{\eta}) = \frac{1}{N}\sum_{k=1}^{N}\left(\frac{1}{N}\sum_{\alpha}\sum_{i=1+k}^{N+k}\sum_{j=1+k}^{N+k}\Theta(j-i)\eta_\alpha(i)\eta_{\alpha+2}(j)\right), \tag{B.3}$$

where one imagines the interval with periodic boundary conditions, such that site $N+m$ refers to site m. This gives

$$\tilde{E}(\underline{\eta}) = \frac{1}{N}\sum_{\alpha}\sum_{i=1}^{N}\sum_{j=1}^{N}\left(\Theta(j-i) + \frac{i-j}{N}\right)\eta_\alpha(i)\eta_{\alpha+2}(j), \tag{B.4}$$

where the interaction term depends upon the distance between sites i and j as well as their order on the line. One may easily rearrange this expression to find

$$\tilde{E}(\underline{\eta}) = \frac{1}{N}\sum_{\alpha}\sum_{i=1}^{N}\sum_{j=1}^{N}\Theta(j-i)\,3\,\frac{N_{\alpha+1}}{N}\,\eta_\alpha(i)\,\eta_{\alpha+2}(j), \tag{B.5}$$

which is identical to (3.6) up to a constant when $v_\alpha\, N = N_\alpha$.

Now let us consider the ground states of the model. As in the standard ABC model, in the $\beta \to \infty$ limit the particle species become phase separated, with the ground states consisting of macroscopic domains of pure A, B, and C particles. The arrangement of these domains may depend upon the v_α as well as the number of each particle species N_α. For values of v_α in regions II and III, where one or two of the v_α is negative, the ground state is completely determined by requiring that all nearest neighbor configurations be stable, i.e., that the energy may not be lowered by making a nearest neighbor exchange. Consider the possible orderings of nearest neighbor pairs

of different particle species: AB, AC, BA, BC, CA, CB. When the v_α do not all have the same sign, the energetically preferred alignment of two nearest neighbor particles of different species will be cyclic for some pairs and anti-cyclic for others. Thus it is not possible to have an arrangement of four or more domains where all nearest neighbor pairs are preferably aligned. Generally, when the v_α lie in region II (III), if $v_\gamma < 0$ (> 0), the ground state is given by three domains arranged in cyclic (anti-cyclic) order, i.e. in a cyclic (anti-cyclic) permutation of **ABC**, with the domain of type γ particles in the middle. For example, if $v_A < 0$ while v_B, $v_C > 0$, the stable nearest neighbor configurations are AB, CB, and CA, thus the ground state must consist of three domains of particles cyclically arranged as **CAB**.

When the v_α lie in region I, the ground states of the ABC model with external fields are closely related to those of the standard ABC model. To show the correspondence, let us consider a rescaling of the energy (3.6), $\tilde{E}(\eta) = E(\eta)/(v_A\, v_B\, v_C)$. The rescaled energy of a sequence of domains, where the ith domain consists of $k_{\alpha,i}$ particles of type α (and no particles of any other type), is up to a constant factor formally identical to the standard ABC energy of the same sequence of domains, but with $k_{\alpha,i}/v_\alpha$ particles in each domain. Of course, $k_{\alpha,i}/v_\alpha$ may not be an integer, which must be taken into account when considering the degeneracy of ground states. One may however apply the same analysis as in [5] to determine the lowest energy configuration of domains. This ground state energy is given, up to a constant factor (see (3.6)), by $\min\{v_A\, r_B\, r_C,\, v_B\, r_C\, r_A,\, v_C\, r_A\, r_B\}$. One then finds that the ground state of the generalized ABC model, with v_α in region I and N_α particles of type α, is arranged in the same order and has the same symmetries as the ground state of the standard ABC model with N_α/v_α particles of type α. There are three different cases.

1. If one of the N_α/v_α is larger than the other two then there exists a unique ground state with three domains arranged in cyclic order, with the particles for which N_α/v_α is largest in the middle. For example if $N_A/v_A > N_{B,C}/v_{B,C}$, the ground state arrangement of domains is **CAB**, with the particles of type A in the middle domain.

2. If two of the N_α/v_α are equal and larger than the term for the third species, the ground state is degenerate, consisting of three or four domains cyclically arranged with the particles for which N_α/v_α is smallest placed on the boundaries of the interval. If for instance $N_B/v_B = N_C/v_C > N_A/v_A$, the ground state is $N_A + 1$ degenerate, with the domains arranged as **ABC**, **ABCA**, or **BCA**; the type A particles may appear on either the left or the right sides of the interval.

3. If all of the N_α/v_α are equal, the ground state is N degenerate, consisting of arbitrary rotations of the domains arranged in **ABC** cyclic order. In this case, as discussed above, the energy of any configuration $\underline{\eta}$ is invariant under rotation.

B.2 The Lotka-Volterra family of centers and ABC-like systems of ODEs

In this section we will demonstrate that the ABC model with external fields is a member of the Lotka-Volterra family of ODE systems when $0 < v_\alpha < 1$ for all α, i.e. when the v_α lie in region I.

First let us change variables from x to $t = 3\beta\sqrt{v_A\, v_B\, v_C}\, x$, a slightly different rescaling than that used in (3.30) which will be convenient in the work that follows. With this change the ELE become

$$\dot{\rho}_\alpha = \rho_\alpha \left(u_{\alpha+1}\, \rho_{\alpha+2} - u_{\alpha+2}\, \rho_{\alpha+1} \right), \tag{B.6}$$

where $u_\alpha = v_\alpha/\sqrt{v_A\, v_B\, v_C}$; the u_α satisfy

$$u_A + u_B + u_C = u_A u_B u_C. \tag{B.7}$$

After eliminating ρ_C via (3.21) and u_C via $u_C = (u_A + u_B)/(u_A\, u_B - 1)$, we obtain the equations

$$\begin{aligned} \dot{\rho}_A &= \rho_A \left[u_B \left(1 - \rho_A\right) - \frac{u_A \left(1 + u_B^2\right)}{u_A\, u_B - 1}\, \rho_B \right], \\ \dot{\rho}_B &= -\rho_B \left[u_A \left(1 - \rho_B\right) - \frac{u_B \left(1 + u_A^2\right)}{u_A\, u_B - 1}\, \rho_A \right]. \end{aligned} \tag{B.8}$$

In this form u_A and u_B are arbitrary positive constants satisfying $u_A\,u_B > 1$, and the stationary point is

$$v_A = \frac{u_A\,u_B - 1}{u_B\,(u_A + u_B)}, \qquad v_B = \frac{u_A\,u_B - 1}{u_A\,(u_A + u_B)}. \tag{B.9}$$

We next shift the origin in the phase plane to the stationary point (B.9) and make a linear change of variables:

$$\begin{bmatrix} x \\ y \end{bmatrix} = T \begin{bmatrix} \rho_A - v_A \\ \rho_B - v_B \end{bmatrix}, \qquad T = \frac{1}{u_A\,u_B - 1} \begin{bmatrix} u_B\left(1 + u_A^2\right) & u_A\,(u_A\,u_B - 1) \\ 0 & u_A\,(u_A + u_B) \end{bmatrix}. \tag{B.10}$$

In these new variables the equations become

$$\begin{aligned} \dot{x} &= -y - bx^2 - cxy + by^2, \\ \dot{y} &= x + xy, \end{aligned} \tag{B.11}$$

where

$$b = \frac{u_A\,u_B - 1}{1 + u_A^2}, \qquad c = \frac{2u_A + u_B - u_A^2\,u_B}{1 + u_A^2}. \tag{B.12}$$

This is the canonical form for the generalized Lotka-Volterra family of centers presented in equation (1) of [66].

Given parameters b and c with $b > 0$ the equations (B.12) can be solved to find

$$u_A = \frac{-c + \sqrt{c^2 + 4b(b+1)}}{2b}, \qquad u_B = \frac{4b(b+1)}{-c + \sqrt{c^2 + 4b(b+1)}} - c. \tag{B.13}$$

Clearly $u_A > 0$ and one finds easily that $u_A\,u_B > 1$, so $u_B > 0$. Thus the set of systems (B.6) with u_A, u_B, $u_C > 0$ corresponds exactly with the family of all generalized Lotka-Volterra systems (B.11) with $b > 0$.

B.3 Restriction on the type of solutions for $r_\alpha \neq v_\alpha$, with v_α in region I

A naive estimate of the cutoff n_{max}, as described in Section 3.3, may be made in the following way. Let us begin with a set of type 1 profiles, with average densities $\tilde{r}_\alpha$. These profiles will be a portion of the type 1 solution for the $r_\alpha = v_\alpha$ case, stretched such that less than one full period of the $\rho_\alpha(x)$ fits inside the interval in $x \in [0, 1]$. We will define the length of the profiles l, $0 < l < 1$, to be the fraction of one full period of

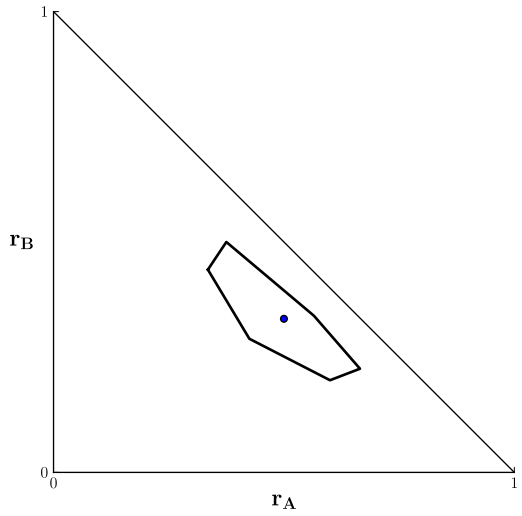

Figure B.1: Restriction on the existence of solutions of type $n = 2$ in the $r_\alpha \neq v_\alpha$ case for $v_A = 1/2$, $v_B = 1/3$, $v_C = 1/6$, using (B.14). For values of (r_A, r_B) outside the bounded region, only type 1 solutions are possible. For $n > 2$, the bounded region in which type n solutions are possible would be smaller.

the $\rho_\alpha(x)$ inside the interval. From these type 1 profiles we may make a set of type n profiles that satisfy the same boundary conditions as the original by rescaling x for the $\rho_\alpha(x)$, such that the original type 1 profiles plus $n-1$ full periods now appear in the interval. Then the average value of the densities for the new type n profiles, $r_{n,\alpha}$, will be given by

$$r_{n,\alpha} = \frac{\tilde{r}_\alpha \, l + n \, v_\alpha}{l + n}. \tag{B.14}$$

As a type n solution of the ELE for $r_\alpha \neq v_\alpha$ will be a profile of this form, if the l and $\tilde{r}_\alpha$ in (B.14) cannot be chosen such that the $r_{n,\alpha}$ are equal to the specified r_α, then this implies that a type n solution does not exist for that case. In Figure B.1 we show an example of the restriction imposed by this simple estimate.

Appendix C

Appendices for Chapter 4

C.1 Proof of maximum entropy

The use of the Ising model is physically motivated by the fact that the Ising model Gibbs measure (4.3) is the maximum entropy measure which satisfies the constraints (4.7). We prove this statement here by showing a more general result, namely, the maximum entropy distribution which satisfies a set of constraints

$$\sum_{\underline{\eta}} f_\alpha(\underline{\eta}) = g_\alpha, \qquad \alpha = 1, \ldots, n, \tag{C.1}$$

if it exists, is given by

$$\mu_{\mathrm{ME}}(\underline{\eta}) = e^{\sum_\alpha \lambda_\alpha f_\alpha(\underline{\eta})}, \tag{C.2}$$

where λ_α is a real number which acts as a Lagrange multiplier.

As a first step we prove Gibbs' inequality, in the method of [19], which states that the Kullback-Leibler divergence (also referred to as the relative entropy) between two probability measures $D_{\mathrm{KL}}(\mu||\mu')$ is nonnegative:

$$D_{\mathrm{KL}}(\mu||\mu') = -\sum_{\underline{\eta}} \mu(\underline{\eta}) \log \frac{\mu'(\underline{\eta})}{\mu(\underline{\eta})} \geq 0. \tag{C.3}$$

We need only consider the subset of configurations $\{\underline{\eta} \,|\, \mu(\underline{\eta}) > 0\}$, as terms with $\mu(\underline{\eta}) = 0$ in (C.3) are zero with the convention $0 \log 0 = 0$. As $\log x$ is concave, we have by Jensen's inequality

$$D_{\mathrm{KL}}(\mu||\mu') \geq -\log \sum_{\underline{\eta} \,|\, \mu(\underline{\eta})>0} \mu(\underline{\eta}) \frac{\mu'(\underline{\eta})}{\mu(\underline{\eta})} = -\log \sum_{\underline{\eta} \,|\, \mu(\underline{\eta})>0} \mu'(\underline{\eta}) \geq 0, \tag{C.4}$$

where equality only holds if $\mu'(\underline{\eta})/\mu(\underline{\eta})$ is constant for all $\underline{\eta}$. Thus we have proven (C.3), assuming the probability measures are normalized such that the sum over all configurations of the system is equal to one.

Now we move to the proof that (C.2), if it exists, is the maximum entropy distribution which satisfies the constraints (C.1). Let us assume that, in addition to the maximum entropy measure (C.2), there exists another measure μ' which also satisfies the constraints (C.1), and has entropy that is greater than or equal to that of the maximum entropy measure,

$$S(\mu') = -\sum_{\underline{\eta}} \mu'(\underline{\eta}) \log \mu'(\underline{\eta}) \geq S(\mu_{\mathrm{ME}}) = -\sum_{\underline{\eta}} \mu_{\mathrm{ME}}(\underline{\eta}) \log \mu_{\mathrm{ME}}(\underline{\eta}). \tag{C.5}$$

By (C.3) we have that

$$-\sum_{\underline{\eta}} \mu'(\underline{\eta}) \log \mu_{\mathrm{ME}}(\underline{\eta}) \geq S(\mu'). \tag{C.6}$$

By the definition of (C.2)

$$\log \mu_{\mathrm{ME}}(\underline{\eta}) = \sum_{\alpha} \lambda_\alpha f_\alpha(\underline{\eta}), \tag{C.7}$$

thus

$$\begin{aligned} -\sum_{\underline{\eta}} \mu'(\underline{\eta}) \log \mu_{\mathrm{ME}}(\underline{\eta}) &= -\sum_{\underline{\eta}} \sum_{\alpha} \lambda_\alpha f_\alpha(\underline{\eta}) \mu'(\underline{\eta}) \\ &= -\sum_{\alpha} \lambda_\alpha g_\alpha, \end{aligned} \tag{C.8}$$

as we have assumed that μ_{ME} and μ' satisfy the same constraints. But then

$$-\sum_{\underline{\eta}} \mu_{\mathrm{ME}}(\underline{\eta}) \log \mu_{\mathrm{ME}}(\underline{\eta}) = -\sum_{\alpha} \lambda_\alpha g_\alpha, \tag{C.9}$$

so

$$S(\mu') - S(\mu_{\mathrm{ME}}) \leq -\sum_{\underline{\eta}} \mu'(\underline{\eta}) \log \mu_{\mathrm{ME}}(\underline{\eta}) - S(\mu_{\mathrm{ME}}) = 0. \tag{C.10}$$

As above, in order for equality to hold in (C.10) we must have $\mu_{\mathrm{ME}}(\underline{\eta}) = \mu'(\underline{\eta})$ for each configuration $\underline{\eta}$. This shows that $S(\mu')$ cannot be larger than $S(\mu_{\mathrm{ME}})$, and further, equality only holds if $\mu' = \mu_{\mathrm{ME}}$. Thus (C.2) is the maximum entropy distribution which satisfies the constraints (C.1).

C.2 Statistical effects of finite sampling

Finite sampling of an experimental system introduces fluctuations which complicate the inverse problem. In this Appendix we discuss the effects of finite sampling noise

on the empirical one- and two-point correlations, and statistical errors on the inferred couplings and fields.

We can estimate the size of the fluctuations we expect for the measured correlations $\{p_i^*\}, \{p_{ij}^*\}$ in the following way. Let us assume the spins are stochastic variables with Gibbs average

$$\langle \eta_i \rangle = p_i^*. \tag{C.11}$$

Their variance is then

$$\sigma_i = \langle \eta_i^2 \rangle - \langle \eta_i \rangle^2 = p_i^*(1 - p_i^*). \tag{C.12}$$

Their average over B independent samples is also a stochastic variable with the same average as above, but with the standard deviation

$$\delta p_i^* = \sqrt{\frac{p_i^*(1-p_i^*)}{B}}. \tag{C.13}$$

Similarly the pair correlations are have the average value

$$\langle \eta_i \, \eta_j \rangle = p_{ij}^*, \tag{C.14}$$

and variance

$$\sigma_{ij} = p_{ij}^*(1 - p_{ij}^*), \tag{C.15}$$

therefore their sampled average over B samples p_{ij} has a standard deviation

$$\delta p_{ij}^* = \sqrt{\frac{p_{ij}^*(1-p_{ij}^*)}{B}}\,. \tag{C.16}$$

To derive an estimate for the statistical fluctuations of the fields and couplings, let us again assume that data are generated from the Ising model (4.1) with fields $\{h_i^*\}$ and couplings $\{J_{ij}^*\}$ which minimize the cross-entropy (4.11). As shown in Section 4.1 the likelihood of infering the interactions $\mathbf{J}$ is proportional to $\exp[-B\, S^*(\mathbf{p}^*, \mathbf{J})]$. When B is very large this probability is tightly concentrated around the minimum of S^*, that is, $\mathbf{J}^*$. The difference between the inferred and the true fields and couplings is encoded in the $\frac{N(N+1)}{2}$-dimensional vector $\mathbf{\Delta J}$ of components $\{\{h_i - h_i^*\}, \{J_{ij} - J_{ij}^*\}\}$. The distribution of this vector is asymptotically Gaussian,

$$\mathcal{L}(\mathbf{\Delta J}) \simeq \frac{\sqrt{\det \chi}}{(2\pi B)^{N(N+1)/4}} \exp\left(-\frac{B}{2}\, \mathbf{\Delta J}^\dagger \cdot \chi \cdot \mathbf{\Delta J}\right). \tag{C.17}$$

Statistical fluctuations of the fields and couplings are therefore characterized by the standard deviations

$$\delta h_i = \sqrt{\frac{1}{B}\left(\chi^{-1}\right)_{i,i}}\,, \quad \delta J_{ij} = \sqrt{\frac{1}{B}\left(\chi^{-1}\right)_{ij,ij}}\,. \tag{C.18}$$

C.3 Gaussian approximation for the inverse Ising problem

The main problem of the minimization of the cross-entropy S^* (4.11) is the calculation of the partition function Z which, if done exactly, requires the sum over all 2^N possible configurations of the system of N spins. Because this sum becomes prohibitive for systems with more than ≈ 20 spins some approximate solution of the inverse problem must be found.

One choice of approximation is to allow the Ising spins η_i take continuous values, while maintaining the same one- and two-point correlations. The Ising model Hamiltonian (4.1) is then replaced by a Gaussian model of interacting pairs of spins, whose entropy is given by the logarithm of the determinant of the covariance matrix. Adding in the contribution from individual spins, we have

$$S_{\rm G}(\mathbf{p}) = S_{\rm ind}(\{p_i\}) + \frac{1}{2}\log\det M(\mathbf{p}), \tag{C.19}$$

where

$$S_{\rm ind}(\{p_i\}) = \sum_i \left[-p_i\,\log p_i - (1-p_i)\,\log(1-p_i)\right] \tag{C.20}$$

is the entropy of independent spin variables with averages $\{p_i\}$, and

$$M_{ij}(\mathbf{p}) = \frac{p_{ij} - p_i p_j}{\sqrt{p_i(1-p_i)p_j(1-p_j)}}, \tag{C.21}$$

which can be calculated in $O(N^3)$ time [45, 58], and is consistent with the so-called TAP equations [64].

The derivatives of $S_{\rm G}$ with respect to the $\{p_{ij}\}$ and $\{p_i\}$ give the value of the couplings and fields,

$$\begin{aligned}
(J_{\rm G})_{ij} &= -\frac{\partial S_{\rm G}}{\partial p_{ij}} = -\frac{(M^{-1})_{ij}}{\sqrt{p_i(1-p_i)p_j(1-p_j)}}\,, \\
(h_{\rm G})_i &= -\frac{\partial S_{\rm G}}{\partial p_i} = \sum_{j(\neq i)} (J_{\rm G})_{ij}\left(c_{ij}\frac{p_i - \frac{1}{2}}{p_i(1-p_i)} - p_j\right)\,,
\end{aligned} \tag{C.22}$$

where $c_{ij} = p_{ij} - p_i p_j$ is the connected correlation.

Vita

John Barton

2006-2012 Ph.D. in Physics, Rutgers University

2002-2006 B.S. in Mathematics and Physics (with distinction), Duke University

2011-2012 Graduate Assistant, Rutgers University

2010-2011 Teaching Assistant, Rutgers University

2009-2010 Graduate Assistant, Rutgers University

2006-2009 Teaching Assistant, Rutgers University

2003-2004 Teaching Assistant, Duke University

Publications

1. John Barton, Joel L. Lebowitz, and Eugene R. Speer. Phase diagram of a generalized ABC model on the interval, *J. Stat. Phys.*, Volume 145, Number 3, 763-784 (2011).

2. John Barton, Joel L. Lebowitz, and Eugene R. Speer. The grand canonical ABC model: a reflection asymmetric mean field potts model, *J. Phys. A: Math. Theo.* **44**, 6, 065005 (2011).

3. John Barton and Simona Cocco. Ising models for neural activity inferred via Selective Cluster Expansion: structural and coding properties, *Accepted*.